A STRESS-BASED DAMAGE CRITERION TO PREDICT ARTICULAR JOINT INJURY FROM SUBFRACTURE INSULT

By

Patrick Joseph Atkinson

A DISSERTATION

Submitted to
Michigan State University
in partial fulfillment of the requirements
for the degree of

DOCTOR OF PHILOSOPHY

Department of Materials Science and Mechanics

1998

ABSTRACT

A STRESS-BASED DAMAGE CRITERION TO PREDICT
ARTICULAR JOINT INJURY FROM SUBFRACTURE INSULT

By

Patrick Joseph Atkinson

Subfracture trauma to articular joints is a routine occurrence in sports, falls, and car accidents. In some cases, the trauma can produce microscopic fractures of bone and cartilage. Approximately 25% of patients sustaining subfracture injuries will experience chronic joint tissue degeneration within several years following the initial injury. Because of the small size of the fractures, subfracture injuries are difficult to detect acutely and patients are typically not treated. Unfortunately, there is no protocol for assessing the injury risk associated with subfracture traumatic events. An established joint injury criterion does exist, however, it is based on gross fracture of bone. The criterion is used by the automotive industry and is based on impact experiments on human cadavers. The criterion states that loads exceeding 10 kN will likely result in gross fracture of bone. Unfortunately, this criterion does not address subfracture injuries. This has led to the current investigation in which theoretical and experimental models were used to develop a stress-based, subfracture injury criterion. The patellofemoral joint served as a representative joint to develop the criterion. Numerous experimental and theoretical investigations were conducted to determine the impact response of the knee to fracture and subfracture level traumas. Impact loads were directed at the patella of 62 pair of isolated human cadaver knees to simulate impact loading which can occur during realistic trauma scenarios such as falls or car accidents. During such traumatic events, body kinematics and the contacting impact surfaces can vary, thus, a range of impact interfaces were used to impact the knee flexed at 60°, 90°, or 120°. Fracture level injuries typically involved transverse and comminuted fractures of the patella. Subfracture impact experiments at approximately 70% of the fracture load produced microscopic cartilage

fissures and occult subchondral bone microfractures. These injuries were documented via histology and were observed for all flexion angles. It was also observed that higher impact loads could be tolerated before fracture or subfracture level injuries were produced with increased contact area over the knee. Increased contact area typically resulted from experiments conducted with padded impact interfaces. A mathematical model was developed to estimate the stresses in the bone and cartilage in an effort to understand the injury mechanism of subfracture injuries. It was found that elevated shear stresses at the cartilage surface were associated with impact induced fissures. Occult injuries at the subchondral plate were associated with elevated shear and tensile stresses. The model showed that increased contact area over the knee significantly reduced tensile stresses in the subchondral plate. The degree to which the tensile stresses were reduced was dependent on the magnitude of the impact load and large contact areas. The reduced incidence of fracture and subfracture injuries was significantly associated with reductions in the tensile stresses in the subchondral bone. This suggested that the load and contact area data could be used as a gross estimation of the stresses in the bone. This concept was expanded to develop an injury criterion based on peak impact load and the contact area on the knee. This criterion is useful for predicting injury in the human cadaver knee, however, experiments conducted by automotive companies typically utilize anthropomorphic dummies for crash simulations. Because studies have suggested that the load-area response of the dummy knee significantly differs from the human knee, a transformation protocol was developed to allow the load-area data from the cadaver experiments to be transposed to the dummy knee. Thus, experimentally derived load-area data points from the dummy were compared to injurious load-area data points from the cadaver. The load-area criterion can be applied in experimental or theoretical studies to optimize the design of car instrument panels, sports padding, etc. Implementation of such improvements may reduce the overall incidence of joint injuries and the associated sequelae of chronic joint morbidity.

DEDICATION

I want to thank the Lord for the opportunities afforded me throughout my life. I want to thank my beautiful wife; I have a deep love and respect for you and my successes are rooted in your support. I want to thank my family: my parents, one of the greatest gifts God has given me; my brothers and sisters for their loving encouragement.

ACKNOWLEDGMENTS

I would like to acknowledge my major professor Dr. Roger Haut for taking a chance on me five years ago. His mentoring, guidance, and encouragement have inspired me throughout my time at Michigan State University.

I am also grateful to Dr. Nicholas Altiero for serving on my committee and playing an important role in developing my understanding and appreciation of engineering.

I would like to acknowledge Dr. Dahsin Liu and Dr. Charles DeCamp for their time and input through serving on my committee.

I would like to acknowledge Dr. Robert Soutas-Little for his time and energy in helping with the analysis of inertial and stress wave effects presented in the concluding chapter.

Finally, I would like to express my graditude to the many collaborators I have had the pleasure of working with on my research. This includes faculty members at Michigan State University, faculty from other universities, members of industry and many of my fellow graduate students.

TABLE OF CONTENTS

LIST OF TABLES

LIST OF FIGURES

CHAPTER 7

CHAPTER 8

CITATIONS OF PUBLISHED WORK CONDUCTED DURING GRADUATE SCHOOL: DISSERTATION RESEARCH

Each chapter in this dissertation represents a complete paper. Following are the citations for those papers.

CHAPTER 1
Atkinson PJ, Walsh JA, Haut RC: The human patella: a comparison of three preparation methods. The Journal of Histotechnology In press.

CHAPTER 2
Atkinson PJ, Newberry WN, Atkinson TS, Haut RC: A method to increase the sensitive range of pressure sensitive film. Journal of Biomechanics. In press

CHAPTER 3
Atkinson PJ, Haut RC: A method for determining regions of diarthrodial joint contact during dynamic loading of the human knee. Transactions of the Orthopaedic Research Society: 656, San Francisco, CA, February, 1997.

CHAPTER 4
Atkinson PJ, Haut RC: Subfracture insult to the human cadaver patellofemoral joint produces occult Injury. Journal of Orthopaedic Research 13:936-944, 1995.

CHAPTER 5
Atkinson PJ, MacKenzie CM, Haut RC: Joint fracture load prediction using geometrical, physical and pathological measures: the human knee. SAE International Congress: paper 980358, 1998.

CHAPTER 6
Atkinson PJ, Garcia JJ, Altiero NJ Haut RC: The influence of impact interface on human knee injury: implications for instrument panel design and the lower extremity injury criterion. 41st Stapp Car Crash Conference, SAE: 167-180. paper 973327, 1997.

CHAPTER 7
Patrick Atkinson, Jose Garcia, Hasnin Ali*, Nicholas Altiero*, Roger Haut: Human Knee Impact Injury Thresholds And Location Vary With Flexion Angle And Impact Interface. 8th Injury Prevention Through Biomechanics Symposium: 8:127-143, 1998.

CHAPTER 8
Patrick Atkinson, Nicholas Altiero, Roger Haut Chris Eusebi, Vivek Maripudi, Tim Hill, Kiran Sambatur: A Proposed Model To Transform Cadaver Knee Injury Criteria To The Hybrid Iii Dummy. 8th Injury Prevention Through Biomechanics Symposium: 8:157-172, 1998.

CITATIONS OF PUBLISHED WORK CONDUCTED DURING GRADUATE SCHOOL: ADDITIONAL PUBLISHED RESEARCH

Atkinson PJ, Oyen-Tiesma M, Decamp CE, Mackenzie CD, Haut RC: Mechanical augmentation of the patellar tendon after removal of its central third helps limit changes in joint tissue. Journal of Orthopaedic Research Conditionally accepted.

Atkinson PJ, Atkinson TS, Lancaster RL, Arnoczky SP, Haut RC, Weisbrode SE: In-Vivo Breaking Strength Retention And Histological Effects of 1.3 mm PDS ORTHOSORB® Absorbable Pins as Seen in Rabbits. Journal of Foot and Ankle Surgery 37(1):42-47, 1998

Patrick Atkinson, Nicholas Altiero, Roger Haut Chris Eusebi, Vivek Maripudi, Tim Hill, Kiran Sambatur: Development of an injury criteria for human surrogates to address current trends in knee-to-instrument panel injuries. 42nd Stapp Car Crash Conference, SAE: paper 98S-25, 1998.

Atkinson PJ, Haut RC: Insult to the human cadaver patellofemoral joint: effects of age on fracture tolerance and occult injury. 39th Stapp Car Crash Conference, SAE: 281-294. paper 952729, 1995.

Atkinson, PJ, Garcia JJ, Altiero NJ, Haut RC:Animal and human studies on injury mechanisms during blunt insult to the knee. 7th Injury Prevention Through Biomechanics Symposium, 1997, 7:53-64.

Atkinson, P, Newberry, W, Staton, T, Garcia, J, Altiero, N, Haut, R:Animal and human studies on injury mechanisms during blunt insult to the knee. 6th Injury Prevention Through Biomechanics Symposium, 1996, 6:137-160.

Newberry, W, Atkinson, P, Li X, Decamp, C, Altiero, N, Haut, R: Tissue injuries resulting from blunt impact on the knee. 5th Injury Prevention Through Biomechanics Symposium, 1995,5:21-39

Haut R, Atkinson P, Garcia J, Altiero N: Impact model for the human patellofemoral joint. 1998 World Congress on Biomechanics. In press.

Haut R, Atkinson P, DeCamp C, MacKenzie D: Augmentation influences joint remodeling after removal of the central third of the patellar tendon. 1998 World Congress on Biomechanics. In press.

Garcia JJ, Newberry WN, Atkinson PJ, Haut RC, Altiero NJ: Comparison of stresses in human and rabbit knees as they pertain to injuries observed during impact experiments. Advances in Bioengineering ASME:315-316, Sun River, OR, June, 1997.

Atkinson PJ, Decamp C, Kamps B, Hespenheide B, Zukosky D, Haut R: Healing response of the patellar tendon after removal of its central third and implantation of an augmentation device. Transactions of the Orthopaedic Research Society : 751, Atlanta, GA February, 1996.

Newberry, W, Shelp, D, Atkinson, P, Haut, R: The effect of temperature on the mechanical response of intact and scarified articular cartilage. Advances in Bioengineering ASME:73-74, Chicago, IL November, 1994.

INTRODUCTION

Knee injury is a considerable problem which currently represents a large economic and societal cost. The knee joint is commonly injured in domestic (States 1970), sports and car accidents. Studies of experienced and amateur football players reveal it is the most injured body region for that sport. For the years 1979-1995, 10% of all injuries associated with car accidents were to the knee. Only the head and face are injured more frequently (Huelke 1991). The knee is commonly injured in car accidents (Huelke 1991) during high speed contact with the instrument panel which can produce subfracture and fracture injuries (Crandall 1995, States 1970) leading to a significant financial burden for acute care. In addition to acute injuries, knee trauma can lead to chronic joint problems such as post-traumatic osteoarthritis which add additional costs and disability (MacKenzie 1988). Osteoarthritis (OA) is documented to be the most prevalent joint disease in the world and has been strongly correlated to injury (Davis 1989). For example, independent clinical studies (Nagel 1976, Volpin 1990, Chapchal 1978) document a 25% or greater chance of developing OA after gross fracture of the knee as early as one year post-insult (Chapchal 1978).

A well established criterion is currently used by the automotive industry to prevent gross bone fracture in the human knee (Viano 1977). The criterion states that loads exceeding 10 kN will likely result in gross fracture of bone. This criterion is used to certify new car models in which crash simulations are conducted using anthropomorphic dummies as human surrogates. However, long-term complications have also been associated with subfracture joint trauma. OA has also been associated with subfracture,

repetitive loading such as occurs during sporting and occupation related activities. For example, mail carriers, farmers, construction workers, and firefighters are significantly predisposed to OA in the absence of fracture. It is hypothesized that the chronic joint problems are a consequence of repetitive microfracture of cartilage and bone. This is confirmed by Radin and coworkers who cyclically loaded the rabbit tibiofemoral joint producing occult microfractures at the bone-cartilage interface which were associated with the development of OA. Unfortunately, the small size and typically occult nature of occult injuries precludes there acute detection and treatment (Tomatsu 1992).

Chronic joint morbidity has also been documented following a single, subfracture joint trauma (States 1970) which causes acute microfracture of cartilage and underlying bone. In as early as 4 years, subfracture traumatic dislocations of the hip lead to OA in 24% of cases (Upadhyay 1983). In experimental studies, a single transarticular blow to the knee at 45% of the energy required to cause fracture produces occult vertical clefts at the bone-cartilage interface which have been associated with ensuing degenerative changes (Donohue 1983, Thompson 1991). Clinical and experimental studies of human (Atkinson 1998) and animal (Newberry 1996, Armstrong 1985, Tomatsu 1992) joint tissues show that the development of cartilage fissures and occult cracks are associated with chronic pain and joint degeneration (Johnson-Nurse 1985, Newberry 1996). Occult bone microfracture can appear *in vivo* as a 'bone bruise' on magnetic resonance images and is associated with superficial degeneration of the overlying cartilage within 6 months (Vellet 1991).

It is hypothesized that the superficial and occult subfracture injuries noted above are associated with elevated shear or tensile stresses (Atkinson 1998, Ateshian 1993, Eberhardt 1991, Thompson 1991). In general, the magnitude and location of these stress maxima are dependent, in part, on the radii of the contacting articular surfaces. For example, contact between disparate radii results in elevated shear stresses at the surface while contact between similar, larger radii result in elevated shear stresses at the bone-cartilage interface (Atkinson 1998, Eberhardt 1991). The relative contact radii in the patellofemoral joint vary with flexion, as evidenced by studies of patellofemoral contact areas associated with passive joint loading. The largest contact areas are documented at 90° of joint flexion with reduced contact areas documented at at flexion angles of 120° and 60° (Huberti 1984). This suggests that trauma at extreme flexion angles may produce more superficial lesions due to the disparate radii which lead to the smaller areas of contact. Alternately, increased intraarticular contact area reflects larger contact radii suggesting deeper lesions would be more frequent at the bone-cartilage interface. The flexion angle at which trauma occurs in car accidents, for example, can range from 70° to 120° at the point of impact with the instrument panel. The relatively large range of flexion angles is attributed to the anthropometry of the individual (Dischinger 1994), the initial distance between the knee and instrument panel and other factors associated with the car interior. Injuries incurred during sports and domestic accidents can also occur at varied flexion angles due to similar reasons. In addition to the influence of flexion angle, past studies suggest that the composition of the impact interface will play an important role in knee injury. Studies conducted with rigid impact interfaces and padded interfaces of

variable thickness and composition show a 65% reduction in patellar fractures with padding (Melvin 1975, Powell 1975, Patrick 1965). Unfortunately, an investigation of subfracture injuries was not conducted. While not measured, the padded interfaces probably produced greater contact areas over the knee than the rigid interface experiments. This shows that increased contact area can prevent fracture level injuries, while it is unknown if it will prevent subfracture injuries.

In the automotive industry, assessments of knee joint injury is predicted via instrumented anthropomorphic dummies. If impact load and contact area are important parameters in predicting injury in the cadaver, then this concept would need to be applied to the dummy knee in the crash environment. However, previous studies suggest that the impact load and contact area response of the dummy knee is significantly different than the cadaver knee (Hering 1977). Thus, a transformation of injurious load and area data in the cadaver will be required for use with the dummy.

The aims of the current study were to investigate the response of the human knee to subfracture transarticular loading with different interfaces at different flexion angles. It was hypothesized that the flexion angle of the knee and the stiffness of the impact interface would play an important role in the incidence of impact-induced subfracture injuries of the knee. Specifically, the study hypotheses were: 1) extreme flexion angles will be associated with more superficial lesions of articular cartilage while median flexion angles will yield deeper, occult injuries; 2) increased contact over the knee will increase the magnitude of the impact load that can be tolerated before injury occurs; 3) parameters

which are determined to be associated with injury in the cadaver can be transformed for use with the dummy knee.

Below is an overview of the chapters contained in this dissertation:

Chapter 1 presents a comparison of three histological methods which can be used to reliably prepare slides for microscopic analysis of subfracture injuries. This study shows that superior results can be achieved without preparation artifact via simple, alternative processing methods.

Chapter 2 presents a new way to use different ranges of pressure sensitive film in recording extraarticular and intraarticular contact areas and contact pressures associated with the impact event. This method increases the sensitivity and accuracy of contact area and contact pressure data.

Chapter 3 outlines a method to identify regions of diarthrodial joint contact on the articular surfaces. This is particularly helpful in determining the correct placement of boundary conditions for mathematical models.

Chapter 4 is the first known subfracture injury study conducted on human joints. Human cadaver knees were impacted at 45% of the energy required to produce fracture with a rigid impactor and the knee flexed 90°. Occult, horizontal microfractures were documented at the bone-cartilage interface in four of seven subjects.

Chapter 5 examines which gross parameters describing test cadaver subjects (age, height, mass, sex, joint pathology, joint geometry, contact area over the knee) might influence the impact response of the knee. It was found that joint geometry and contact area significantly affected the impact loads and bone and cartilage stresses.

Chapter 6 followed from the findings in the preceding chapter. Paired experiments were conducted on cadaver knees in which consistent impact loads were delivered with the load distributed over significantly different contact areas. Small contact areas produced gross and microscopic injuries while large contact areas prevented injury.

Chapter 7 studied the impact response of the knee by conducting experiments with different interfaces and with the knee flexed at a range of flexion angles. It was found that rigid interfaces produced small contact areas and a high incidence of injuries at all flexion angles. These injuries were associated with elevated tensile and shear stresses in the subchondral plate. Padding significantly reduced these stresses and the associated incidence of injury.

Chapter 8 takes the findings from the cadaveric studies and applies them to the anthropomorphic dummy commonly used as a human surrogate in car crash simulations. Thus, the experimental findings of the current dissertation are applied in a pragmatic to estimate the injury potential of a traumatic event. This will allow the design of countermeasures which could prevent knee injuries.

Chapter 9 is a concluding chapter which provides an overview of the findings in the dissertation such as injury classifications and probable mechanisms as well as potential injury countermeasures. In addition, some analyses are presented for the first time in this chapter: 1) inertial effects and stress waves are studied with regard to their injury potential in the knee, 2) injury risks based on regression analyses of the experimental data, and 3) modeling of the anthropomorphic dummy in simulated car crashes.

REFERENCES

1. Armstrong C, Mow V, Wirth C (1985) Biomechanics of impact-induced microdamage to articular cartilage: a possible genesis for chondromalacia patella. In: Amer Acad of Orth Surg Symp on Sports Med, ed by G Fenerman. pp70-84

2. Ateshian GA, Lai WM, Zhu WB, Mow VC (1994) An asymptotic solution for the contact of two biphasic cartilage layers. *J Biomechanics* 27(11):1347-1360

3. Atkinson, T.S., Haut, R.C., and Altiero, N.J. (1998) An Investigation of Biphasic Failure Criteria for Impact Induced Fissuring of Articular Cartilage. J of Biomechanical Engineering (In Press)

4. Chapchal G (1978) Posttraumatic osteoarthritis after injury of the knee and hip joint. *Reconstr Surg Trauma* 16:87-94

5. Crandall J, Kuhlmann T, Pilkey W (1995) Air and knee bolster restraint system: laboratory sled tests with human cadavers and the Hybrid III dummy. J Trauma 38: 517-520

6. Davis M, Ettinger W, Neuhaus J, Cho S, Hauck W (1989) The Association of Knee Injury and Obestiy with Unilateral and Bilateral Osteoarthritis of the Knee. American Journal of Epidemiology 130(2): 278-288

7. Dischinger PC, Kerns TJ, Kufera JA (1995) Lower extremity fracturesin motor vehicle collisions: the role of gender and height. Accident Analysis and Prevention 27(4): 601-606

8. Donohue MJ, Buss D, Oegema T, Thompson R (1983) The Effects of Indirect Blunt Trauma on Adult Canine Articular Cartilage. The Journal of Bone and Joint Surgery 65-A(7): 948-957

9. Eberhardt, A., Keer, L., Lewis, J., and Vithoontien, V. (1990) An Analytical model of joint contact. Journal of Biomechanical Engineering 112:407-413

10. Hering W, Patrick L (1977) Response Comparisons of the Human Cadaver Knee and a Part 572 Dummy Knee to Impacts by Crushable Materials. Twenty-First Stapp Car Crash Conference 21: 1015-1053

11. Huberti H, Hayes W, Stone J, Shybut G (1984) Force ratios in the quadriceps tendon and ligamentum patellae. Journal of Orthopaedic Research 2: 49-54

12. Johnson-Nurse C, Dandy D (1985) Fracture-Separation of Articular Cartilage in the Adult Knee. The Journal of Bone and Joint Surgery 67-B(10: 42-43

13. MacKenzie EJ, Siegel JH, Shapiro S, et.al. (1988) Functional Recovery and Medical Costs of Trauma: An analysis by Type and Severity of Injury. Journal of Trauma 28: 281-298

14. Melvin J, Stalnaker R, Alem N, Benson J, Mohan D (1975) Impact Response and Tolerance of the Lower Extremities. Stapp Car Crash Conf 19: 543-559

15. Nagel D, States J (1977) Dashboard and bumper knee-will arthritis develop? AAAM proceedings 21: 272-278

16. Newberry W, Haut R (1996) The effects of subfracture impact loading on the patellofemoral joint in a rabbit model. 40th Stapp Car Crash Conference 149-159

17. Patrick L, Kroell C, Mertz H (1965) Forces on tehehuman body in simulated Crashes. Stapp Car Crash Conf 9: 237-259

18. Powell W, Ojala S, Advani S, Martin R (1975) Cadaver Femur Responses to Longitudinal impacts. Stapp Car Crash Conf 19: 561-579

19. Radin E, Parker H, Pugh J, Steinberg R, Paul I, Rose R (1973) Response of joints to impact loading-III relationship between trabecular microfractures and cartilage degeneration. *J Biomech* 6:51-57

20. States J (1970) Traumatic Arthritis-- A Medical and Legal Dilemma. Ann Conf of the Amer Assoc for Automotive Med 14: 21-28

21. Thompson RC, Oegema TR, Lewis JL, Wallace L (1991) Osteoarthritic changes after acute transarticular load. The Journal of Bone and Joint Surgery 73-A(7): 990-1001

22. Tomatsu T, Imai N, Takeuchi N, Takahashi K, Kimura N (1992) Experimentally produced fractures of articular cartilage and bone. J Bone Joint Surg 3:457-461, 1992

23. Upadhyay S, Moulton A, Srikrishnamurthy K (1983) An analysis of the late effects of traumatic posterior dislocation of the hip without fractures. J Bone Joint Surg 65: 150-152

24. Vellet AD, Marks PH, Fowler PJ, Munro TG (1991) Occult post-traumatic osteochondral lesions of the knee: prevalence, classification, and short-term sequelae evaluated with MR imaging. Radiology 178(1):271-276

25. Viano D (1977) Considerations for a femur injury criterion. 21st Stapp Car Crash Conference 445-473

26. Volpin G, Dowd G, Stein H, Bentley G (1990) Degenerative arthritis after intra-articular fractures of the knee. Long-term results. J Bone Joint Surg Br 72: 634-638

CHAPTER 1

DETECTION OF EXPERIMENTALLY PRODUCED OCCULT MICROCRACKS AT THE BONE-CARTILAGE INTERFACE

Atkinson PJ [&#], Walsh JA [&], Haut RC [&#]

&Orthopaedic Biomechanics Laboratories, College of Osteopathic Medicine

and the # Department of Materials Science and Mechanics, College of Engineering

Michigan State University, East Lansing, MI

ABSTRACT

We compared 3 histological preparation methods to detect experimentally produced occult microcracks in decalcified human patellae: a paraffin tape-transfer technique, a paraffin slab-cut method, and a paraffin method with methyl salicylate as the clearing agent. Microcracks were observed at the bone-cartilage interface and were oriented either parallel or perpendicular to the tidemark. Both types of microcracks were documented with each preparation method. The slab-cut method was time consuming, however, the section thickness allowed a detailed analysis of the architecture of microcracks as they passed into the depth of the section. The methyl salicylate method was efficient and produced thin, serial sections of good morphological detail, and minimal cutting artifact. Reliable histological data were also derived from the tape-transfer technique, however, this method was inconsistent. The methods summarized here for

processing decalcified human joint tissues provide a basis for future orthopaedic studies investigating occult microfractures at the bone-cartilage interface.

INTRODUCTION

Clinical (Kern 1988, States 1970) and experimental (Donohue 1983, Newberry 1996, Newberry 1997, Radin 1978, Radin 1973, Shimizu 1993, Thompson 1991, Vener 1992) studies suggest that impact-induced trauma can initiate a chronic joint disease (i.e. osteoarthrosis). The disease pathogenesis can be associated with an acute gross fracture or occult microfracture involving bone and cartilage. The microcracks have been documented as open cracks oriented perpendicular or parallel to the articular surface occurring in areas of high intraarticular contact stress (Atkinson 1997). The microcracks do not normally exist in untraumatized human joint tissues (Atkinson 1995). While gross fractures can be documented via conventional techniques (i.e. radiographs, palpation, etc.), occult microfractures are more difficult to diagnose. Currently, the sole diagnostic technique for *in vivo* detection of occult microfractures in humans and animals relies on specific Magnetic Resonance Imaging (MRI) protocols (i.e. STIR). 'Bone bruises' associated with the microfracture can be detected with MRI (Vellet 1991), however, this requires that a basal blood pressure exists to form the bone bruise. Unfortunately, this technique is not suitable for *in vitro* studies. Histology is the only established technique in documenting occult microfractures from experimental joint trauma studies (Atkinson 1995, Thompson 1991, Vener 1992). However, consistent and reliable methods are needed. Recent studies (Thompson 1991, Vener 1992) base the interpretations on

whether the microfractures exist in serial sections. This study was designed to determine reproducible preparation methods that yielded consistent sections of decalcified human patella. The resulting sections were then analyzed to investigate experimentally induced microfractures.

METHODS AND MATERIALS

Tissues

18 knee joints were harvested from human cadavers with no prior history of joint trauma and/or evidence of advanced joint pathology. The femur and tibia were transected and all musculature was removed. The knee joints were attached to a special fixture, flexed 90° and impacted once at a subfracture load using a previously described protocol (Atkinson 1995). The patellae were then dissected free.

Processing and Decalcification

The patellae were fixed in 10% neutral buffered formalin for 9-12 days. Formic acid (20%) was used to decalcify the tissue. Decalcification solutions were changed every 3 days at which time a precipitate test was performed using ammonium oxalate (Lillie 1954). The decalcification endpoint was determined with 2 successive negative precipitate tests. Both fixation and decalcification were performed with continuous, moderate agitation.

Following decalcification, samples were taken from each patellae (3-5 mm thick, approximately 50 mm wide, 8 mm depth). 6 patellae each were randomly assigned to be processed according to one of three methods: paraffin slab-cut method, paraffin tape-transfer method, or a paraffin method using methyl salicylate. The processing schedules

for each method have been previously described (Atkinson 1998). A synopsis of each method follows.

Slab-cut Method: Samples were dehydrated, infiltrated and embedded in paraffin. The block was cut into 500μm slabs on an Isomet low speed saw (Buehler Ltd., Lake Bluff, IL) using a diamond blade. The slabs were stained with safranin O-fast green and coverslipped (Rosenburg 1971).

Paraffin Tape-Transfer Method: Samples were dehydrated, infiltrated and embedded in paraffin. Sections were cut at 8μm on a rotary microtome using a 150 mm stainless steel knife. As the sections were cut, they were captured on 50.8 mm sealing tape (3M Scotch 375, 3M St Paul MN) (Sterchi, D.L. and Eurell, J.C. 1990), floated on a water bath at 45°C, retrieved on slides, coated with Poly-l-Lysine (Sigma, St. Louis, MO), and placed on a warming plate. The slides were covered with a strip of plastic wrap, stacked, clamped together in a vise and maintained at 60°C overnight followed by an additional 24 hr at 37°C. The slides were placed in xylene at room temperature overnight to remove tape. The sections were stained with safranin O-fast green and coverslipped.

Paraffin Method using Methyl Salicylate: Samples were slowly dehydrated in a series of increasing alcohols followed by three changes of methyl salicylate (Skinner 1986). Times for methyl salicylate ranged from 3-6 hr with agitation. Infiltration occurred in 3 changes of paraffin (6 hr each) at 60-65°C under vacuum (15-18 psi). Samples were embedded in paraffin and cured at 4°C. A block softener was used in addition to icing the block face for 10-15 minutes immediately prior to sectioning. A rotary microtome was used to section the blocks at 6-9 μm. The resulting sections were

floated in a 45-48°C water bath and retrieved on slides. No slide adhesive was used. The slides were warmed in 2 steps: 53-55°C for 10 min and 62-75°C until the section was flat. The sections were then dried overnight at 37°C, stained with safranin O-fast green and coverslipped.

The resulting sections from each patellae were examined independently with light microscopy by two of the authors (P.A., J.W.) for structural detail and then photographed.

RESULTS

Vertical (perpendicular to the articular surface) and horizontal (parallel to the articular surface) occult microcracks were documented in approximately 50% of all patellae using each method (Figure 1, A-F). All cracks were 'open', involving a separation of bone and/or cartilage. The horizontal cracks were observed with a magnification of 40 power at the subchondral bone-calcified cartilage interface in one of three areas: a delamination of the cartilage from the calcified cartilage, a delamination of the calcified cartilage from the subchondral bone, or a crack confined to the subchondral plate. The vertical cracks typically initiated in the trabecular bone near the subchondral plate, and extended across the subchondral plate and the tidemark into the cartilage. While these cracks did not communicate to the articular surface, they were visually discernible on some tissues as a faint shadow when viewing the articular surface of the patella prior to cutting. The appearance of the microcracks was consistent, regardless of the processing method. With higher magnification (100-400X), a previously established protocol (Frost 1960) was used to document the existence of small, intact cracks oriented vertically in the calcified cartilage of some patellae. These cracks have been previously

described as normally occuring in human tissues, indicative of joint morbidity (Sokoloff 1993; Villanueva 1994). Therefore, these microcracks were considered a preexisitng condition and not included for analysis in the current study.

Intact sections suitable for the detection of microcracks were procured with varying levels of effort using the three methods. While serial sections were easily taken with the slab-cut technique, it was very time consuming, requiring 3 to 5 hours to cut 1 block. A top-lit stereomicroscope was found to be the best method of providing a detailed analysis of the microcracks. Analysis with standard light microscopy was hindered by reduced light transmission due to the thickness of the slab. However, because of the section thickness, this method gave the added dimension of depth to the microcracks which often communicated to both sides of the section (Figure 2). It was difficult to obtain serial sections with the tape-transfer technique. Typically, 5 of 20 sections were considered suitable for staining. The sections that were stained were of good quality. Analysis with light microscopy at a range of magnifications (40-400X) showed the cartilage, bone and tidemark to be free of preparation artifact. The methyl salicylate method produced serial sections with considerable ease. Analysis with light microscopy showed good cartilage, bone and cellular detail and the absence of preparation artifact. While increased time was required for dehydration and clearing, the improved quality of cutting was significant. Using a block softener and icing the block face before sectioning for 10-15 min greatly enhanced the ease of cutting.

DISCUSSION

This study presents a comparison of 3 histologic preparation methods applied to decalcified human patellae. It was designed to identify a reproducible method which consistently produces high quality serial sections to allow the detection of occult microfractures in the human patella. The detection of occult microfractures is currently limited to histological methods for *in vitro* studies. This underscores the need to identify suitable methods for continued study in this area.

Experimentally produced 'open' vertical and horizontal occult microfractures were documented using all three methods. The architecture of the microcracks was visually similar from all methods, and similar to past studies using a single method. For example, animal and human experimental studies have shown horizontal (Armstrong 1985; Atkinson 1995, Radin 1978; Radin 1973; Zimmerman 1988) and vertical (Donohue 1983; Thompson 1991; Vener 1992) occult microcracks at the bone-cartilage interface.

Additional studies have documented a variety of *in vivo* (preexisting) occult microcracking. While it is difficult to establish the exact cause of the microcracks, they may be due to a single trauma (subfracture joint insult) (Thompson 1991), repetitive microtrauma (Radin 1973), or a consequence of aging/joint morbidity (Villanueva 1994). Studying the canine, Van Sickle and Evander (1997) document open, horizontal microfractures at the bone-cartilage that are visually similar to the horizontal cracks in the current study. Villanueva, et al. (1994) retrieved typically degenerated femoral heads during prosthetic surgery and discovered small, vertically oriented, 'closed' (intact)

microcracks in the subchondral bone and/or calcified cartilage. Sokoloff (1993) documents similar closed microcracks confined to the calcified cartilage. The appearance of the *in vivo*, closed microcracks described in these studies differ from the experimentally produced occult microfractures documented in the current study and the past studies noted above. We hypothesize there may be two different explanations for this variation in appearance. First, the mechanism of microfracture may be different. The larger, open microfracture may be the result of a more acute injury associated with a high energy joint insult. Alternately, the smaller, intact microfractures may be a chronic phenomenon (i.e. associated with tissue remodeling). A second, related possibility is that the larger, open microcracks may close as the tissue heals; eventually they may reduce in size taking on the appearance of the smaller, closed microcracks.

In the current study, the presence of occult microcracks was verified *a priori* via faint shadows observed on the articular surface of some patella prior to any cutting. If this visualization is possible for *in vivo* tissues, it may provide a helpful tool for clinical detection of subfracture joint injuries, in addition to MRI (i.e. via arthroscopy).

The methods outlined in this study provides flexibility for studies investigating occult microfractures when processing decalcified human joint tissues. For example, while the slab-cut method was time consuming, it allowed a detailed analysis of the architecture of microcracks as they passed into the depth of the section. This method also facilitated taking serial sections free of cutting artifact. Alternately, the methyl salicylate method should be used if thin sections are required. This method resulted in easy cutting, consistent serial sections, good morphological detail, and a reduction of cutting artifact.

Reliable histological data were also derived from the tape-transfer technique, however, this methods was inconsistent. The methods summarized here may provide a basis for future orthopaedic studies investigating disruptions at the bone-cartilage interface.

ACKNOWLEDGMENTS

This study was supported by a grant (R49/CCR503607) from the Centers for Disease Control and Prevention. Its contents are solely the responsibility of the authors and do not necessarily represent the official views of the Centers for Disease Control and Prevention. We are indebted to Mr. Rick Shumaker and the Michigan Tissue Bank for solicitation of donors and retrieval of joints.

REFERENCES

1. Armstrong, C., Mow, V., Wirth, C. 1985. Biomechanics of impact-induced microdamage to articular cartilage: a possible genesis for chondromalacia patella. *American Academy of Orthopaedics Surgical Symposium on Sports Medicine*, ed. G. Fenerman, pp. 70-84.

2. Atkinson, P.J., Walsh, J. and Haut, R.C. 1998. The human patella: a comparison of three preparation methods. 1998. 21(2) Journal of Histotechnology (In Press)

3. Atkinson, P.J., Garcia, J.J., Altiero, N.J. and Haut, R.C. 1997. The influence of impact interface on human knee injury: implications for istrument panel designa and the lower extremity criterion. 41st Stapp Car Crash Conference. 41:167-180.

4. Atkinson, P.J. and Haut, R.C. 1995. Subfracture insult to the human cadaver patellofemoral joint produces occult injury. Journal of Orthopaedic Research 13, 936-944.

5. Donohue, M.J., Buss, D., Oegema, T. and Thompson, R. 1983. The effects of indirect blunt trauma on adult canine articular cartilage. The Journal of Bone and Joint Surgery 65-A(7), 948-957.

6. Frost, H.M. 1960. Presence of microscopic cracks *in vivo* in bone. Henry Ford Hospital Medical Bulletin. 8:25-35.

7. Kern, D., Zlatkin, M. and Dalinka, M. 1988. Occupational and post-traumatic arthritis. Radiologic Clinics of North America. 26:1349-1358.

8. Lillie, R. 1954. *Histologic Technic and Practical Histochemistry.* McGraw Hill, NY, p. 424.

9. Newberry, W.N., Garcia, J.J. and Haut, R.C. 1996. The effects of subfracture impact loading on the patellofemoral joint in a rabbit model. 40th Stapp Car Crash Conference SAE paper 962422, 149-159.

10. Newberry, W.N. and Haut, R. 1997. A single blunt impact to a rabbit patello-femoral joint induces OA changes in cartilage and subchondral bone. Journal of Orthopaedic Research 15, 450-455.

11. Radin, E., Ehrlich, M., Chernack, R., Abernethy, P., Paul, I. and Rose, R. 1978. Effect of repetitive impulsive loading on the knee joints of rabbits. Clinical Orthopaedics and Related Research 131:288-293.

12. Radin, E., Parker, H., Pugh, J., Steinberg, R., Paul, I. and Rose, R. 1973. Response of joints to impact loading-III relationship between trabecular microfractures and cartilage degeneration. Journal of Biomechanics 6:51-57.

13. Rosenburg, L. 1971. Chemical basis for the histological use of Safranin O in the study of articular cartilage. Journal of Bone and Joint Surgery 53(A):69-82.

14. Shimizu, M., Tsuji, H., Matsui, H., Katoh, Y. and Sano, A. 1993. Morphometric analysis of subchondral bone of the tibial condyle in osteoarthrosis. Clinical Orthopaedics 293:229-239.

15. Skinner, R.A. 1986. The value of methyl salicylate as clearing agent. Journal of Histotechnology 9(1):27-28.

16. Sokoloff, L. 1993. Microcracks in the calcified layer of articular cartilage. Archives of Pathology and Laboratory Medicine 117:191-195.

17. States, J. 1970. Traumatic arthritis--a medical and legal dilemma. Annual Conference of the American Association for Automotive Medicine 14:21-28.

18. Sterchi, D.L., Eurell, J.C. 1990. Tape-transfer technique for large paraffin blocks. Journal of Histotechnology 13(3):207-208.

19. Thompson, R.C., Oegema, T.R., Lewis, J.L. and Wallace, L. 1991. Osteoarthritic changes after acute transarticular load. The Journal of Bone and Joint Surgery 73-A(7), 990-1001.

20. Van Sickle, D. and Evander, S. 1997. The enigma of adult and immature articular cartilage. Journal of Histotechnology 20(3):243-252.

21. Vellet, D., Marks, P., Fowler, P. and Munro, T. 1991. Occult posttraumatic osteochondral lesions of the knee; prevalence, classification, and short-term sequelae evaluated with MR imaging. Journal of Radiology 178:271-276.

22. Vener, M.J., Thompson, R.C., Lewis, J.L. and Oegema, T.R. 1992. Subchondral damage after acute transarticular loading - an invitro model of joint injury. Journal of Orthopaedic Research. 10:759-765.

23. Villanueva, A.R., Longo, J.A. and Weiner G. 1994. Staining and histomorphometry of microcracks in the human femoral head. Biotechnic and Histochemistry. 69(2):81-88.

24. Zimmerman, N.B., Smith, D.G., Pottenger, L.A., Cooperman, D.R. 1988. Mechanical disruption of human patellar cartilage by repetitive loading in vitro. Clinical Orthopaedics and Related Research 229:302-307.

FIGURES

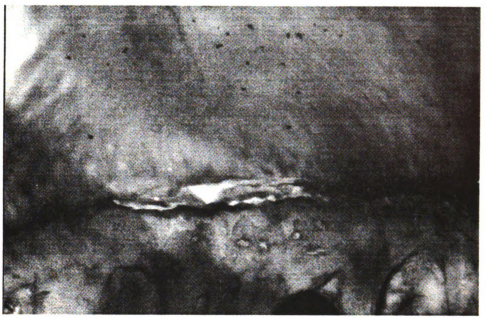

A

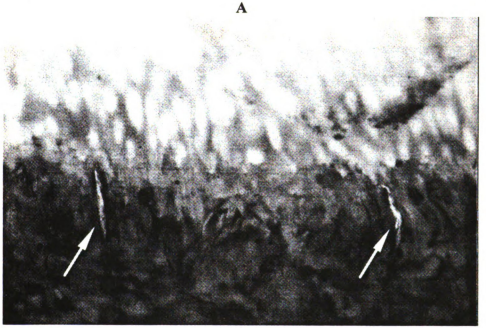

B

Figure 1: See subsequent page for caption.

C

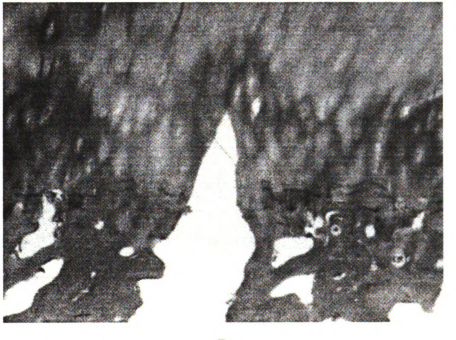

D

Figure 1: See subsequent page for caption.

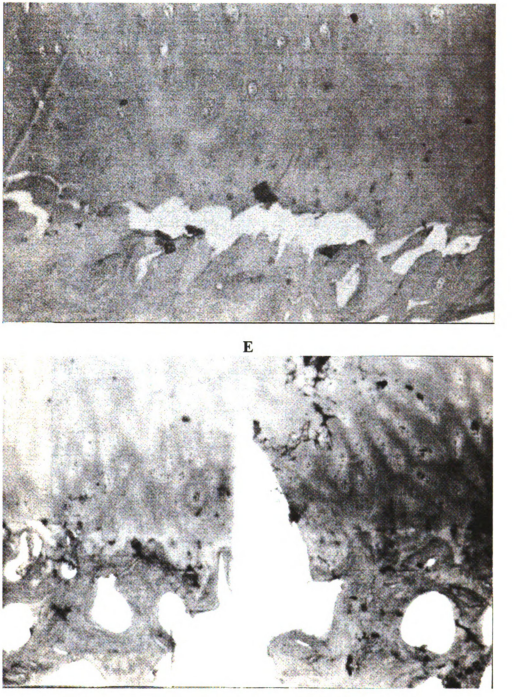

E

F

Figure 1

Figure 1: Photomicrographs of horizontal and vertical occult microcracks prepared by: 1) slab-cut method (A,B arrows point to occult injury; 40X), 2) paraffin tape-transfer method (C,D; 40X), and 3) paraffin method using methyl salicylate (D,E; 40X). Note: a microcrack at the calcified cartilage-subchondral bone interface (A,C), and a microcrack at the tidemark (E).

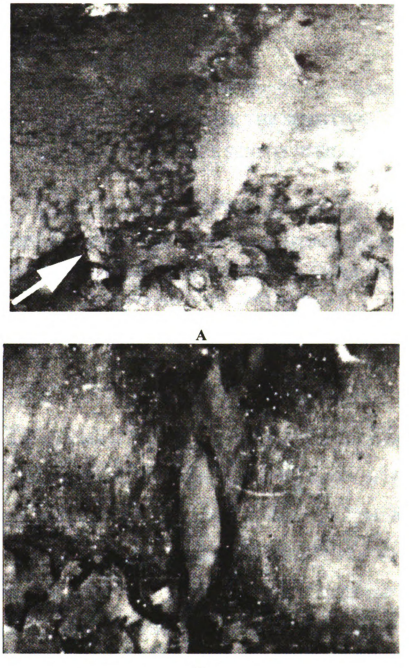

A

B

Figure 2: Photomicrographs of both sides (A,B; 18X) of a section (slab-cut method) showing a vertical, occult microcrack which passes through the section thickness. The microcrack initiates in the trabecular bone and terminates in the middle zone of the cartilage. The thickness of the section gave the added dimension of depth and allowed meaningful data to be derived from both sides of the section. Note: the light area in A (arrow) is where the microcrack exits the section on the reverse side (shown in B).

CHAPTER 2

A METHOD TO INCREASE THE SENSITIVE RANGE OF PRESSURE SENSITIVE FILM

Atkinson PJ, Newberry WN, Atkinson TS, Haut RC
Orthopaedic Biomechanics Laboratories, College of Osteopathic Medicine
and the Department of Materials Science and Mechanics, College of Engineering
Michigan State University, East Lansing, MI

ABSTRACT

Pressure sensitive film is frequently used in biomechanics to document intra- and extra-articular contact pressures. This often involves the contact of two surfaces of varying curvature producing non-uniform pressure distributions. The purpose of this study was to determine the feasibility of using multiple films in such experiments to yield accurate pressure and contact area data. A composite arrangement of film was dynamically loaded using cylindrical indenters of five radii. An analytical model of each indentation was constructed to provide a standard for error analysis. The study showed that several ranges of pressure sensitive film can be used simultaneously to accurately transduce contact pressures arising from loading scenarios that produce contact pressure gradients and contact pressures that involve suprathreshold loading of a given film range.

INTRODUCTION

Pressure sensitive film commonly used in biomechanics is constructed of a color developing layer sandwiched by a polyethylene terephthaylate (PET) base and a microcapsule layer. The film comes in several ranges (i.e. low range, 2-10 MPa; medium range, 10-50 MPa; high range, 50-130 MPa) and has been extensively used to transduce intra- and extra-articular dynamic (a:Atkinson 1995, Newberry 1996, Haut 1995, Haut 1989, Vener 1992, Li 1995) and quasi-static loading (Huberti 1984, Fukubayashi 1980). Because only a single range of film was used in these studies, contact area and/or pressure data may have been inaccurate (Atkinson 1997, Vener 1992). For example, low range film can yield accurate contact areas due to its sensitivity to low contact pressure. However, pressure data may be erroneous if the experimental contact pressure field exceeds the relatively low upper threshold of the film. Errors in contact area and pressure measurements may also exist for films that have higher ranges of sensitivity. By incorporating more than one range of film into experimental studies, more accurate contact area and pressure data can be transduced.

The purpose of the current study was to determine the feasibility of using multiple films simultaneously in a given dynamic experiment to yield accurate pressure data and measures of contact area. Low, medium and high range pressure sensitive film coupons were dynamically loaded in a composite arrangement (high, low and medium ranges) by means of cylindrical indentations. Digital analysis of the film documented the mean

contact pressure and contact area. An analytical model of each indentation was constructed to provide a standard for error analysis.

METHODS AND MATERIALS

Experimental Protocol

Idealized contact stress distributions were obtained experimentally by indenting packets of pressure sensitive film coupons (described below) with cylindrical indenters (Hale 1992) of five different radii (5.5, 12, 19, 66.5 and 94 mm). The film packets were compressed between the cylinder and a thick plate to produce a contact pressure distribution along the transverse axis. The length of the cylinder was much greater than the contact width, so that the longitudinal variation in contact stress was negligible. The cylinders and plate were machined from stainless steel and polished to a smoothed finish. The packets were loaded via a 60 Hz haversine pulse in a materials testing machine (model 1331, retrofitted 8500 electronics, Instron, Canton, MA) to simulate pulses derived from transarticular loading experiments (b:Atkinson 1995, Newberry 1997, Thompson 1991). The indenters were attached to the machine actuator, and the plate was supported by a load cell which was mounted on the fixed lower base of the machine. Load data was sampled at 5 kHz on a storage oscilloscope. Multiple indentation experiments were conducted for each indenter radius. A representative experiment was then analyzed per methods described below.

The packets consisted of pressure sensitive film coupons (Fuji Film Prescale, Itochu, Int., Montreal CA) of three ranges: dual sheet low (L W R270 10M), and single sheet medium (M S R270 10M) and high (H S R270 10M). The stacked coupons were

inserted into a polyethylene packet to reduce shear loading artifact (Huberti 1984) and to simulate how the film is commonly protected from moisture when used in hydrated environments (articular joints). The overall thickness of the packet was 0.44 mm (high and medium range film = 0.085 mm each, low range film 'A' and 'C' sheets = 0.08 mm each, two-ply polyethylene packet = 0.04 mm/ply). The packets were indented to achieve a nominal peak contact pressure of 60 MPa to ensure that the high pressure film (lower threshold of 50 MPa) reacted to the different loading scenarios.

The film was calibrated by conducting additional indentation tests on the stacked film packets described above with a plane ended square indenter (1 cm square). A wide range of loads was applied via a 60 Hz pulse. Pilot experiments showed wide variations in pressure stains with regard to the stacking order, loading rate and whether the film coupons were loaded separately or stacked. Therefore, the loading rate and film packet construction were consistent for all tests in the current study. The coupons were stacked in the following order: high, low and medium with the PET surfaces oriented in a consistent direction. The peak applied load divided by the area of the steel indenter was taken as the experimentally applied pressure. Following load application, the film was removed from the packet and digitized on a scanner (Scanmaker MRS-1200E6, Microtek, Taiwan) using commercially available software (Photostyler, version 1.1A, Aldus Co., Seattle WA) at 150 dpi in 8-bit gray scale (0 = white, 255 = black) within four hours of testing. The mean image density for each loading was determined using an image analysis program (Image, version 1.6, NIH). A calibration table was made from the mean image

densities and experimentally applied pressure data for each range of film. Third order polynomial curves were fit to these data ($r^2 \geq 0.98$).

The pressure sensitive film coupons from the cylindrical indentation experiments were analyzed separately (by film range) by taking an image slice several pixels thick along the transverse axis of contact. Polynomial fits of each range of film were determined for a given experiment (Figure 1). For example, a polynomial was fit to the low range film over its usable range (2-10 MPa). Similar curves were made for the medium and high range films over their respective ranges. The contact width was determined by calculating the roots of the polynomial for a given range of film at the lower threshold of that film (Mathematica, version 3.0, Wolfram Research, Champagne IL). The mean contact pressure was determined for each range of film for a given experiment by integrating the respective polynomial and dividing by the contact width. For instance, the mean pressure predicted by the low range film was calculated as the area under its respective polynomial curve. The area was bounded at each end by the intersection of the curve with the lower boundary of the film (2 MPa). Finally, to incorporate data from all pressure ranges, a 'composite' curve was made by fitting a polynomial to the data points from all pressure ranges. For the composite curve, only the non-thresholded data points were used from the low and medium range films. The mean contact pressure was also determined for the composite curves.

Theoretical validation

A mathematical model of the cylindrical indentation was made as an independent comparison for the experimental data (Hale 1992). A plane strain contact model

consisting of a rigid indenter, film packet, and rigid plate was constructed using a commercial code (Abaqus, version 5.6-1) to predict the half-width contact pressures for each experiment. The film packet was assumed to be a homogeneous solid and was modeled using 80, 8-noded elements. The composite modulus of the packet, 22 MPa, was determined by matching the contact area of a 12 mm radius pilot experiment then iterating on the modulus to minimize the difference between the pressures predicted by the model and those in the experiment. Indentations with the remaining indenter radii were simulated by indenting the film packet layer until the contact width of the model matched that predicted by the composite film. Poisson's ratio was assumed to be zero as this parameter had a minimal influence on the predicted contact pressures. The difference in the half-width contact pressure profiles between the composite curves and the model were quantified by calculating the Chi-squared difference.

RESULTS

Correlation coefficients for the polynomial fits of the experimental data were typically high (mean $r^2 = 0.929 \pm 0.09$, Figure 1). In all cases the composite film exhibited the least error in mean contact pressure and peak pressure compared to the theoretical solution (Table 1). The mean pressure and peak pressure recorded with the composite film were within 5% and 6% of the theoretical, respectively. The high pressure film documented mean and peak pressures that were 38% and 10% greater than theoretical, respectively. Mean and peak pressures for medium film were less than the theoretical by 10% or less for all radii with the exception of 94.0 mm. For 94.0 mm radius indenter these errors were approximately 25% and 45%, respectively. The higher errors for low

and medium film for the 94.0 mm radius are a result of the higher applied pressure for this case. Mean and peak pressures for low film were less than theoretical by approximately 80% for all radii. The pressure distributions predicted by the theoretical model and those documented experimentally using composite film were visually consistent for all radii, as evidenced by the low chi-squared values (Table 1, Figure 2). The composite film typically predicted a contact half width within less than 10% of the low pressure film (Table 2). The medium pressure film typically underrepresented the contact half width predicted by the low film by 15% to 22%, and the high pressure film underrepresented this contact half width by 50% to 80%.

DISCUSSION

This study documented that several ranges of pressure sensitive film can be used to accurately transduce contact pressures and areas in load scenarios which produce: 1) contact pressure gradients, and 2) contact pressures which involve suprathreshold loading of a given film's pressure range. Such loading scenarios can occur during loading of articular joints. For example, contact in the patellofemoral or tibiofemoral joints involves two surfaces of varying curvature (i.e. the 'curved' femoral condyle contacting the flat tibial plateau). This results in peak contact pressures at the center of contact, and gradually reduces to zero pressure at the edge of contact (Hayes 1978). If the contact pressures extend beyond a given film's threshold limits, contact area and pressure data will be compromised. In such cases, pilot experiments should be conducted to determine the appropriate ranges of film needed to accurately transduce both contact area and pressure. Pilot studies also showed that the image produced on the film can be influenced by the

stacking arrangement and therefore the calibration of stacked pressure sensitive film should be performed in the desired stack sequence. Finally, due to the film's rate sensitivity (Haut, 1989), the film should be calibrated with a load pulse that approximates the anticipated experimental conditions for which the film will be used.

While the composite curves best agree with the theoretically predicted contact pressure distributions, small differences did exist, possibly due to our analysis technique. Polynomial fits of the data were used for analysis, instead of the raw data. This protocol was adopted to allow calculations to be performed (i.e. contact area, mean pressure) without the influence of local discontinuities in the raw data. Further, the correlation coefficients were typically high, suggesting that the polynomials adequately described the raw data. In addition, the theoretical curves were obtained by modeling the layered packet as a homogeneous body. It is possible that interactions between the film layers contributed to differences between the model and experiments, however these interactions were likely small given the fit of the model to the experimental data.

In the current study, data from all film ranges was used to produce a composite curve that closely approximated the theoretical peak and mean pressure, and contact pressure profile for a one-dimensional problem. The composite curve, because it contains pressure data from the low pressure film, provides an excellent measure of contact area. This method could also be applied to two-dimensional pressure data, such as that arising from contact between two articular surfaces. The pressure image from a given film range can be easily represented as a two-dimensional array of calibrated pressure data. The arrays from different film ranges chould then be added, cell by cell, to yield the composite

pressure distribution. Pertinent data can then be deduced from the composite array of data. The methods outlined here provide a new approach for accurate measures of contact area and pressure during dynamic loading of a diarthrodial joint.

ACKNOWLEDGMENTS

This study was supported by a grant (R49/CCR503607) from the Centers for Disease Control and Prevention. Its contents are solely the responsibility of the authors and do not necessarily represent the official views of the Centers for Disease Control and Prevention.

REFERENCES

1. a:Atkinson, P.J. and Haut, R.C. (1995). Subfracture Insult to the Human Cadaver Patellofemoral Joint Produces Occult Injury. Journal of Orthopaedic Research 13, 936-944.

2. b:Atkinson, P. and Haut, R. (1995). Insult to the human cadaver patellofemoral joint: effects of age on fracture tolerance and occult injury. 39th Stapp Car Crash Conference 281-294.

3. Atkinson, P.J. and Haut, R.C. (1997). A Method for Determining Regions of Diarthroidal Joint Contact During Dynamic Loading of the Human Knee. Proc. 44th Annual Meeting Orthopaedic Research Society 656.

4. Fukubayashi, T. and Kurosawa, H. (1980). The Contact Area and Pressure Distribution Pattern of the Knee. Acta Orthop. Scand. 51, 871-879.

5. Hale, J.E. and Brown, T.D. (1992). Contact stress gradient detection limits of pressensor film. J of Biomechanical Engineering 114, 352-358.

6. Haut, R. (1989). Contact Pressures in the Patello-femoral Joint during Impact Loading on the Human Flexed Knee. Journal of Orthopaedic Research 7, 272-280.

7. Haut, R., Ide, T. and DeCamp, C. (1995). Mechanical responses of the rabbit patello-femoral joint to blunt impact. Journal of Biomechanical Engineering

8. Hayes, W., Swenson, L. and Schurman, D. (1978). Axisymmetric finite element analysis of the lateral tibial plateau. Journal of Biomechanics 11, 21-33.

9. Li, X, Haut, R. and Altiero, N. (1995). An analytical model to study blunt impact response of the rabbit P-F joint. Journal of Biomechanical Engineering 117, 485-491.

10. Newberry, W.N., Garcia, J.J. and Haut, R.C. (1996). The effects of subfracture impact loading on the patellofemoral joint in a rabbit model. 40th Stapp Car Crash Conference SAE paper 962422, 149-159.

11. Newberry, W.N., Zukosky, D.K. and Haut, R.C. (1997). Subfracture insult to a knee joint causes alterations in the bone and in the functional stiffness of overlying cartilage. Journal of Orthopaedic Research 15, 450-455.

12. Thompson, R.C., Oegema, T.R., Lewis, J.L. and Wallace, L. (1991). Osteoarthritic changes after acute transarticular load. The Journal of Bone and Joint Surgery 73-A(7), 990-1001.

13. Vener, M., Thompson, R., Lewis, J. and Oegema, T. (1992). Subchondral Damage after acute transarticular loading: an in vitro model of joint injury. Journal of Orthopaedic Research 10, 759-765.

TABLES

Table 1. *Mean pressure (over the half-width contact) and peak pressures (presented in MPa as mean pressure / peak pressure) predicted by the theoretical model and documented from the composite, high, medium, and low pressure film data.*

Radius (mm)	Theoretical	Chi-squared fit*	Composite pressure film	High pressure film	Medium pressure film	Low pressure film
5.5	41.5 / 55.9	2.0	41.2 / 56.8	57.2 / 60.7	37.8 / 50.0	9.0 / 10.0
12.0	41.7 / 55.0	0.2	41.6 / 55.5	55.5 / 58.2	37.9 / 50.0	9.2 / 10.0
19.0	43.0 / 55.9	8.0	44.3 / 59.2	56.2 / 59.4	40.6 / 50.0	9.2 / 10.0
66.5	47.4 / 63.6	32.3	52.6 / 71.5	67.6 / 76.3	38.8 / 50.0	8.8 / 10.0
94.0	59.4 / 90.0	6.3	61.9 / 90.5	79.9 / 95.0	44.3 / 50.0	10.0 / 10.0

* Chi-squared fit: This represents a normalized measure of the summed difference between the theoretical and composite film data.

Table 2. *Contact half-width (mm) predicted by the theoretical model and documented by low, medium, and high pressure film data.*

Radius (mm)	Composite pressure film	High pressure film	Medium pressure film	Low pressure film
5.5	0.82	0.24	0.75	0.88
12.0	0.82	0.19	0.72	0.92
19.0	0.72	0.28	0.65	0.80
66.5	1.42	0.46	1.30	1.41
94.0	3.94	2.26	3.76	4.26

FIGURES

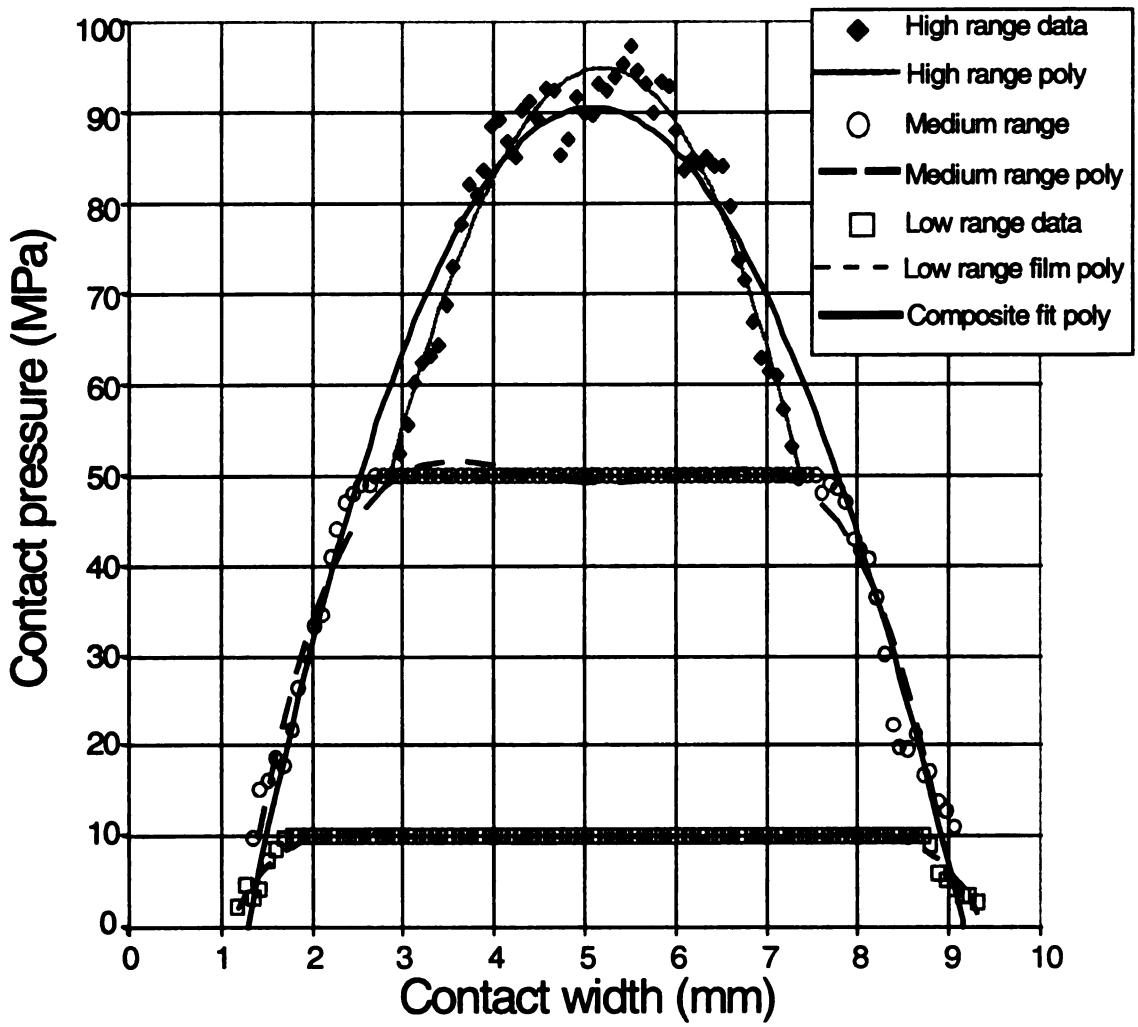

Figure 1. Plot of the calibrated pressure film data and the corresponding polynomial fits (poly) used for data analysis. Contact half-width, mean and peak pressures were calculated individually for the three ranges of film (low, medium and high) and for the composite fit.

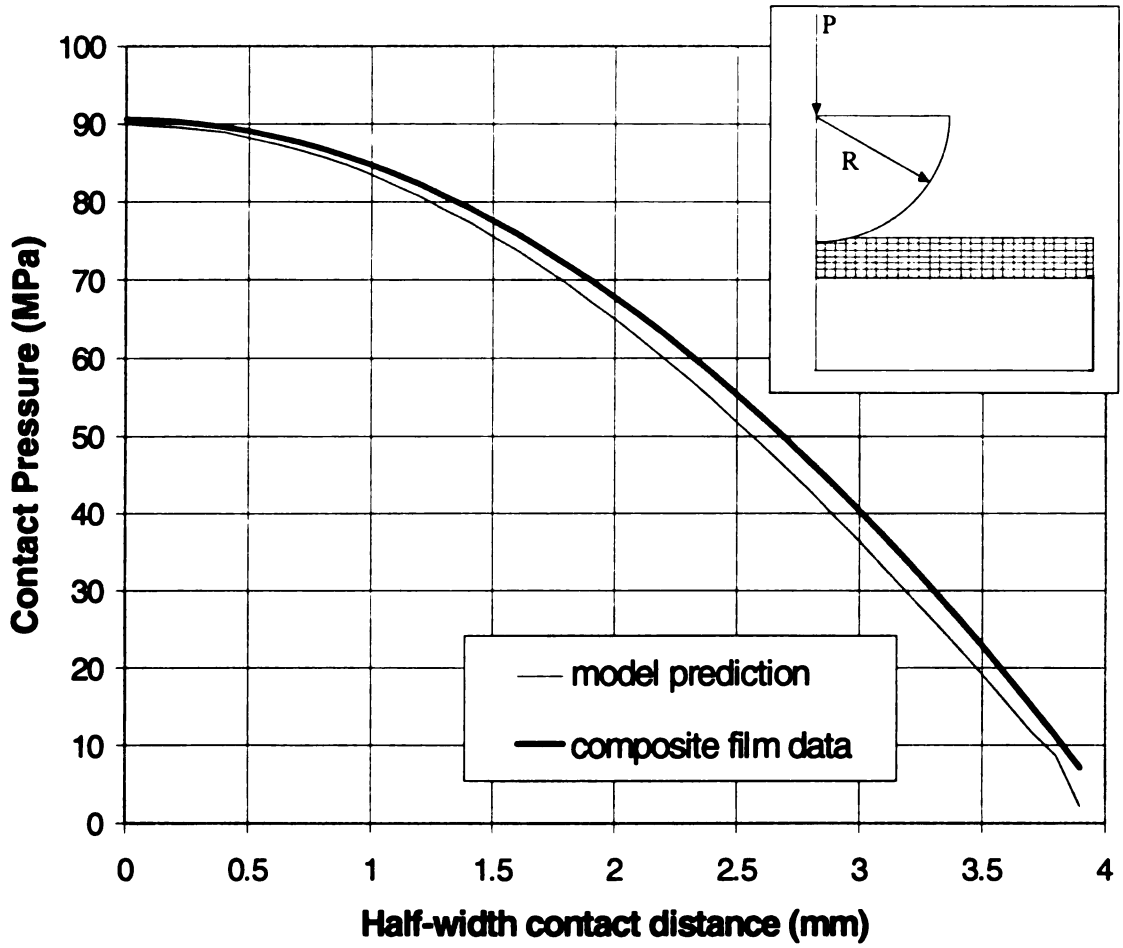

Figure 2. Plot of the half-width contact pressure profile (r = 94 mm) from the composite polynomial fit of the experimental data and the profile predicted by the mathematical model. The film packet was compressed between a cylindrical indenter and a flat plate in the mathematical model (inset).

CHAPTER 3

A METHOD FOR DETERMINING REGIONS OF DIARTHRODIAL JOINT CONTACT DURING DYNAMIC LOADING OF THE HUMAN KNEE

Atkinson PJ, Haut RC
Department of Materials Science and Mechanics
Michigan State University, East Lansing, MI

ABSTRACT

Areas of joint contact are necessary to understand joint pathologies and joint mechanics. In this study a method is described for contact area measurement from dynamic loading.

INTRODUCTION

Accurate determination of diarthrodial joint contact is necessary for theoretical modeling of joint contact mechanics. Stresses on articular cartilage and bone arise from both static and dynamic loading. Accurate predictions of these stresses can aid in the understanding of tissue modeling and remodeling, and the development of stress based damage criteria for cartilage and bone. For example, recent studies propose stress based criteria for diarthrodial joints to explain how high levels of stress in bone and cartilage may cause osteoarthrosis (Atkinson 1995, Donohue 1983, Ateshian 1994) and chondromalacia patellae (Goodfellow 1976, Minns 1979). A number of methods have been employed to determine joint contact area under static loading (Ateshian 1994, Huberti 1984). Pressure

sensitive film has been shown suitable for use during dynamic loading of joints to quantify both contact pressure and area (Atkinson 1995, Vener 1992). However, because the film is designed to function within certain pressure ranges, joint contact area at pressures less than the film's minimum pressure threshold is not recorded. Further, it is unknown where contact occurs on the articular surfaces. In this study, we investigated the effectiveness of biological stains in producing a permanent record of dynamic joint contact. Water soluble stains were eliminated as they could not differentiate contact areas in the hydrated joint. The ideal stain would be sensitive to low contact pressures and react to loads over short time durations.

METHODS

Sudan Black adipose stain was selected for this study after pilot investigations on numerous other biological stains. A packet was prepared using medium Fuji pressensor film (10-50 MPa, dynamically) encased in thin polyethylene film (Figure 1). Double sided tape affixed to the outside of the packet acted as the Sudan stain carrier. The technique was evaluated during blunt insult experiments on the 90° flexed human knee joint (Atkinson 1995). The packet was inserted into the patellofemoral joint of 5 human cadavers with grossly healthy articular surfaces. The joints were impacted (Figure 2) with a free flight inertial mass of 4.5 kg at an average energy of 27J. After insult the articular surfaces were irrigated and photographed. The stained contact area was manually outlined on a thin plastic sheet. The contact areas from the pressure film and plastic sheet were measured using a previously documented computerized technique (Atkinson 1995).

RESULTS

The blunt insults on the human knee generated average contact loads of 5 kN in 7 ms. No bone fractures were generated in 4/5 experiments. The images of the contact areas generated by the stain after irrigation had the same general shape as the contact area recorded by the film. The stained area on the articular surface, however, was 12% larger (Table 1) on average. The stained area on the patellar and femoral surfaces were visually consistent (Figure 3). The variations in contact area between the stain and film methods were small within specimens, but there were large variations between specimens.

DISCUSSION

We present a simple, quick, inexpensive, noninvasive technique for measurement of contact areas in diarthrodial joints during impact loading. Sudan stain on a film packet records articular joint contact in the same regions where the film records contact pressure. The larger contact area produced by the stain suggests it reacts at pressures less than the minimum threshold of the film (10 MPa). This suggests the stain yields a more accurate contact area in addition to being able to locate contact area on articular surfaces. Comparisons of this method with others will be difficult during dynamic loads because of the biphasic nature of cartilage. A 'low pressure' film (2.5-10 MPa) would have yielded more accurate contact area, however, the film would be saturated by pressures (15-20 MPa) resulting from dynamic loading of the human patellofemoral joint (Atkinson 1995). The Sudan or a similar stain could be used to provide important positioning information for 3-D analytical models or, in conjuction with the pressure film data, indicate the most appropriate orientation for 2-D analytical models. The marking also provides a means by

which areas of potential damage might be isolated for histologic analysis. In a clinical setting the method may assist those investigating the influence of flexion and Q-angle on knee joint contact areas for *in vitro* and possibly *in vivo* studies.

We hypothesize two possible mechanisms by which the Sudan technique may function. The Sudan stain may be loosely impacted into the superficial layer of the cartilage. Alternately, the Sudan stain may be reacting with small, freshly exposed areas of fat in areas of joint contact - in essence reacting in areas of very subtle damage. Therefore, this method may also highlight areas of existing damage to articular surfaces and play a role in advanced diagnosis of a chronic disease.

ACKNOWLEDGMENTS

Supported by the Centers for Disease Control and Prevention (R49/CCR503607).

REFERENCES

1. Atkinson P, Haut R (1995) Insult to the human cadaver patellofemoral joint: effects of age on fracture tolerance and occult injury. 39th Stapp Car Crash Conference 281-294

2. Donohue MJ, Buss D, Oegema T, Thompson R (1983) The Effects of Indirect Blunt Trauma on Adult Canine Articular Cartilage. The Journal of Bone and Joint Surgery 65-A(7): 948-957

3. Ateshian G, Kwak S, Soslowsky L, Mow, V (1994) A stereophotographic method for determining in situ contact areas in diarthrodial joints, and a comparison with other methods. Journal of Biomechanics 27(1): 111-124

4. Goodfellow J, Hungerford D, Woods C (1976) Patellofemoral joint mechanics and pathology: chondromalcia patellae. The Journal of Bone and Joint Surgery 58B(3):291-99

5. Minns RJ, Birnie AJM, Abernethy PJ (1979) A stress analysis of the patella, and how it relates to patellar articular cartilage lesions. Journal of Biomechanics 12: 699-711

6. Huberti H, Hayes W, Stone J, Shybut G (1984) Force ratios in the quadriceps tendon and ligamentum patellae. Journal of Orthopaedic Research 2: 49-54

7. Vener MJ, Thompson RC, Lewis JL, Oegema TR: Subchondral damage after acute transarticular loading: an in vitro model of joint injury. Journal of Orthopaedic Research 10:759-765, 1992

Table 1: *Human patellofemoral contact area (mm^2) data*

Specimen	Contact Area: Sudan Stain	Contact Area: Pressure Film
1	460	433
2	408	377
3	354	334
4	350	305
5	653	514

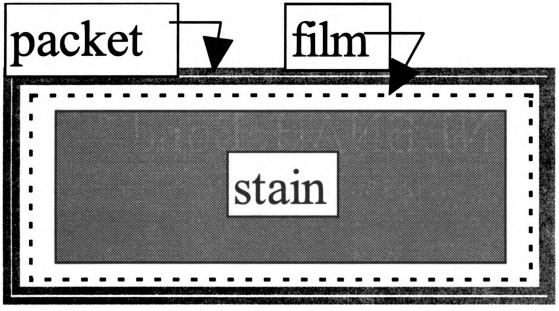

Figure 1: A schematic of the prepared film packet.

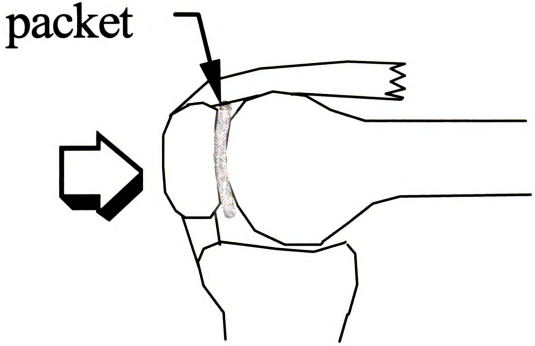

Figure 2: A side view of the knee showing placement of the film packet in the patellofemoral joint. The arrow points in the direction of the impact force.

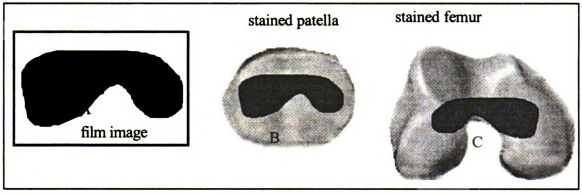

Figure 3: A typical imprint from the pressure sensitive film (A). The film image superposed on schematics of the patellar (B) and femoral (C) articular surfaces.

CHAPTER 4

SUBFRACTURE INSULT TO THE HUMAN CADAVER PATELLOFEMORAL JOINT PRODUCES OCCULT INJURY

Patrick J. Atkinson and Roger C. Haut
Department of Materials Science and Mechanics
Orthopaedic Biomechanics Laboratories
Michigan State University

ABSTRACT

The current criterion used by the automotive industry for lower extremity injury is based on visible bone fracture. Studies suggest, however, that chronic joint degeneration may occur after subfracture impact loads on the knee. We hypothesized that subfracture loading of the patellofemoral joint could result in previously undocumented microtrauma in areas of high contact pressure. In the current study, seven human cadaver patellofemoral joints were each impacted with successively greater energy until visible fracture was noted. Transverse and comminuted fractures of the patella were noted at 6.7 kN of load. Forty-five percent of that impact energy was then delivered to the contralateral joint. Subfracture loads of 5.2 kN resulted in no gross bone fracture in five of seven specimens. Histological examination of the patellae revealed occult trauma in four of seven subfracture specimens consisting of a horizontal split fracture in the subchondral bone, at the tidemark, or at the calcified cartilage-subchondral bone interface. The trauma appeared predominantly on the lateral facet, adjacent to, or directly beneath

preexisting fibrillation of the articular surface. Surface fibrillation was noted in histological sections of non-impacted control patellae, but occult damages were not observed. While the mechanism of this occult trauma is unknown, similar damage has been shown to occur from direct shear loading. Since these microcracks can potentiate a disease process in the joint, this study may suggest that the current injury criterion, based on bone fracture alone, is not sufficiently conservative.

INTRODUCTION

Traumatic injury is the third leading cause of death in the U.S., surpassed by heart disease and cancer, and motor vehicle injuries rank second to cancer in total societal cost (Rice 1989). While more recent statistics suggest a lowering of fatalities from motor vehicle accidents (likely due to the mandated use of seatbelts and airbags), more cases of less severe injury are being reported. A high frequency of lower extremity injuries, in particular, are showing up even with seat belt restrained drivers (Dischinger 1992). The currently accepted criterion for prediction of a lower extremity injury during a motor vehicle accident is based on bone fracture alone. The injury criterion for knee contact with the instrument panel is 10 kN, based on femur forces measured in an anthropomorphic dummy (Nyquist 1985). This criterion is based on knee contact forces from seated, human cadavers that cause fracture of the femur or a split fracture of the patella (Patrick 1965, Melvin 1975, Powell 1975).

An additional complication associated with lower extremity trauma is post-traumatic osteoarthrosis (States 1970). Clinical studies have long associated mechanical insult with the onset of disease (Davis 1989, Johnson-Nurse 1985, Kellgren 1958).

Animal studies have been conducted in order to establish a correlation between mechanical insult and the onset of a progressive disease. Donohue et al. (1983) reported changes in the zone of calcified cartilage of the canine patello-femoral joint two weeks after transarticular loading at 45% of the energy needed to cause visible fracture of bone. More recent canine studies report vertically oriented microfractures in calcified cartilage prior to bone fracture, without disruption of the articular surface (Donohue 1983, Thompson 1991, Vener 1992). These researchers suggest that changes in the calcified cartilage and underlying bone form the basis for development of a diseased state in the joint. The hypothesis is consistent with earlier studies of Radin and colleagues (1973) who theorize that microdamage and subsequent stiffening of the underlying subchondral bone results in abnormal stresses in the overlying cartilage, leading to a progressive degeneration of this soft tissue layer. Shimizu et al. (1993) studied the human tibial plateau and found degradation in the underlying bone preceding changes in the overlying cartilage. A recent clinical study of high energy knee injuries indicate changes in the subchondral bone detected by magnetic resonance imaging that were associated with "overt cartilage loss or defect in 48% of the patients evaluated 6 months after injury" (Vellet 1991).

Past studies on the mechanisms of human osteoarthrosis have attempted to identify which factors play a role in initiating joint degeneration. It has been suggested that microcracking at the cartilage-bone interface (Minns1979) in the human joint may be due to high shear stresses. A recent mathematical model of the impacted human patellofemoral joint indicates large shear stresses along the zone of calcified cartilage on the lateral patellar facet (Shelp 1994). A study on the impact response of human cartilage

biopsy samples to impact loading concluded that 25 MPa is a damage threshold of human cartilage (Repo 1977). However, pressures averaging of approximately 25 MPa in the human cadaver patellofemoral joint are only reached or exceeded at loads causing bone fracture (Haut 1989).

While clinical associations have been made between joint insult and subchondral bone damage, there are no experimental data documenting such occult types of injury from impact on the human knee. If the injury does exist prior to visible bone fracture, then the current lower extremity injury criterion may not be a conservative enough measure for the long term health of a diarthrodial joint under blunt insult.

The primary objectives of the current study was to conduct subfracture experiments on the flexed human knee joint and examine joint tissues for occult injury. Specifically, we hypothesized: 1) subfracture blunt insult to the human cadaver knee would produce microcracks in the calcified cartilage and/or subchondral bone; 2) subfracture contact loads would be less than 10 kN; and 3) that microfractures would occur at contact pressures less than 25 MPa.

METHODS AND MATERIALS

Blunt impact was delivered to isolated, flexed knee joints of seven human cadavers aged 46ñ9 years of age (1 female, 6 males). Tissue from an additional four specimens aged 40ñ22 years (seven total patellae), was used as histological controls (Table 1). Tissues were procured by the Tissue Bank (see Acknowledgment) from donors with no prior history of joint trauma and/or evidence of advanced joint pathology (areas of denuded bone, advanced chondromalacia, etc.). Shortly after death, the patellofemoral

joint was examined through a medial incision. Joint preparations were excised approximately 15 cm from the knee proper within 4 hours of death and stored at 4° C in 17mg/ml L-15 culture medium (Sigma Chemical, St. Louis, MO) with 85mg/ml Gentamicin Sulfate (Gibco/BRL, Gaithersburg,MD) for approximately 3 days prior to use in this study. Superficial tissues proximal to the femoral condyle were excised and the femoral shaft was cleaned with alcohol. The femur was potted in a cylindrical steel sleeve with room temperature curing epoxy, and was mounted to a rigid test frame (Haut 1989). Each specimen was maintained at a flexion angle of 90° prior to impact with a loosely knotted tether tied to the quadriceps tendon. The knot was such that minimal load was required to cause slippage, thus minimizing tensile loads in the tendon during impact. The patella was brushed with India ink and photographed prior to impact to document any baseline surface roughness or fibrillation.

A 4.5 kg impact mass was accelerated to a given pre-impact velocity, while aligned on two steel guide rails and supported on four nylon blocks to minimize friction. A 15.3 cm diameter, 6061-T6 aluminum impact interface was mounted to the front of a load transducer (Model 3173-2k, Lebow Products, Troy, MI, USA). While a rigid impact interface does not model the energy absorbing characteristics of an instrument panel, this surface provided baseline results that could be compared to previous studies (Haut 1989, Powell 1975). The impact mass was selected based on a previous study (Haut 1989). The resonant frequency of the load cell with the impact interface attached was 1333 Hz. Pilot studies indicated that the load transducer and attached mass would not resonate during impact on the human knee. Load data were recorded continuously on a personal

computer via a 16 bit A/D board (Model DAS 1600, Computer Boards, Inc., Mansfield, MA, USA). Load data were inertially compensated (Beckman 1969) and sampled at 10,000 Hz.. The impacting mass was accelerated to a predetermined velocity by adjusting pressure in a mass accelerator tank. Velocity of the mass was measured prior to impact on the knee using two infrared optical sensors (Part No. OR518-ND, Digi-Key Corporation, Thief River Falls, MN). These sensors are designed with a 5 mm separation between the emitter and detector. A tab connected to the impact mass crossed the 5 mm gap interrupting the first sensor and then the second. The individual sensors were separated by 76.2 mm to eliminate cross-talk. The test protocol consisted of sequentially increasing the velocity of the impact mass, so as to progressively increase the impact energy (3, 11, 22, 38, 61 J). The experiment was terminated when impact loading resulted in a visible fracture of bone. Damage was assessed by visual inspection through lateral and medial incisions in the joint, palpation and documented photographically. The contralateral limb of each specimen was impacted with 45% of the energy that caused bone fracture in the first limb.

A medium range (7-40 MPa) pressure sensitive film (Prescale, single sheet, Fuji Film, Ltd., Tokyo, Japan) was inserted into the joint prior to each impact through the medial and lateral incisions. The film was encased in two sheets of polyethylene film approximately 0.05 mm thick to prevent exposure to body fluids and help reduce shear loading artifacts (Huberti 1984). The strips of film were sufficiently long to pass through the patellofemoral joint and cover the anterior surface of the patella to measure the location and distribution of the contact load on the knee. This also minimized frictional

forces between the rigid impactor and the knee. Prior to impact, one mm diameter holes were drilled at the proximal and distal poles through the patella in an anterior to posterior direction. After impact, needle probes were inserted through the holes to pierce the film and help locate position of the film with respect to the patellar facets.

The pressure sensitive film was calibrated in a servohydraulic testing machine (Model 1330, Instron, Canton, MA, USA) using a previous methodology (Haut 1989). The film showed the highest sensitivity over the range of approximately 8 to 30 MPa (Haut 1991). Briefly, the film was encased in the polyethylene packet and loaded with a 100 ms load-controlled haversine pulse. The films were analyzed within one day using a video scanner (Model MSF-300Z, MicroTek International Incorporated, Hsinchu, Taiwan, ROC) with a sensitivity of 11.8 pixels per mm^2. The analysis of the exposed film was performed with Image 1.44 public domain software (National Institutes of Health, ftp Wayne@helix.nih.gov). The distribution of contact pressures and contact areas were determined within the patello-femoral joint. The image was divided to analyze the medial and lateral pressures and areas. A characteristic vertex present in most images corresponded to the median patellar ridge separating the image into medial and lateral facets (Figure 1). Technical difficulties during scanning the film from specimen H03 resulted in no pressure or area data from that specimen.

Following the mechanical test, or in the case of controls following harvest of the tissues, patellae were placed in 10% buffered formalin for approximately seven days. The tissue was decalcified in 20% formic acid for approximately 14 days. Due to the size of the human patella, only one 2-3 mm block was excised between the pin holes and used in this study (Figure 2). Blocks were cut medial to lateral across the entire patella. The

blocks were processed for routine paraffin embedding. Eight micron thick sections were cut (33), stained with Safranin O-Fast Green and examined in light microscopy at 12-400 power.

The experimental data resulting from analysis of the load-time curve and the pressure sensitive film were analyzed with a commercial statistics package (Excel 5.0, Microsoft Corporation, Redmond, WA) to calculate means and standard deviations. The peak contact load, average contact pressure, average medial pressure, average lateral pressure, contact area, time to reach peak load and contact duration (pulse) were the dependent variables. Both linear and second-order polynomial functions were used to identify the functional dependence of each dependent variable with impact energy. Correlation coefficients were computed for each fit.

RESULTS

A typical impact on the knee for the impacts leading to fracture resulted in a short period of low contact load followed by a sharp rise to a peak in 5.3ñ3.1 ms. The contact load declined gradually yielding a total contact duration of 16.1ñ6.2 ms. These data did not vary significantly with input energy. A second order polynomial was used to correlate peak contact force and pressure in successive impacts leading to fracture for impact energies of 3, 11, 22, 38 and 61 J. Peak contact force increased with increasing energy (r^2=.82) delivered to the knee (Figure 3). The average patellofemoral contact pressures increased with increasing energy (r^2=.85) delivered to the knee (Figure 4). The pressure over the lateral facet was consistently higher than on the medial facet, but no statistical differences were documented. Contact pressures were uniform (standard deviations less

than 2 MPa) over the facets (Figure 1). The lateral contact area was greater than the medial area.

At approximately 60±25 J of energy and a contact force of 6.7±2.1 kN visible failure of bone was noted (Table 2). Four specimens suffered transverse fractures of the patella, two specimens suffered comminuted fractures of the patella, and one had a significant disruption of articular cartilage and underlying bone. The average patellofemoral contact pressure and contact area was 15.5±1.6 MPa and 677±177 mm^2, respectively, in these fracture-producing experiments.

The average input energy for the subfracture experiments was 26ñ10 J, which was 43.4% of the energy for the fracture-producing group. This level of input energy resulted in a contact force of 5.2±2.1 kN (Table 2). Gross evaluation of the specimens revealed no visible bone fracture in five of seven cases. The average contact pressure and contact area were 11.8±5.5 MPa and 461±111 mm^2, respectively for the sub-fracture experiments.

Gross evaluation of the fracture and subfracture knee joints prior to testing revealed baseline pathology in the form of varying levels of chondromalacia in all patellae. This generally included local softening, mild surface roughness and surface fibrillation of the articular cartilage. No specimens exhibited denuded bone in the contact areas.

Analysis of the patellar histology from the subfracture experiments revealed occult injuries in four of seven patellae. The injury was visible at 12 power and was observed in the deep zones of the articular cartilage, the zones of calcified cartilage and the subchondral bone. The traumas were observed as horizontal (parallel to the articulating surface) occult cracks approximately one-third the width of the patella, located under the

lateral facet. The characteristic shape was that of an open slit. The cracks were identified as two types. The first type involved a split confined to the subchondral bone (Figure 5) and was observed in three specimens. The entire inner surfaces of the split were jagged. The surface of the crack involved a thin layer of subchondral bone still fully intact along the calcified cartilage. In two of these specimens the occult traumas occurred adjacent to areas of surface fibrillation (Figure 6). The fibrillation appeared as a rough, uneven surface across the articular cartilage. The second type of trauma, observed in one specimen, was a split at the subchondral bone and calcified cartilage interface. The edge of the crack along the calcified cartilage was smooth, while the other edge along the subchondral bone was jagged.

Analysis of histological slides from the fractured specimens also revealed occult trauma in four of seven patellae. The characteristic shape and size of these occult traumas were similar in shape and size to the traumas observed in the subfracture experiments. The cracks were again classified as two types. The first type involved, as in the subfracture experiments, cracks confined to the subchondral bone. This type of trauma was observed in two specimens. They were contralateral patellae from the subfracture group with the same occult trauma. One of these fractured specimens (H07) had an occult trauma adjacent to minor surface pathology. The other specimen (H08) suffered a transverse fracture of the patella contiguous with the pin hole used to locate the film. Each of these two specimens showed the same type of occult trauma in the contralateral patellae after subfracture loading. The second type of trauma involved a crack at the tidemark and was noted in the other two specimens. Both edges of this crack appeared

smooth. Occult traumas occurred directly beneath surface fibrillation for both specimens. One of these specimens (H03) had an occult split of the subchondral bone in the contralateral subfracture experiment. The other specimen did not appear to have an occult trauma in the contralateral subfracture experiment.

Because the occult fractures were observed after subfracture and fracture experiments on four specimens, we considered the possibility that these damages were not impact induced, but rather were pre-existent in the joint. To help ensure that these occult damages were experimentally induced, seven unimpacted patellae from four subjects were histologically processed. They were viewed in light microscopy at a range of powers similar to the impacted patellae. Although baseline pathologies existed in the form of articular surface fibrillation, multiplication of tidemark and loss of proteoglycan staining, no horizontal occult traumas were observed. The cartilage, calcified cartilage and subchondral bone appeared intact with no horizontal splits.

DISCUSSION

The primary objective of this study was to examine the human knee for occult trauma following blunt insult which did not produce visible fracture of bone. A second objective was a comparison of the peak fracture and subfracture contact loads with the bone fracture criterion of 10 kN. A final objective was to determine if microcracks occurred at contact pressures less than 25 MPa.

Our histological findings revealed horizontal, occult fractures involving the subchondral bone, calcified cartilage and articular cartilage at subfracture loads averaging 5.2 kN. This load was 22% less than that required to produce visible fracture of bone in

the contralateral limb. These subfracture loads were also 48% less than the current lower extremity injury criterion for new automobile certification using anthropomorphic dummies. The location of the occult traumas was predominantly on the lateral facet for pressures less than 25 MPa. To our knowledge, this is the only study to document controlled, experimentally induced, occult microcracks at the cartilage-bone interface in the human knee. Previous studies impacted the human cadaver knee with similar experimental methods, but microtrauma of the joint tissues was not investigated.

A limitation of the current study was the location of histological sectioning. Excision of the 3 mm block from the patella, between the pin holes, was the basis of a mathematical model predicting maximal interface shear stresses on the lateral facet (Shelp 1994). While this sectioning method resulted in the observation of occult traumas in four of seven cases in both fracture and subfracture experiments, other sections may have shown occult damage in the remaining 3 cases. In addition, it is unknown at which energy or contact load occult damages actually occurred during the fracture experiments. The study was also limited to a rigid interface condition. While this type of interface was used by Powell (1975), whose data largely serves as the basis for the current injury criterion, automotive occupants commonly interact with more deformable structures. During this more typical situation some portion of the contact load might be supported by structures surrounding the patella, such as the femoral condyles (Haut 1989). Furthermore, it is known that for more rigid impacts, femur loads in the current anthropomorphic dummy typically exceed those measured in a human cadaver under similar impact conditions (Hering 1977). Thus, while occult traumas have been reported in cadavers for loads less

than the current injury criterion, the direct applicability of these data to the automotive setting with anthropomorphic dummies needs further clarification.

Comparison of the peak contact loads at fracture with the bone fracture criterion reveals a difference of approximately 3 kN. Since this injury criterion was based on studies using seated cadavers, those impact loads also resulted in inertial acceleration of the specimen (Patrick 1965, Powell 1975, Melvin 1975). More energy is being used to actually deform tissues in the current isolated joint experiments. On the other hand, a previous study with older cadavers (72±11 years) utilized the same experimental setup as the current study, and reported a fracture load of 8.5±3.0 kN that often resulted in split fracture of the femoral condyles (Haut 1989). While no absolute explanation can be given for the lower fracture loads in the current study, one possible factor could be the influence of small pin holes inserted into the patella to help locate the pressure sensitive film. These holes may have produced stress concentrations and local weaknesses in the patella. Yet, in only one case was fracture actually contiguous with a pin hole. Another possible explanation may be related to the relatively good quality, thickness and overall distribution of articular cartilage in the patellofemoral joint of the younger specimens. Haut (1989) and most previous studies, use specimens 70 years and older. Though not documented in all studies, with this advance in age a high degree of joint pathology would be expected, possibly involving areas of denuded bone (Haut 1989). The absence of cartilage in the joint can result in the transmission of high loads to the femur yielding higher shear stresses in the femur to possibly cause split fractures of the condyles. Alternately, the presence of

a soft layer of cartilage in the young joint can yield high localized shear stresses in the patella that could yield more patellar fractures.

Tomatsu et al. (1992) recently reported horizontal split fractures comparable to the current study during shear loading of the porcine femoral condyle. The horizontal microcracks we observed closely resemble his IB and IIB injury classifications. That study suggests the location of trauma is dependent on the mass and velocity of the impactor. Tomatsu et al. conclude that high impact speeds and light masses tend to rupture the cartilage, resulting in open lesions. Low impact speeds and high masses more often generate occult damage in the underlying bone. As the speed is increased, combined injury to the bone and cartilage occurs. The higher speeds used in our fracture group also resulted in visible fractures of bone and gross disruption of the articular cartilage. It is possible the occult traumas recorded in the fractured specimens may have also been produced in one of the subfracture impacts at a lower velocity, and therefore, lower energy. The results of Tomatsu et al. suggest that the occult microfractures observed in the current study could be largely due to our use of a relatively large mass and a corresponding low velocity of impact. Since impact trauma during an automobile collision can occur at speeds of 30 mph or more, it may be questioned whether these occult traumas would be generated. Clinical studies of joints after high energy insult, however, have suggested the possible presence of microfractures at the tidemark or in subchondral bone (Vellet 1991).

While many of these microcracks were confined to the subchondral bone, we also observed cracks at the tidemark. Earlier studies investigating mechanisms of human

osteoarthrosis suggest microdamage at the interface between hyaline and calcified cartilage is due to excessive shear stresses (Meachim 1978, Minns 1979). Armstrong et al. (1985) suggested that a separation of cartilage and bone following high energy loading of the porcine patellofemoral joint is due to high shear stresses. A recent theoretical model studied the contact between two biphasic cartilage layers and shows that sudden loading results in high shear stress at the cartilage-bone interface (Ateshian 1994). Our recent mathematical analysis of the human patellofemoral joint also indicates high levels of shear stress are developed in bone underlying the lateral patellar facet during impact loading (Haut 1994). This being the most common area of occult microfracture suggests that excessive shear stresses may be the major factor causing impact injuries in the current study. Interestingly, our studies indicate that these occult microfractures occur under and adjacent to existing surface pathology. Since other studies indicate that bone seems to remodel before histological changes occur in the overlying cartilage (Radin 1973, Shimizu 1993), perhaps these specimens were predisposed to microcracks because of a weakened subchondral bone plate. On the other hand, a weakened and fibrillated layer of cartilage could also expose the underlying subchondral bone to localized areas of high shear stress during the blunt insult.

Repo and Finlay (1977) document visible damage to human articular cartilage and death of chondrocytes at 25 MPa of contact pressure. Impact studies on the canine report no damage to the surface tangential zone or calcified cartilage at pressures of 17 MPa (Chin 1986). Thompson (1991) suggests damage to the canine patellar articular surface occurs at pressures greater than 25 MPa. Vener et al. (1992) indicates 40 MPa is a

threshold pressure for damage in the canine phalangeal joint. In contrast, contact pressures of 15-17 MPa resulted in gross fracture of bone in the current study. The contrasting results from human and animal studies may be due to anatomical differences between joints, or possible differences in material properties of various joint tissues.

Fuji pressure sensitive film was used in the above mentioned studies and a number of others (Fukubayashi 1980, Haut 1989, Huberti 1984) to record intra-articular contact pressures. The accuracy of the film in transducing pressure gradients is recently reported to be 10 MPa/mm for the more commonly used dual layer type of film (Hale 1992). Since, pressures in the current study predominantly ranged from 9 to 22 MPa for the fracture and subfracture impacts, the film functioned in its most sensitive range. Dynamic calibration of the pressure-sensitive film has been performed in the rabbit knee by the product of contact pressure and patellofemoral contact area (Haut 1991). A similar calculation in the current study was difficult because the human patellar facets are more complex and largely inclined with respect to the line of the impacting force (Haut 1989).

Finally, recent studies have focused on identifying occult bone trauma and relating it to clinical findings. "Radiographically occult injuries to the bone, otherwise referred to as occult fractures, bone bruises, or microtrabecular trauma/fracture, may account for patient pain" (Kapelov 1993), perhaps by impeding venous drainage through extraosseous veins (Arnoldi 1991). Complaints of joint pain immediately following insult to a joint has been reported in approximately 88% of patients eventually progressing to osteoarthrosis (Chapchal 1978). Engebretsen et al. (1993) suggests injury to the anterior cruciate ligament often results in "bone bruises" that can be seen on MRI and provide a basis for

joint pain and a subsequent arthrosis. It is tempting to speculate that split fractures of subchondral bone might be associated with post-traumatic knee pain with a corresponding appearance of a "bone bruise" by MRI.

ACKNOWLEDGMENT

This study was supported by a grant (R49/CCR503607) from the Centers for Disease Control and Prevention. Its contents are solely the responsibility of the authors and do not necessarily represent the official views of the Centers for Disease Control and Prevention. The authors wish to gratefully acknowledge Ms. Jane Walsh for help in the interpretation of histological slides, Mr. Cliff Beckett for technical support, and Mr. Richard Dalimonte for his assistance with the experiments. We are also indebted to Mr. Rick Shumaker and the Michigan Tissue Bank for solicitation of donors and retrieval of joints.

REFERENCES

1. Armstrong C, Mow V, Wirth C: Biomechanics of impact-induced microdamage to articular cartilage: a possible genesis for chondromalacia patella. In: *Amer Acad of Orth Surg Symp on Sports Med,* ed by G Fenerman. pp70-84, 1985

2. Arnoldi C: Patellar Pain. *Acta Orthop Scand* 62:1-29, 1991

3. Ateshian GA, Lai WM, Zhu WB, Mow VC: An asymptotic solution for the contact of two biphasic cartilage layers. *J Biomechanics* 27(11):1347-1360, 1994

4. Beckman DC, Palmer MF: Thoracic force-deflection studies in primates. *Proc 3rd Biomech Factors Conf, ASME*, Ann Arbor, MI Paper 69-BHF-12:1969

5. Chapchal G: Posttraumatic osteoarthritis after injury of the knee and hip joint. *Reconstr Surg Trauma* 16:87-94, 1978

6. Chin M, Donohue J, Erdman A, Oegema T, Thompson R: Biomechanical analysis of an adult canine patella under an indirect blunt trauma. *Trans Orthop Res Soc* 11:232, 1986

7. Davis M, Ettinger W, Neuhaus J, Cho S, Hauck W: The association of knee injury and obesity with unilateral and bilateral osteoarthritis of the knee. *American J Epidem* 130(2):278-288, 1989

8. Dischinger P, Cushing B, Kerns T: Lower extremity fractures in motor vehicle collisions: influence of direction of impact and seatbelt use. *Proc 36th Conf AAAM* Portland, OR pp319-326, 1992

9. Donohue MJ, Buss D, Oegema T, Thompson R: The effects of indirect blunt trauma on adult canine articular cartilage. *J Bone Joint Surgery* 65-A(7):948-957, 1983

10. Engebretsen L, Arendt E, Fritts HM: Osteochondral lesions and cruciate ligament injuries. *Acta Orthop Scand* 64:434-436, 1993

11. Fukubayashi T, Kurosawa H: The contact area and pressure distribution pattern of the knee. *Acta Orthop Scand* 51:871-879, 1980

12. Hale JE, Brown TD: Contact stress gradient detection limits of pressensor film. *J Biomech Eng* 114:352-358, 1992

13. Haut R, Dalimonte R, Li X, Altiero N: Mechanical damage in the human P-F joint after blunt impact loading. *Proc Second World Conf Biomech* 2:297, 1994

14. Haut R: Contact pressures in the patello-femoral joint during impact loading on the human flexed knee. *J Orthop Res* 7:272-280, 1989

15. Haut RC, Ide TM, DeCamp CW: Impact-induced damage to articular cartilage of the patello-femoral joint. *First Injury Through Biomech Symp*13-26, 1991

16. Hering WE, Patrick LM: Response comparisons of the human cadaver knee and a part 572 dummy knee to impacts by crushable materials. *Twenty-First Stapp Car Crash Conf* 21:1015-1053, 1977

17. Huberti H, Hayes W: Patellofemoral contact pressure. *J Bone Joint Surg* 66-A(5):715-724, 1984

18. Johnson-Nurse C, Dandy D: Fracture-separation of articular cartilage in the adult knee. *J Bone Joint Surg* 67-B(10:42-43, 1985

19. Kapelov R, Teresi L, Bradley WG, Bucciarelli NR, Murakami DM, Mullin WJ, Jordan JE: Bone contusions of the knee; increased lesion detection with fast spin-echo MR imaging with spectroscope fat saturation. *Radiology* 901-904, 1993

20. Kellgren J, Lawrence J: Osteoarthritis and disk degeneration in the urban population. *Annals Rheum Diseases* 17:386-396, 1958

21. Meachim G, Bentley G: Horizontal splitting in patellar articular cartilage. *Arthr Rheum* 21:669-674, 1978

22. Melvin J, Stalnaker R, Alem N, Benson J, Mohan D: Impact response and tolerance of the lower extremities. *Nineteenth Stapp Car Crash Conf* 19:543-559, 1975

23. Minns R, Birnie A, Abernethy P: A stress analysis of the patella and how it relates to patellar articular cartilage lesions. *J Biomech* 12:699-711, 1979

24. Nyquist G, King A: Lower extremities. *Rev Biomech Impact Res Inj Auto Env* 6:163-201, 1985

25. Patrick L, Kroell C, Mertz H: Forces on the human body in simulated Crashes. *Ninth Stapp Car Crash Conf* 9:237-259, 1965

26. Powell W, Ojala S, Advani S, Martin R: Cadaver femur responses to longitudinal impacts. *Nineteenth Stapp Car Crash Conf* 19:561-579, 1975

27. Radin E, Parker H, Pugh J, Steinberg R, Paul I, Rose R: Response of joints to impact loading-III relationship between trabecular microfractures and cartilage degeneration. *J Biomech* 6:51-57, 1973

28. Repo R, Finlay J: Survival of articular cartilage after controlled impact. *J Bone Joint Surg* 59-A(8):1068-1076, 1977

29. Rice D, MacKenzie E, et al : *Cost of Injury in the United States: A Report to Congress 1989*. Atlanta, GA, 1989

30. Shelp D, Newberry W, Li X, Dalimonte R, DeCamp C, Altiero N, Haut R: Tissue damage resulting from blunt impact on the knee: animal and cadaver studies. *4th Inj Prevention Through Biomech Symp* 4:43-62, 1994

31. Shimizu M, Tsuji H, Matsui H, Katoh Y, Sano A: Morphometric analysis of subchondral bone of the tibial condyle in osteoarthrosis. *Clin Orthop* 229-239, 1993

32. States J: Traumatic arthritis--a medical and legal dilemma. *Ann Conf of the Amer Assoc for Automotive Med* 14:21-28, 1970

33. Sterchi DL, Eurell JC: A new method for preparation of undecalcified bone sections. *Stain Tech* 64:201-205, 1989

34. Thompson RC, Oegema TR, Lewis JL, Wallace L: Osteoarthritic changes after acute transarticular load. *J Bone Joint Surg* 73-A(7):990-1001, 1991

35. To
fractur

36. V
lesion
imagi

37. V
transa

TAB

Tab

35. Tomatsu T, Imai N, Takeuchi N, Takahashi K, Kimura N: Experimentally produced fractures of articular cartilage and bone. *J Bone Joint Surg* 3:457-461, 1992

36. Vellet AD, Marks PH, Fowler PJ, Munro TG: Occult post-traumatic osteochondral lesions of the knee: prevalence, classification, and short-term sequelae evaluated with MR imaging. *Radiology* 178(1):271-276, 1991

37. Vener MJ, Thompson RC, Lewis JL, Oegema TR: Subchondral damage after acute transarticular loading: an in vitro model of joint injury. *J Orthop Res* 10:759-765, 1992

TABLES

Table 1. *Donor profiles*

Specimen #	Sex	Age	Mass (kg)	Height (m)	Cause of Death
Test Specimens					
H02	F	39	79.5	1.6	colon cancer
H03	M	39	44.5	1.7	renal failure
H04	M	49	95.0	1.8	colon cancer
H05	M	52	81.8	1.8	myocardial infarction
H06	M	59	88.6	1.8	myocardial infarction
H07	M	42	75.0	1.8	myocardial infarction
H08	M	34	68.2	1.8	myocardial infarction
Control Specimens					
H13	F	27	71.3	1.7	suicide
H14	M	71	95.5	1.9	cardiac arrest
H15	M	42	-	-	-
H16	F	21	-	-	-

Table 2. *Fracture and subfracture producing experimental data.*

Spec.	Peak contact force (kN)	Impact Energy (J)	Average patello-femoral contact pressure (MPa)	Gross Visual Damage	Occult Trauma
Fracture producing experimental data.					
H02	4.9	24	12.4	Transverse fracture of the patella	No observable damage
H03	3.2	45	-	Comminuted fracture of the femur	Split at tidemark
H04	9.4	90	18.4	Gross disruption of cartilage	Split at tidemark
H05	7.7	64	15.2	Transverse fracture of the patella	No observable damage
H06	6.6	43	12.7	Transverse fracture of the patella	No observable damage
H07	8.1	92	19.4	Comminuted fracture of the patella	Split in subchondral bone
H08	6.8	65	21.3	Transverse fracture of the patella	Split in subchondral bone
Subfracture-producing experimental data.					
H02	3.9	10	9.4	Transverse fracture of patella	No observable damage
H03	4.8	31	-	Failure of lateral condyle	Split in subchondral bone
H04	4.8	30	9.7	No gross visual damage	No observable damage
H05	5.6	27	12.7	No gross visual damage	No observable damage
H06	3.4	18	4.4	No gross visual damage	Split at calcified cartilage/subchondral bone
H07	8.2	41	13.6	No gross visual damage	Split in subchondral bone
H08	5.7	27	20.8	No gross visual damage	Split in subchondral bone

FIGURES

Figure 1: Successive film imprints of the patellofemoral joint resulting from increasing load delivered across the joint. The final imprint coincides with a fracture of the patella. The arrow indicates a characteristic vertex which corresponded to the median ridge and was used to separate the imprint into median and lateral halves.

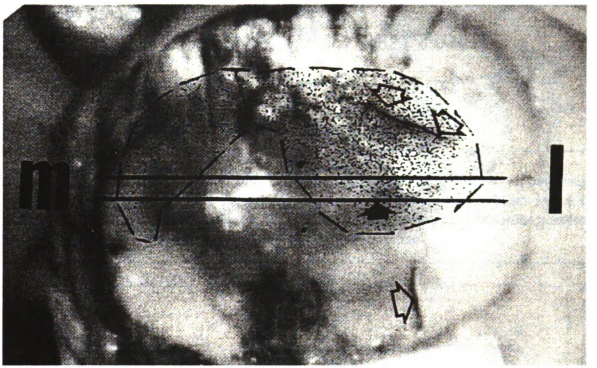

Figure 2: A fractured patella with the superimposed image of the pressure distribution as recorded by the pressure sensitive film (m=medial, l=lateral). The horizontal lines pass through areas of high pressure adjacent to the fracture and indicate where sections were taken for histology. The open arrows indicate two areas of impact induced trauma. The solid arrow indicates the location of an occult split in the subchondral bone. The two small dots represent the location of the 1 mm pin holes used for location of the pressure sensitive film.

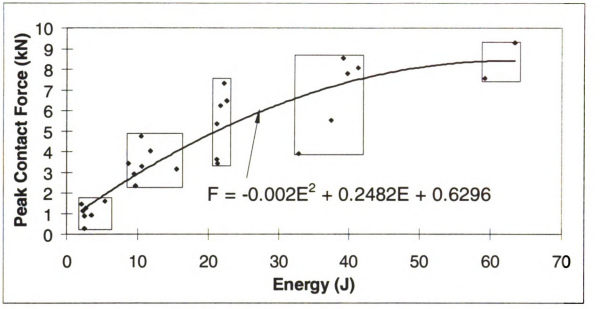

Figure 3: Experimental impact load data from successive impacts leading to an observed fracture of bone. Impacts were delivered at increasing energy levels; the boxes indicate the range of data for each energy level. Not all specimens required the entire impact series to fracture. The second-order polynomial fit of the data is shown.

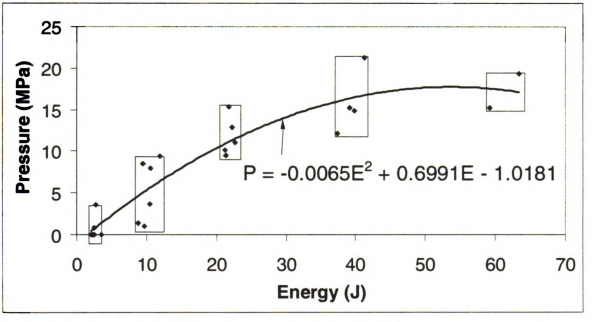

Figure 4: Experimental data from successive impacts leading to an observed fracture of bone. The pressure has been averaged over the patellofemoral contact area. Impacts were delivered at increasing energy levels; the boxes indicate the range of data for each energy level. Not all specimens required the entire impact series to fracture. The second-order polynomial fit of the data is shown.

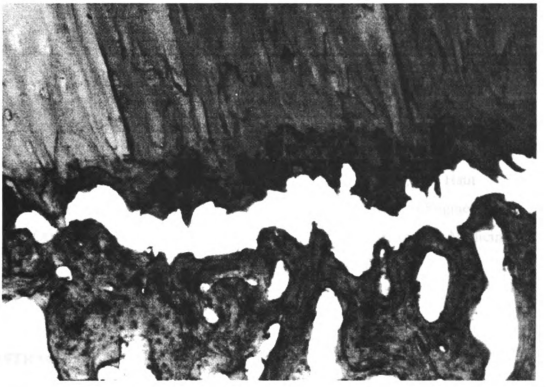

Figure 5: Transverse section of the patellae (hematoxylin and eosin 40X) showing a representative occult split fracture confined to the subchondral bone.

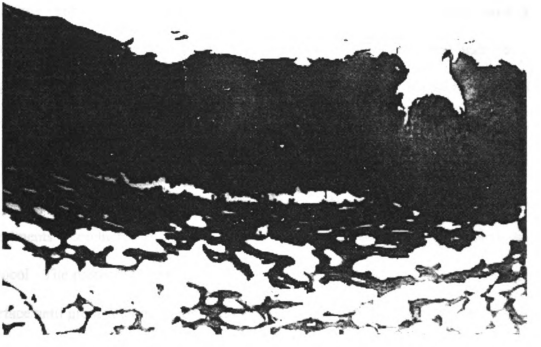

Figure 6: Transverse section (hematoxylin and eosin 25X) of the lateral patellar facet showing proximity of surface pathology (fibrillation) to an occult trauma.

CHAPTER 5

PATELLOFEMORAL JOINT FRACTURE LOAD PREDICTION USING PHYSICAL AND PATHOLOGICAL PARAMETERS

Patrick J. Atkinson, Charles M. Mackenzie* and Roger C. Haut
Department of Materials Science and Mechanics, College of Engineering,
Orthopaedic Biomechanics Laboratories, College of Osteopathic Medicine
*College of Veterinary Medicine
Michigan State University

ABSTRACT

Lower extremity (knee) injury prediction resulting from impact trauma is currently based on a bone fracture criterion derived from experiments on predominantly aged cadavers. Subsequent experimental and theoretical studies indicate that more aged, pathological specimens require higher, not lower, loads to initiate bone fracture. This suggests that a bone fracture criterion based solely on aged specimens may not be representative of the current driving population. In the current study, we sought to determine if cadaver age, physical size, sex, baseline joint pathology, or patellar geometry correlated with fracture load. An analysis was made of data from previous impact experiments conducted on fifteen isolated cadaver knees using a consistent impact protocol. The protocol consisted of sequentially increasing the impact energy with a rigid interface until gross fracture. Gross bone fractures occurred at loads of 6.9±2.0 kN (range 3.2 to 10.6 kN) using this protocol. Regression analyses revealed that fracture load was predicted by only one parameter: patellar geometry. Alternately, we developed a 2-D

mathematical model of the human knee to explore parameters that might influence the loads required to cause gross bone fracture. In support of our recent experimental studies using rigid and padded impact interfaces, the model suggested that load intensity and it's distribution over the knee play a role in defining the fracture load as well as the site (patella or femur) of patellofemoral joint injury.

INTRODUCTION

Numerous studies have described the in vivo and in vitro response of human and animal joints to impact loading. Such data are necessary to understand joint mechanics during dynamic loading and to establish injury criteria. In particular, whole human cadaver studies were conducted in the 1960's and 70's to establish a lower extremity injury criterion to address bone fracture injury sustained during loading through the knee in automotive accidents (Patrick 1965, Melvin 1975, Powell 1975). The average age of the specimens was 64 years, perhaps, due in part to the availability of the more aged subject and because these early studies hypothesized that the more aged cadaver would result in a more conservative benchmark for lower extremity injury. Indeed, Patrick, et al., note: "The fact that all of the subjects used exceeded fifty years of age and that all were embalmed should render the foregoing data somewhat conservative..." (Patrick 1965). However, more recent studies suggest that some aged cadavers require higher loads to cause bone fracture (Atkinson:a 1995, Haut 1989). Isolated knee joints from a group of 'aged' (72 yrs) versus 'young' (46 yrs) cadavers require 8.5 kN and 6.7 kN, respectively, to initiate gross bone fracture. In fact, the aged group typically suffered split femoral condylar fractures, while patellar fractures were more common in the younger specimens. The difference in injury modalities might be explained by the overall health of

the joints. The study involving aged cadavers documented advanced joint pathology in the test subjects involving areas of denuded bone. This likely resulted in increased stress transmission across the joint leading and may explain the femoral fractures (Atkinson:b 1995). The study involving the younger group of cadavers documented a complete and healthy distribution of cartilage in the patellofemoral joint. This scenario likely results in elevated stresses in the patella, and might explain the higher frequency of patellar fractures in younger cadavers. These differences suggest that age and/or the pathological state of the joint might influence fracture patterns in this isolated joint model, and that a criterion based solely on aged specimens may not be representative of the current driving population.

In the current study, an analysis of data was performed of blunt insult experiments on isolated human cadaver knees from a prior study. Additionally, specimen age, physical sizes, patellar geometry and degree of joint pathology on fracture load was investigated using regression methods. Because a previous study (Atkinson:a 1997) suggests that contact area and peak load might influence knee joint fracture, theoretical parametric analyses were performed on a finite element model of the patellofemoral joint in an effort to more completely understand parameters that may influence fracture of this joint.

METHODS AND MATERIALS

Statistical Regression Analyses

The current investigation was an analysis of a previous study (Atkinson:b 1995). In that study, blunt impacts were delivered to isolated, flexed knee joints of fifteen cadavers with the following physical characteristics: 12 males and 3 females aged 58.5±14.7 years old, weighing 78.6±21.9 kg and a height of 1.77±0.14 meters. The

specimens were procured by a tissue bank shortly after death from donors with no prior history of joint trauma and presenting a wide range of joint health: from no gross evidence of joint disease to advanced joint pathology, including areas of denuded bone, advanced chondromalacia, etc. The impact protocol has been previously described (Atkinson 1995, Haut 1989). Briefly, the patellofemoral joint was examined through a medial incision. Joint preparations were excised approximately 15 cm from the knee proper. The femur was potted in a cylindrical steel sleeve and attached to a rigid frame such that the long axis of the femur was oriented horizontally. Each specimen was maintained at a flexion angle of 90° prior to impact with a loosely knotted tether tied to the quadriceps tendon. A 4.9 kg impact mass was pneumatically accelerated to a given pre-impact velocity. A 15.3 cm diameter, 6061-T6 aluminum impact interface was mounted to the front of a load transducer (Model 3173-2k, Lebow Products, Troy, MI, USA) attached to the impact mass. The resonant frequency of the load cell with the impact interface attached was approximately 1300 Hz. Load data was inertially compensated (Atkinson 1997) and recorded on a personal computer via a 16 bit A/D board at a sampling frequency of 20 kHz (Model DAS 1600, Computer Boards, Inc., Mansfield, MA, USA). Velocity of the mass was measured prior to impact on the knee using two infrared optical sensors (Part No. OR518-ND, Digi-Key Corporation, Thief River Falls, MN). The test protocol, which has been in used in numerous studies by our laboratory (Atkinson:a 1995, Atkinson:b 1995, Haut 1989) consisted of sequentially increasing the velocity of the impact mass in 1 m/s increments starting at 1 m/s, so as to progressively increase the impact energy (2.5, 10, 22, 38, 61, 88 J). The experiment was terminated when impact loading resulted in a

visible fracture of bone. Damage was assessed by visual inspection through lateral and medial incisions in the joint, palpation and documented photographically.

Each subject's patellar geometry was also quantified on the unimpacted, contralateral knee using a previously described technique (Grelsamer 1994). Briefly, the length of the bone and articular cartilage surface were measured along a mid-sagittal plane (Figure 1). The ratio of bone to cartilage length (the morphology ratio) was then computed.

Parametric Study of Load and Contact Area

To investigate some of the potential effects of load intensity and distribution in determining stress states in various knee joint tissues, a parametric study was performed using a plane strain finite element model of the patellofemoral joint (Garcia 1997). The model (Figure 2) geometry was taken from a transverse slice taken through a 90 degree flexed human cadaver knee. Due to the short duration of impact loading in which there is insufficient time for fluid flow in the biphasic cartilage, the cartilage was considered to be an incompressible elastic isotropic material (Eberhardt 1990). A quasistatic analysis was adopted due to the negligible effect of tensile stress wave transmission through the knee joint for short duration loading (Anderson 1991). The articular cartilage, subchondral bone, and trabecular bone were modeled with isoparametric elements. Values for Young's modulus and Poisson's ratio were taken from the literature (Atkinson:b 1997, Mente 1994, Repo 1977, Townsend 1975): 20 MPa and 0.49 for cartilage, 3750 MPa and 0.30 for subchondral bone, and 300 MPa and 0.30 for trabecular bone.

Pilot studies determined that 45 MPa of pressure applied to the anterior of the patella was sufficient to reach referenced bone failure stresses in the human knee joint

(Garcia 1997). Areas of load contact on the patella were 25, 40, 55, 65, 75, and 80% of the available contact area for the patella in this study (Figure 2). The contact problem was solved assuming finite displacement and the iterative solutions were written to an output file for post-processing. These solutions were reviewed to determine which load step coincided with documented failure stresses of the subchondral plate and articular cartilage of the patella and femoral condyles (Garcia 1997). The failure stresses for the subchondral plate were taken to be 42 MPa and 78 MPa, respectively, in tension and shear. Both stresses were considered because injury may result from high levels of either stress (Atkinson:a 1997). Failure of the articular surface has been documented to be mediated most significantly by high levels shear stress (Atkinson:b 1997). Thus, articular cartilage failure was based on a shear stress of 6 MPa. The failure load in the plane of the model was calculated by integrating the applied boundary condition. To estimate the corresponding failure load on a whole knee, the calculated failure load from the 2-D model was multiplied by $\pi * a^2$ (a is the half-width of contact). This procedure was adopted because previous studies by our group have shown that blunt insult to the patella results in an approximately circular area of contact.

To quantify the health of patellar bone and cartilage histological sections were prepared. Following the mechanical test, the patellae were placed in 10% buffered formalin for approximately seven days and decalcified in 20% formic acid for approximately 28 days. One 2-3 mm block was cut medial to lateral across the entire patella in an area of high contact pressure adjacent to cartilage and bone trauma (Atkinson:a 1995)). The blocks were processed for routine paraffin embedding. Eight micron thick sections were cut and stained with Safranin-O and examined under light

microscopy. Patellar sections were scored in a randomized, blinded fashion by one of the authors (C.M.) using a modified Mankin scale (Mankin 1971). The cartilage was scored for: structure (possible score of 0-4), cellular appearance (0-6) and tidemark integrity (0-1) and was modified to include a three point pathological measure of the subchondral plate: 0=normal, 1=moderate changes, 2=advanced pathological changes. The total possible combined histopathological score was 13, where lower numbers indicate healthy tissue.

Subject age, sex, mass, height, histopathological score, fracture load and morphology ratio were analyzed using linear regression (SigmaStat, Jandel Corp., San Rafael CA) to identify correlations in the data. Specifically, fracture load, histopathological score and morphology ratio were first analyzed by conducting separate univariate regression analyses versus each remaining predictor variable (Table 2). Multiple linear regression analyses were conducted by using all possible combinations of the predictor variables in stepwise fashion to predict fracture load, histopathological score and morphology ratio. Subject age, mass, height, histopathological score, fracture load and morphology ratio data were then separated by sex and compared with the unpaired Student's t-test to determine if these data varied by sex. Statistical significance was set at $p \leq 0.05$.

RESULTS

Typical impacts causing fracture resulted in a short period of low contact load followed by a sharp rise to a peak in 5 ± 2.6 ms (Figure 3). The contact load declined gradually yielding a total contact duration of 12.2 ± 3.2 ms. All knee joints did not require the full series of impact energies to fracture. Peak contact force increased with increasing

energy delivered to the knee. Visible bone fracture occurred for a range of energies (24-92 J) and contact forces (3.2-10.6 kN) (Table 1). There were nine transverse fractures of the patella, two comminuted fractures of the patella, two distal femoral fractures, one significant disruption of articular cartilage, and one joint presented no gross visual damage.

Regression Statistics

The regression analyses of various subject parameters revealed two significant correlations using univariate regression and no significant correlations using multivariate models. First, the fracture load was statistically correlated with the morphology ratio (Table 2). As the morphology ratio decreased, the load required to cause gross fracture of bone significantly increased (Figure 1). Second, the patellar histopathological score significantly increased with increasing subject mass. The morphology ratio, however, was not predicted by any of the subject parameters. Analysis of the patellae revealed a median morphology ratio of 1.30 (range 1.17-1.38) and a median histopathological score of 5 (range 2-8).

Paramteric Study Findings

The theoretical parametric analysis revealed that increasing contact area increased the load tolerance of the patella and femur. For small contact areas (<40%) the shear and tensile failure stresses in the patella occurred before those in the femur. For larger contact areas, femoral fracture was the limiting criterion. Failure of the patellar or femoral cartilage due to large shear stresses occurred at higher loads than for bone fractures for the 90 degree flexed knee.

DISCUSSION

In this study we hypothesized that joint pathology and other physical parameters which describe impact test subjects would influence the load to cause fracture of bone from a blunt insult to the human knee. The study indicated that subject age, joint pathology score, sex, height and mass did not correlate with the impact load required to cause bone fracture in the isolated human knee using a rigid interface. Patellar geometry (the morphology ratio) was, however, found to be a predictor of fracture load. This suggested that joint geometry may play a significant role in determining fracture load.

It is important to note that the fracture load data presented in the current study was thought to be conservative, and may not reflect the realistic impact event for several reasons. Previous investigators (Patrick 1965, Melvin 1975, Powell 1975), directed impact missiles at the 90 degree flexed knee of seated cadavers using both single and sequential impact protocols. They documented fracture loads of approximately 10-17 kN, significantly higher than those of the current study. Firstly, the sequential impact protocol used in the current study was not ideal, as "this technique introduces the uncertainty of progressive predamage to the skeletal structure"(Powell 1975). Repeated impacts likely result in accumulated bone microdamage leading to a reduced load at gross fracture. Impact trauma at subfracture levels to the human knee is known to result in occult microcracking in the subchondral plate of the patella (Atkinson:a 1995, Atkinson:b 1997). These types of experimentally produced defects in the bone likely introduce stress concentrations which may reduce the load necessary to initiate a gross bone fracture. On the other hand, all specimens in this study were exposed to the same protocol. It seems reasonable to assume that the accumulation of microdamage in the bone would be

consistent across all specimens, or perhaps, even more pronounced in the more fragile specimens. Yet, age, pathology, etc. did not correlate with the final fracture load. A second reason for the lowered fracture loads in the study versus earlier studies using the whole cadaver was the use of isolated knee preparations. The impact loads in this case were generated by deformation of the joint tissues. In an automotive crash event, however, loads derived by contact with a knee bolster, for example, would be the result of tissue/knee bolster deformation, as well as inertial motion of the occupant. Another reason for the lower expected fracture loads in the current study was the use of a rigid impact interface. This allowed us to make more unambiguous comparisons to past studies. The earlier studies with rigid interfaces largely serve as the basis for the current injury criterion. Yet, automotive occupants commonly interact with more deformable structures, such as the instrument panel. This type of interaction may result in injury to the femoral condyles versus the patella, as described in the model analysis.

In this study we proposed the idea of a stress based injury criterion for the patellofemoral joint. Fundamentally, the state of stress in a body is due to three main parameters: geometry, material properties and boundary conditions. While the morphology ratio is admittedly a very simple measure of patellar geometry, it is a step towards quantifying the shape of the knee. Since the morphology ratio relies only on one lateral 2-D view, medial-lateral geometrical variations are not included. Yet, this simple anatomical ratio was found to significantly correlate with fracture load.

The material properties of the knee joint tissues from each cadaver was not quantified in the current study. This is a difficult problem due to their spatial variation

within subjects and the inherent variability between subjects. The latter may be due, in part, to confounding parameters not measured in this study, such as heredity, physical demands during life, etc.

Finally, the influence of the impact boundary conditions on the state of stress in the knee was studied with the 2-D human knee model. A uniform boundary condition of varying contact width was applied in an iterative fashion to identify injurious levels of stress in the patella and femur. Clearly, the shape of the curves is a direct result of our modeling protocol, and the curves might shift with variations in modeling protocol. For example, the failure stresses in the current study require additional study and further scrutiny as more experimental/theoretical data become available. Currently, the geometry is limited to a single knee at 90 degrees flexion with uniform loading. Different flexion angles will change the boundary conditions by altering patellofemoral contact and contact between the knee and impact interface. Further, a hyperbolic, versus a uniform load profile would concentrate load at the center of the contact area, potentially resulting in an altered stress state for a given contact area. It is possible then that contact area and load intensity might not be sufficient in accurately predicting tissue stresses. Knowledge of contact pressure gradients, such as if the occupant contacts the corner of a heater vent, glove box knob, etc., resulting in small areas of high contact pressure, would also be needed to assess the state of stress in the interior of the joint. We believe the model ultimately can have the utility to investigate different impact interfaces and load profiles, making it a valuable tool to predict stresses in the human knee. Ultimately, it will be necessary to adjust the injury curves to be relevant to the crash environment. This will

involve a transformation of the isolated human cadaver knee data to the current dummy knee, and then to the whole body setting in the crash environment. Simple methods, such as the use of pressure sensitive film on the dummy knee might be used to record the contact area and distribution of contact pressures over the dummy knee. These efforts represent a first step towards a more comprehensive injury criterion for the human knee.

ACKNOWLEDGMENTS

This study was supported by a grant (R49/CCR503607) from the Centers for Disease Control and Prevention. Its contents are solely the responsibility of the authors and do not necessarily represent the official views of the Centers for Disease Control and Prevention. The authors wish to gratefully acknowledge Ms. Jane Walsh and Mr. Marc Newmark for help in the histological slides, Mr. Cliff Beckett and Hasnin Ali for technical support and Mr. Rick Shumaker and the Michigan Tissue Bank for solicitation of donors and retrieval of joints.

REFERENCES

1. Anderson DD, Radin EL: Stress wave effects in a finite element analysis of an impulsively loaded articular joint. Journal of Engineering in Medicine 205:27, 1991

2. Atkinson PJ, Haut RC: Subfracture Insult to the Human Cadaver Patellofemoral Joint Produces Occult Injury. Journal of Orthopaedic Research 13:936, 1995

3. Atkinson P, Garcia J, Altiero N, Haut R: The influence of impact interface on human knee injury: implications for instrument panel design and the lower extremity injury criterion. 41st Stapp Car Crash Conference 167, 1997

4. Atkinson P, Haut R: Insult to the human cadaver patellofemoral joint: effects of age on fracture tolerance and occult injury. 39th Stapp Car Crash Conference 281, 1995

5. Atkinson T, Haut R, Altiero N: An investigation of failure criteria for impact induced fissuring of articular cartilage. Injury prevention through biomechanics symposium 85, 1997

6. Eberhardt AW, Keer LM, Lewis JL, Vithoontien V: An Analytical Model of Joint Contact. Journal of Biomechanical Engineering 112:407, 1990

7. Garcia J, Newberry W, Atkinson P, Haut R, Altiero N: Comparison of stresses in human and rabbit knees as they pertain to injuries observed during impact experiments. ASME Bioengineering conference 315, 1997

8. Grelsamer R, Proctor C, Bazos A: Evaluation of patellar shape in the sagittal plane: A clinical analysis. Amer J Sports Med 61, 1994

9. Haut R: Contact Pressures in the Patello-femoral Joint during Impact Loading on the Human Flexed Knee. Journal of Orthopaedic Research 7:272, 1989

10. Mankin H, Dorfman H, Lippiello L, Zarins A: Biochemical and Metabolic Abnormalities in Articular Cartilage from Osteo-arthritic human Hips. J of Bone and Joint Surgery 13:523, 1971

11. Melvin J, Stalnaker R, Alem N, Benson J, Mohan D: Impact Response and Tolerance of the Lower Extremities. Stapp Car Crash Conf 19:543, 1975

12. Mente P, Lewis J: Elastic modulus of calcified cartilage is and order of magnitude less than that of subchondral bone. Journal of Orthopaedic Research 12:637, 1994

13. Patrick L, Kroell C, Mertz H: Forces on the human body in simulated crashes. Stapp Car Crash Conf 237, 1965

14. Powell W, Ojala S, Advani S, Martin R: Cadaver Femur Responses to Longitudinal impacts. Stapp Car Crash Conf 19:561, 1975

15. Repo R, Finlay J: Survival of Articular Cartilage after Controlled Impact. The Journal of Bone and Joint Surgery 59-A(8):1068, 1977

16. Townsend P, Raux P, Rose R, Miegel R, Radin E: The Distribution and Anisotropy of the Stiffness of Cancellous Bone in the Human Patella. Journal of Biomechanics 8:363, 1975

TABLES

Table 1: *Impact and subject parameters*

Specimen	gross injury (fx=fracture)	impactor energy (J)	fx load (kN)	morphology ratio	histology score	sex	age	height (m)	mass (kg)
H02	Transverse fx of the patella	24	4.9	1.38	3.5	f	39	1.62	79.5
H03	Comminuted fx of the femur	45	3.2	1.32	5.5	m	39	1.74	44.5
H04	Gross disruption of cartilage	90	9.4	1.26	3.0	m	49	1.83	95.0
H05	Transverse fx of the patella	64	7.7	1.17	5.0	m	52	1.87	81.8
H06	Transverse fx of the patella	43	6.6	1.23	6.5	m	59	1.87	88.6
H07	Comminuted fx of the patella	92	8.1	1.26	4.5	m	42	1.83	75.0
H08	Transverse fx of the patella	65	6.9	1.22	3.0	m	34	1.87	68.2
H10	No gross visual damage	89	10.6	1.24	5.5	m	61	1.83	95.4
H18	Femur shaft fx	63	5.6	1.36	6.5	m	70	1.83	113.6
H20	Transverse fx of the patella	62	8.9	1.29	2.5	m	72	1.87	40.9
H21	Transverse fx of the patella	38	6.0	1.29	2.5	f	62	1.36	77.5
H23	Transverse fx of the patella	59	6.9	1.23	2.0	m	73	1.92	50.9
H25	Transverse fx of the patella	52	8.9	1.18	7.0	m	85	1.76	68.2
H26	Comminuted fx of patella	33	5.2	1.30	8.0	f	70	1.76	120.5
H27	Transverse fx of the patella	37	4.6	1.36	5.5	m	70	1.65	79.5

Table 2: *Linear regression results*

Predicted Variable	Predictor Variables	Univariate Linear Regression
1) Fracture Load	**1) Morphology ratio**	**1) p=0.012**
	2) Sex	2) p=0.153
	3) Height	3) p=0.208
	4) Age	4) p=0.476
	5) Histopathological score	5) p=0.505
	6) Mass	6) p=0.962
2) Histopathological Score	**1) Mass**	**1) p=0.030**
	2) Age	2) p=0.269
	3) Fracture load	3) p=0.505
	4) Height	4) p=0.523
	5) Morphology ratio	5) p=0.917
	6) Sex	6) p=0.974
3) Morphology Ratio	**1) Fracture load**	**1) p=0.041**
	2) Sex	2) p=0.192
	3) Height	3) p=0.275
	4) Mass	4) p=0.421
	5) Age	5) p=0.838
	6) Histopathological score	6) p=0.917

FIGURES

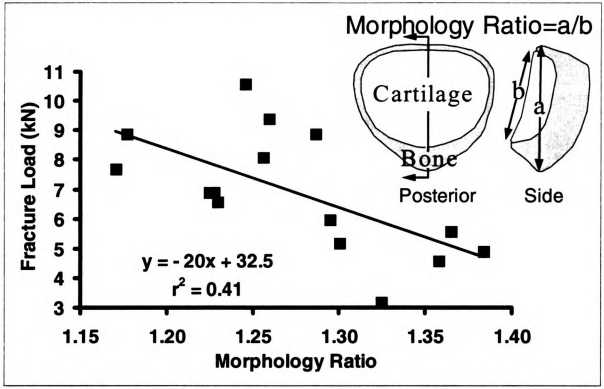

FIGURE 1: Fracture load significantly decreased with increasing morphology ratio. The morphology ratio is a measure of the proximal-distal patellar bone length on a mid-sagittal plane divided by the length of the articular surface.

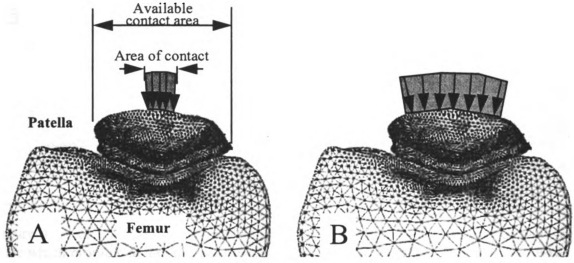

FIGURE 2: A 2-D contact model was developed from a transverse slice taken centrally through a typical cadaver knee flexed at 90 degrees. The influence of load intensity and contact area on injurious levels of stress was investigated by considering a range of contact areas (A: small area of contact, B: large area of contact). The tissue failure stresses are taken from Garcia, et al., 1997.

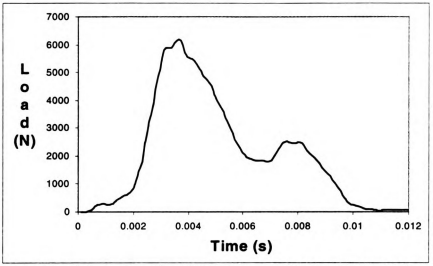

Figure 3: Typical load-time trace for blunt trauma to the isolated knee by a free flight inertial mass.

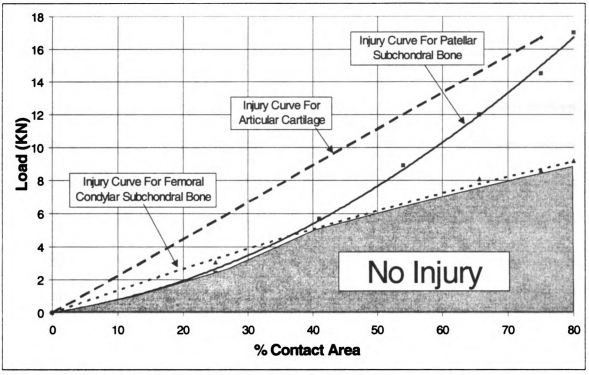

Figure 4: A plot of the combination of impact load intensity and contact area over the knee which produce failure levels of stress. Combinations of contact area and load which are below the curves would probably not result in injury. The horizontal axis is the area of contact divided by the total available contact area (see Figure 2). For small contact areas (<40%) the patellar bone is apparently more susceptible to injury, while the femoral condylar bone is more susceptible to injury with larger areas of contact. The patellofemoral articular cartilage does not appear to be the limiting injury factor for the range of contact areas and loads studied.

CHAPTER 6

THE INFLUENCE OF IMPACT INTERFACE ON HUMAN KNEE INJURY: IMPLICATIONS FOR INSTRUMENT PANEL DESIGN AND THE LOWER EXTREMITY INJURY CRITERION

Patrick J. Atkinson, Jose J. Garcia, Nicholas J. Altiero, Roger C. Haut
Department of Materials Science and Mechanics, College of Engineering
Orthopaedic Biomechanics Laboratories, College of Osteopathic Medicine
Michigan State University

ABSTRACT

Injury to the lower extremity during an automotive crash is a significant problem. While the introduction of safety features (i.e. seat belts, air bags) has significantly reduced fatalities, lower extremity injury now occurs more frequently, probably for a variety of reasons. Lower extremity trauma is currently based on a bone fracture criterion derived from human cadaver impact experiments. These impact experiments, conducted in the 1960's and 70's, typically used a rigid impact interface to deliver a blunt insult to the 90° flexed knee. The resulting criterion states that 10 kN is the maximum load allowed at the knee during an automotive crash when certifying new automobiles using anthropomorphic dummies. However, clinical studies suggest that subfracture loading can cause osteochondral microdamage which can progress to a chronic and debilitating joint disease. Additional studies suggest that the stiffness of the impact interface influences knee injury modalities resulting from impact loading. In the current study, a single impact at 27 J of

energy with a rigid interface was delivered to one knee of isolated joint preparations of six cadavers resulting in an average peak load of 5 kN. Contralateral knees were impacted with a padded interface at an additional level of energy at approximately the same load. All rigid impact experiments resulted in some form of injury to the patella including occult microcracking and gross fracture of the patella. No injuries were detected in the knees from the padded experiments. Math modeling of the patellae showed significantly reduced tensile and shear stresses in the bone with padding. This study suggests that the current lower extremity injury criterion, based solely on load, may not be sufficiently conservative. Increasing contact area over the knee reduces stresses in the bone and prevents both gross bone fracture and bone and cartilage microdamage. Such data may be useful in future instrument panel designs and might suggest revision to the current lower extremity injury criterion.

INTRODUCTION

Three extensive field studies conducted in 1977 examined the frequency of injuries associated with automotive accidents (Nagel 1977, Hartemann 1977, Bourret 1977). The studies found as many as 37% of automotive accident survivors sustained injuries involving the lower extremity (foot, knee, thigh or hip). Injury typically involved gross fracture of bone and the knee accounted for approximately a third of these injuries. This suggests that approximately one in ten automotive accidents resulted in knee injury two decades ago. Knee injury typically resulted from high speed contact with the instrument panel (Hartemann 1977, Bourret 1977). It was estimated in 1977 that 900,000 knee injuries associated with motor vehicle accidents occurred per year in the United States.

Severe injury to articular joints, such as those incurred to the knee during automotive accidents, are difficult to treat (Huelke 1982, Pattimore 1991, Hayashi 1996) and are implicated in chronic joint morbidity and pain (Nagel 1977, Radin 1972, Upadhyay 1983, Radin 1973, Radin 1978, Donohue 1983, Nyquist 1985, Thompson 1991, Vellet 1991, Gardner 1994, Volpin 1990, Chapchal 1978, Arnoldi 1991). In 1976 a federally regulated injury criterion (FMVSS 208) was adopted to address lower extremity injury. The criterion states that axial femoral loads cannot exceed 10 kN when certifying new automobiles with anthropomorphic dummies at a crash velocity of 13.4 m/s (30 mph). The criterion is based on a bone fracture threshold derived from human cadaver impact experiments (Patrick 1965, Melvin 1975, Powell 1975, Viano 1977, Viano 1980).

Analysis of more recent injury incidence studies conducted in the 1990's shows that the incidence of lower extremity injury has not decreased over the past twenty years and has, in fact, increased in some analyses (Pattimore 1991, Siegal 1993, Morgan 1991, Thomas 1995, Otte 1996). These results are attributed to the increased safety of automobiles following the mandated use of seat belts and the fleetwide phase-in of air bags into production vehicles from 1987-97. In 1995 it was documented that seat belts and air bags are 42% and 15% effective, respectively, in preventing fatal injuries (Lund 1995, Viano 1995). A decrease in the incidence of fatalities associated with severe crashes has resulted in a higher incidence of non-life threatening injuries, such as those involving the lower extremity. While seat belts and air bags are effective in protecting vital organs (Mackay 1995) from injurious impact with the windshield, steering wheel, etc., the lower extremity may be the sole site of unprotected contact between the occupant and the

automotive interior (Hartemann 1977, Bourret 1977, Pattimore 1990, Siegal 1993, Morgan 1991, Thomas 1995, Otte 1996, Mackay 1995, Crandall 1995). Currently, 4,800,000 injuries are attributed to automotive accidents each year (King 1995) and 500,000 injuries are serious enough to require hospitalization. Estimates of the current incidence rate of lower extremity injury are 30% (Morgan 1991), 37% (Pattimore 1991), 50% (Huelke 1982) and as high as 58% (Siegal 1993). This suggests between 150,000-300,000 lower extremity injuries per year require treatment. Eight per cent of the total treatment cost from motor vehicle accidents is due to the lower extremities (Malliaris 1982). In 1993, the overall cost associated with treating injured automotive occupants was approximately $55,000 per occurrence (Siegal 1993), suggesting that lower extremity injury may account for $2,200,000,000 annually.

In addition to gross, acute trauma, clinical studies suggest irreversible injury may occur in the absence of bone fracture (States 1986, MacKenzie 1988). Acute post-traumatic pain and a subsequent disease (osteoarthrosis or osteoarthritis, known as OA) are complications commonly associated with joint trauma (Nagel 1977, Radin 1972, Upadhyay 1983, Radin 1973, Radin 1978, Donohue 1983, Nyquist 1985, Thompson 1991, Vellet 1991, Gardner 1994, Volpin 1990, Chapchal 1978, Arnoldi 1991, States 1986). OA may account for a societal cost of $54,000,000,000 annually in both treatment costs and lost work days. OA affects cartilage and subchondral bone of articulating joints (Hamerman 1989). While the etiology of OA is not well understood, subfracture mechanical insult has long been associated with its development via controlled in vivo animal experiments (Radin 1972, Radin 1973, Radin 1978, Donohue 1983, Thomspon

1991). These studies suggest that bone microdamage, and its subsequent healing, causes sclerosis of the underlying subchondral bone inducing abnormally high stresses in the overlying cartilage. This leads to progressive cartilage degeneration and loss of this tissue.

Clinical and post-mortem studies have been conducted on the human in an effort to understand joint disease pathogenesis and progression. Shimizu et al. (1993) studied biopsy tissues from the human tibial plateau and found degradation in the underlying bone preceding changes in the overlying cartilage. A recent clinical study of high energy knee injuries indicates changes in the underlying subchondral bone as detected by magnetic resonance imaging (MRI). These injuries were associated with "overt cartilage loss or defect in 48% of the patients evaluated 6 months after injury" (Vellet 1991). "Radiographically occult injuries to the bone, otherwise referred to as occult fractures, bone bruises, or microtrabecular trauma/fracture, may account for patient pain" (Kapelov 1993), perhaps by impeding venous drainage through extraosseous veins (Arnoldi 1991). Additional clinical studies document a strong correlation between a history of joint trauma and the development of osteoarthritis (Davis 1989, Kellgren 1958). Indeed, complaints of joint pain immediately following insult to a joint has been reported in approximately 88% of patients eventually progressing to osteoarthrosis (Chapchal 1978). Additionally, Johnson-Nurse and Dandy (1985) document that 50% of osteoarthritic patients recall a traumatic injury to the diseased joint in years prior to the development of symptoms.

Recent studies by our laboratory have shown that occult microcracks can be produced near the cartilage-bone interface following blunt subfracture insult to the 90° flexed human knee (Atkinson:a 1995, Atkinson:b 1995). The microcracking is evident at

approximately 70% of the load required for gross fracture of bone in the knee. These microcracks may yield the so-called "bone bruises" in MR images. Because these injuries occur below the gross fracture tolerance of bone, the current criterion used in the automotive industry may not be sufficiently conservative to protect the long term health of the joint. Two-dimensional mathematical models of the human knee suggest that these occult microcracks may be the result of excessive shear stresses (Atkinson:b 1995). Parametric studies performed on these models indicate the distributions of stress in articular cartilage and bone depend on the input boundary loads and joint geometry (Hayashi 1996, Li 1995, Atkinson 1996, Newberry 1996). For example, distributing impact loads over a greater area (i.e. padded interface) might limit injury to bone and cartilage (Hayashi 1996). Theoretical models suggest shear stresses are reduced by more than 50% with a padded versus rigid impact interface (Hayashi 1996, Newberry 1996).

While the field investigation data presented above show lower extremity injury to be a significant problem, numerous experimental studies attempting to simulate contact between the knee and instrument panel, have also been undertaken in an effort to identify injury thresholds and mechanisms. The experimental studies are advantageous over field observations since tests can be conducted in a controlled, repeatable manner with the ability to obtain detailed data. Alternately, field observations are made after the incident has taken place. Assumptions must be made as to vehicle/occupant kinematics, contact points, etc. Therefore, to quantify what is already known, a retrospective analysis was conducted of four main experimental impact studies using whole cadavers (Patrick 1965, Melvin 1975, Powell 1975, Viano 1980). A total of 68 limbs were tested. Typically, the

cadaver was seated with the knee at 90° flexion and an impact missile of variable mass (10-50kg) was directed at the knee at various velocities (5-13.4 m/s). In 32 tests the impact missile was faced with a flat, rigid plate. In the remaining 36 tests, the plate was covered by pads of variable thickness and composition. The incidence of fracture to the patella, femoral condyles, femoral shaft, femoral neck and pelvis are shown in Table 1.

The majority of fracture injuries occur in the knee with the rigid interface in which the patella, femoral condyles or both suffered gross fracture. The localized distribution of load on the patella has been implicated in the high incidence of knee injuries with the rigid interface (Hayashi 1996, Powell 1975). The contact between the rigid impact interface and the bony anterior surface of the patella likely resulted in a very localized distribution of the impact load. The flesh thickness over the anterior patella is approximately 4.8 mm (Hering 1977), offering little protection to a rigid impact. Alternately, padding likely resulted in a distribution of the impact force over part or all of the patella and possibly the femoral condyles (Hayashi 1996). This resulted in a significant reduction of knee injuries. These studies suggest that the distribution of impact load over the knee is an important factor in injury prevention.

The lower extremity injury criterion currently utilized in the automotive industry (FMVSS 208) is based, in part, on experimental studies using a rigid interface. This suggests that the criterion is a somewhat conservative predictor of lower extremity injury since typical instrument panels are not rigid, thus offering some degree of protection by distributing impact load over the knee. However, as mentioned above, recent field reports document that lower extremity injury persists at or above past incidence rates, probably

for a variety of reasons. While increasing the amount of contact area over the anterior surface of the knee decreases the incidence of injury, the criterion is based solely on peak impact force and does not take into account how the force is distributed. Currently, it is not possible to quantify the contact area required to prevent injury at loads less than 10 kN, based on an analysis of the whole cadaver experiments cited above, due to the following:

1) While load data was measured in all of the past studies, the contact area over the knee was not measured (i.e. with pressure sensitive film, etc.).

2) Intrastudy comparisons/contrasts of specific data may not be valid due to variations in protocol (i.e. impact energy, pre-impact cadaver positioning).

3) Between-subject comparisons may not be valid due to the large variability documented in fracture load and energy with cadaver age, height and sex (Powell 1975.

4) Between-subject comparisons may not be valid due to anthropometric variations of the anterior surface of the knee (size variations of 20% in a random sample of knees) (Hering 1977).

Anterior knee surface geometry is of particular interest because the contact of the impact interface with this anatomy influences, in large part, the distribution of load over the knee. For example, scaled shape differences can lead to larger or smaller contact areas, whereas, local anatomical incongruities could lead to load distribution gradients in the area of contact. Intersubject articular joint geometrical variation may be due to a variety of effects including age, sex, height, weight and heredity (Grelsamer 1994). In general, joint geometry probably reflects the demands placed on the joint during normal

activities such as ambulation, rising from a chair, etc. Patellar geometry is a significant predictor of anterior knee pain (Grelsamer 1994) and may indicate a predisposition to early joint pathology which may influence knee joint injury mechanisms (Atkinson:b 1995).

The objective of the current study is to investigate the relationship between load and contact area while addressing the concerns noted above. The goal was to investigate how different distributions of a given load would affect impact biomechanics and macro/micro injuries to the knee. Therefore, paired experiments were conducted on human cadaver knees with rigid and padded interfaces at consistent 'within subject' impact loads. Each patella was theoretically modeled to investigate whether the state of stress in the bone and cartilage correlated with injury. A geometrical measure was also made of each patella to investigate how individual joint geometry may have affected the theoretical and experimental results. Subsequent gross and histological examinations were conducted and injury to bone and cartilage were documented.

METHODS AND MATERIALS

Experimental Methods

Impact experiments were conducted on six pairs of isolated human knee joints (65±12 years). The sample size was selected following a confidence interval analysis to determine how many subjects would be required to yield sufficient statistical power. The premortem age of the subjects was not of particular interest for the specific type of testing performed in the current study. While other studies have documented age effects in the properties of joint tissues, a previous study showed that cadaver age is not a significant

predictor of impact biomechanics or injury (gross or microdamage) to the human knee (Atkinson:b 1995). Advanced joint pathology, however, may affect joint injury and impact biomechanics. Therefore, gross joint inspection was used to select the sample pool of test subjects. Tissues were procured by the Tissue Bank (see Acknowledgment) from donors with no prior history of joint trauma and/or evidence of advanced joint pathology (areas of denuded bone, advanced chondromalacia, etc.). Shortly after death, the patellofemoral joint was examined through a medial incision. Joint preparations were excised approximately 15 cm from the knee proper within 4 hours of death and stored at -20° C until the day of testing. Superficial tissues proximal to the femoral condyle were excised and the femoral shaft was cleaned with alcohol. The femur was potted in a cylindrical steel sleeve with room temperature curing epoxy, and was mounted to a rigid test frame (Haut 1989). Each specimen was maintained at a flexion angle of 90° prior to impact with a loosely knotted tether tied to the quadriceps tendon. The knot was such that minimal load was required to cause slippage, thus minimizing tensile loads in the tendon during impact. One knee from each subject was impacted once (see below for details) with a rigid interface at an impact energy of 27 J. This energy was selected following a logistical regression analysis of a previous experimental study involving twenty human cadavers (Atkinson:b 1995). The analysis suggested that 27 J of energy would provide the greatest chance of producing an occult trauma while accepting a 50% chance of gross bone fracture (Figure 1).

Following the rigid interface experiment on one knee of each subject, the contralateral knee was impacted once with a padded interface (Hexcel, 1.35 MPa crush

strength) at an energy which resulted in approximately the same load. A greater impact energy was required to achieve the same load as in the rigid interface experiments, due to the deformable characteristics of the padding. Pilot impact experiments were conducted on a knee analog to determine the relationship between energy and peak contact load for the rigid and padded interfaces. The knee analog was constructed from a short length of 10 cm x 10 cm wood block covered by a 6.4 mm thick rubber sheet (Figure 2). Experiments with a rigid and padded interface using a 4.8 kg mass were conducted at a range of velocities. This data was crossplotted to eliminate the influence of the knee analog and to develop a functional relationship between the padded and rigid interface. The increased impact energy required for padded interface experiments to yield the same load as rigid experiments could then be determined (Figure 3).

The data is presented as a so-called 'energy multiplier' plotted versus the rigid interface peak impact load. While the impact energy was consistent for all rigid interface experiments, the impact load was variable for all cadavers. Therefore, following the rigid experiment for each cadaver, the increased energy required to produce the same peak load with the padded interface was determined by looking up the energy multiplier (Figure 3). The rigid impact energy (27 J) was then multiplied by this factor and the contralateral knee was impacted with the padded interface at that energy.

Impact was delivered to the knees via a 4.8 kg missile accelerated to the pre-impact velocity required for each experiment. The missile was aligned on two steel guide rails and supported on four nylon blocks to minimize friction. A 7.5 x 8 cm, 6061-T6 aluminum impact interface was mounted to the front of a load transducer (Model 3173-2k,

Lebow Products, Troy, MI, USA). The impact mass was selected based on a previous study (Haut 1989). The resonant frequency of the load cell with the impact interface attached was 1333 Hz. Pilot studies indicated that the load transducer and attached mass would not resonate during impact on the human knee. Load data was recorded continuously on a personal computer via a 16 bit A/D board (Model DAS 1600, Computer Boards, Inc., Mansfield, MA, USA). Load data were inertially compensated (Atkinson 1995) and sampled at 20,000 Hz. The velocity of the mass was measured prior to impact on the knee using two infrared optical sensors (Part No. OR518-ND, Digi-Key Corporation, Thief River Falls, MN). These sensors were designed with a 5 mm separation between the emitter and detector. A tab connected to the impact mass crossed the 5 mm gap interrupting the first sensor and then the second. The individual sensors were separated by 76.2 mm to eliminate cross-talk.

A medium range (7-40 MPa) pressure sensitive film (Prescale, single sheet, Fuji Film, Ltd., Tokyo, Japan) was inserted into the joint prior to each impact through medial and lateral incisions of sufficient size to allow the film to pass through. The film was encased in two sheets of polyethylene film approximately 0.05 mm thick to prevent exposure to body fluids and help reduce shear loading artifacts (Huberti 1984). The strips of film were sufficiently long to pass through the patellofemoral joint and cover the anterior surface of the patella to measure the location and distribution of the contact pressure in the patellofemoral joint and at the impactor-anterior patella interface. This also minimized frictional forces between the impactor and the knee. A method for indicating regions of articular cartilage contact suitable for impact loading was also

employed (Atkinson 1997). This method semipermanently colors the area of intraarticular contact and allows documentation of the contact area to aid in locating the contact pressure boundary condition for math modeling.

The pressure sensitive film was calibrated in a servohydraulic testing machine (Model 1330, Instron, Canton, MA, USA) using a previous methodology (Haut 1989). The film showed the highest sensitivity over the range of approximately 8 to 30 MPa. Briefly, the film was encased in the polyethylene packet and loaded with a 40 ms time to peak load-controlled haversine pulse. The films were analyzed within one day using a video scanner (Model MSF-300Z, MicroTek International Incorporated, Hsinchu, Taiwan, ROC) at 150 dpi. . The average pressure over that length was determined using the public domain NIH image program, version 1.6 (developed at the U.S. National Institutes of Health and available on the internet at http://rsb.info.nih.gov/nih-image/). The distribution of contact pressures and contact areas were determined within the patellofemoral joint.

Following the mechanical test the patellar geometry was quantified using the method of Grelsamer, et al. (1994), in which the so-called 'morphology ratio' is determined. The ratio is the quotient of the mid-sagittal length of the patellar bone divided by the sagittal length of the articular surface ('a' and 'b', respectively, in figure 4). The morphology ratios were used to categorize each patella into one of three categories: Type I patellae, $1.2 \leq a/b \leq 1.5$; Type II patellae, $a/b > 1.5$, Type III patellae, $a/b < 1.2$. Type I patellae are typical of 94% of the population (Grelsamer 1994).

The patellae were placed in 10% buffered formalin for 10-14 days. The tissue was decalcified in 20% formic acid. Each patella was transected into three to five 2-3 mm

sample blocks, processed for routine paraffin embedding, slab-cut and stained with Safranin O-Fast Green. All sections were examined in light microscopy at 12-400 power and photographed.

The experimental data resulting from analysis of the load-time curve and the pressure sensitive film were tabulated and statistically analyzed. The time to peak load, contact duration, peak contact load, average anterior patella contact pressure and area, average patellofemoral contact pressure and patellofemoral contact area data from rigid interface and padded interface experiments were compared with paired t-tests (Sigmastat). A regression analysis was conducted to determine the influence of cadaver age, sex, height, weight and patellar geometry on peak load, average anterior patella contact pressure and area and average patellofemoral contact pressure and patellofemoral contact area.

Theoretical Modeling

The cartilage, trabecular and cortical bone geometry of the patellae from all rigid and padded interface experiments were digitized into a commercial CAD software (AutoCAD, version 12) (Figures 5,6). The geometry was taken from a transverse plane in the area of highest patellofemoral contact pressure (Atkinson:b 1995). Twelve 2-D mathematical models (ANSYS, version 5.3) were developed to analyze each patella along that plane. The patella was meshed with 8 node elements and elastic isotropic behavior was assumed for the analysis with the material properties in Table 2. The assumption of elastic behavior is based on the work of Eberhardt, et al (1991). Cartilage and, to a lesser extent bone, are commonly considered viscoleastic and are typically modeled with a rate

dependent, biphasic analysis (Setton 1990, Mow 1984). However, impact loading (<200ms) results in negligible differences between the linear elastic and biphasic analyses. The model was run assuming static loading since stress wave transmission through articular joints causes little deviation from the quasistatic stress state (Anderson 1990, Anderson 1991).

The patellofemoral pressure distribution from the subfracture impact experiment was discretized and applied as a compressive elemental pressure to the retro-patellar surface of the model. The pressure distribution was located by the intraarticular contact method (Atkinson 1997). A one pixel slice of the pressure film image, consistent with the 2-D model, was discretized into 1 mm lengths. The average pressure over that length was determined using the public domain NIH Image program, version 1.6 (developed at the U.S. National Institutes of Health and available on the internet at http://rsb.info.nih.gov/nih-image/). The resulting pressure distribution was then applied to the posterior surface of the patella. The anterior surface of the patella was fixed in the area of contact with the impactor. Three areas were investigated: the cartilage surface, the subchondral bone, and the trabecular bone. The maximum principal stress, maximum shear stress and their respective locations were tabulated. The stresses from the rigid and padded experiments were compared with a paired t-test (Sigmastat). A regression analysis was conducted to determine the influence of cadaver age, sex, height, weight and patella geometry on the maximum stresses predicted by the model.

RESULTS

Experimental Results

The typical load-time response was a symmetrical haversine. The time to peak load (loading rate) and contact duration (pulse) for rigid experiments were 4.14±0.45 ms and 11.33±3.0 ms, respectively. These data were significantly less than padded experiments which had a time to peak load of 7.01±1.54 ms and a contact duration of 17.03±3.9 ms. A typical load time curve (H34) (Figure 7) shows similar peak loads with different loading rates and contact durations. The impactor-patella average contact pressure and contact area were different between rigid and padded interfaces. The rigid interface contacted a small area in the center of the anterior patellar surface. The average anterior patellar contact pressure and area were 18.2±4.7 MPa and 247±87 mm^2. With padding the entire patella was contacted resulting in significantly increased knee contact area and reduced contact pressure. The anterior patellar contact area was approximately 2000 mm^2 and the contact pressure was 1.4 MPa. There was no statistical difference detected for peak contact load or patellofemoral contact pressure between rigid and padded experiments. While the patellofemoral contact area tended to be larger with the rigid interface, this difference was not significant (Table 3). The patellofemoral contact was typically proximal and adjacent to the femoral notch on the femur (Figure 8) and centrally located on the patella (Figure 9). The contact area had a 'kidney' shaped appearance. The dark areas in Figures 8 and 9 illustrate regions of intraarticular joint contact.

Two rigid interface experiments resulted in gross transverse fracture of the patella (H32, H33) (Figure 9, 10) and one resulted in gross transverse patella fracture and gross fracture of the femoral condyles (H36). While two patellar fractures were full thickness through the patella (H33, H36), the fracture in the remaining specimen (H32) was partial thickness and emanated from the posterior surface. Analysis of the histological sections from all rigid interface experiments revealed occult microcracking in four of six specimens (H31, H32, H35, H36). No gross bone fracture or microdamage was detected in padded experiments.

Categorization of the patellae by morphology ratio (Table 4) revealed that five of six were of Type I and one was of Type II (H31). Therefore, data from H31 was therefore not included in regression analyses including the morphology ratio. Regression analyses of biomechanical impact data (Table 3) against cadaver, age, sex, height, and weight were not statistically significant. Regression analyses of the data against patella morphology ratio revealed a significant influence of decreasing peak contact force with an increasing morphology ratio (Figure 13). In addition, the three fracture specimens (H32, H33, H36) exhibited a significantly ($p<0.05$, unpaired t-test) higher morphology ratio (1.35 ± 0.03) than specimens which did not fracture (H34, H35: morphology ratio=1.268 ± 0.02).

Theoretical Results

Stresses in the cartilage and trabecular bone were not statistically different with rigid or padded interfaces. In the subchondral bone for both padded and rigid interface experiments, the minimum principal stress field was compressive and minimal compared to

the maximum shear stress and maximum principal stress, which was tensile. The maximum principal stress was tensile. Maximum principal ('Normal') and shearing stresses occurred in the subchondral bone and were significantly reduced with padding (Table 5). The stress distributions presented in Figures 14, 15 (H36) are typical stress distributions. Light areas indicate regions of larger magnitude stresses (tensile: 55-145 MPa; shear >40-80 MPa) and dark areas represent lower magnitude stresses (<30 MPa). The distributions are restricted to the posterior half of a transverse section through the patella.

The high stresses documented in the subchondral bone in the rigid interface experiments (Figure 16,a) were due to either global (Figure 16,b,c) of the patella or local (Figure 17) bending of the subchondral plate. Maximum tensile and shear stresses were documented on the lateral facet and at the median ridge. Compressive pressure from contact with the femur that was medial or lateral with respect to the area of contact with the rigid impactor on the anterior surface apparently caused the global bending phenomenon. In all cases, global bending was maximal on the lateral facet and coincided with the highest levels of stress in the subchondral bone. Global bending on the medial facet was minimal and the state of stress was reduced in this region. Alternately, local bending was observed in regions of high contact pressure. Due to the low compressive stress field, the distribution of maximum tensile and shearing stresses appeared to be consistent in each model of rigid interface experiments. Because the average maximum tensile and shear stresses were both near the failure stresses (shear, σy=68 MPa; tension,

σy=133 MPa, (Hayes 1991)), it was not clear if injury was related to tensile or shearing stresses.

Padding supported the entire anterior surface of the patella, eliminating global bending and reducing local bending of the subchondral plate. This resulted in an 80% decrease in the normal stress and a 70% decrease in the maximum shear stress (Table 5, Figure 15). With padding the magnitude of these stresses was significantly reduced and more nearly approximated the magnitude of the minimum principal stress. Therefore, the distribution of maximum tensile and shearing stresses was different for each padded interface experiment.

DISCUSSION

The specific aims of the current study were to experimentally and theoretically investigate the influence of padding on the impact response of the human knee. Padding was experimentally and theoretically shown to prevent gross bone fracture and occult microdamage and to limit normal and shearing stresses in the subchondral bone plate of the patella. Paired impact experiments were conducted with rigid and padded interfaces to limit test variability. Both knees from a given cadaver were impacted at approximately the same impact load. While the padding better reflects more realistic impact scenarios (i.e. knee impacting the instrument panel), it also served to significantly change the boundary conditions at a given impact load. The rigid impact interface only contacted a small portion of the central anterior patella. Independent, outboard reactions from the medial and lateral femoral condyles resulted in approximately three point global bending of the patella. This may explain the elevated stresses in the subchondral plate for rigid

interface experiments. Alternately, padding provided greater support across the entire anterior surface of the patella resulting in less bending and drastically reduced stresses in the subchondral bone. This may help explain the genesis of microcracking in the subchondral bone.

Hayashi and coworkers (1996) also conducted impact experiments on the 90° flexed knee using different impact interfaces. In that study, a rigid interface and a variety of Hexcel interfaces were used to conduct several experiments with each interface at a fixed impact energy. A direct comparison to the current study may not be possible because in a majority of the experiments the same interface was used on both limbs of the test subjects. In general, however, Hayashi, et al. (1996), showed similar results to the current study whereby padding can prevent transverse patellar fractures.

In the current study, normal and shearing stresses in the cartilage and trabecular bone were not different between rigid and padded interface experiments, however, the subchondral bone state of stress was significantly reduced with padding. Rigid interface experiments resulted in gross bone fracture in two specimens and occult microcracking in the subchondral bone was detected in three specimens. No gross fracture of bone or occult microdamage was detected in contralateral padded experiments. Further, because the impact loads were not different in paired experiments, and the state of stress in the cartilage and trabecular bone were consistent, these data may suggest that gross fracture of bone initiates in the subchondral plate. This assumes that patellar fracture initiates near the retropatellar surface. Viano and Stalnaker (1980) impacted whole, human cadavers and documented patella fractures which appeared to emanate from the posterior surface.

This is supported by the results of our math model which predicts high stresses, both gobally and locally, in the subchondral bone on the posterior surface.

The patella has been documented to predominantly fracture transversely in both past investigations (Hayashi 1996, Melvin 1975, Patrick 1965, Powell 1975, Atkinson:a 1995, Atkinson:b 1995, Haut 1989) and in the current study. This is suggestive of a tensile failure in which the tension is directed proximal-distal. Such tensile stresses are predicted in a stress analysis of the whole patella conducted by Minns and coworkers (1979). The model also predicts high shear stresses near the bone cartilage interface as seen in the current study. These results suggest the subchondral bone may be acting like a shell subjected to an externally applied compressive traction through contact with the femur. Because the patellofemoral contact area is much wider medial-lateral than in the transverse proximal-distal direction, the very stiff subchondral bone is essentially subjected to a narrow medial to lateral loading in the middle of the patella. The model used in the current study may be somewhat limited because the model geometry is taken from a transverse plane and the model is analyzed with the assumption of plane strain.

Even though a consistent flexion angle and impact energy were used with all rigid impact interface experiments, a range of peak contact loads and injuries were documented in the current study. These differences may be related to subject-to-subject variability's in the strength of the bone and cartilage, the relative size of the knees and the relative position of the patella to the femoral condyles during the impact event. Because the premortem state of the subjects can involve extended illnesses, long periods of bedrest may be expected to lead to some level of tissue atrophy. As such, the peak loads may be a

somewhat conservative measure of the current driving population (Viano 1980). While admittedly unlikely, if a consistent knee stiffness was true for all subjects, the size of the knee may then be expected to result in peak loads which scale with the size of the knee. Even with the same knee stiffness and size, more subtle joint geometry differences may affect joint impact response. Hence, the geometry of the patellae in the current study was quantified with the so-called 'morphology ratio' in effort to determine if impact biomechanics and the state of stress predicted by the math model would vary with patella geometry in a random sample of six human subjects. The morphology ratio is easily found as the ratio of two linear dimensions of patella bone and cartilage. While other investigators have used more complex methods (i.e. topographical maps, stereophotogrammetry) (Minns 1975, Mcleod 1977, Eckstein 1992, Ateshian 1994, Blenkevoort 1991, Ateshian 1991) to quantify joint geometry, the morphology ratio was sufficiently fine to detect differences in peak load and the incidence of gross bone fracture. Alternately, gross test subject parameters (i.e. height, weight, sex, age) did not significantly correlate with impact biomechanics in the current study or in past investigations (Powell 1975, Atkinson:b 1995). While considering which independent variables might correlate best with impact biomechanics and injury, it is interesting to note the predictive power of the logistical regression used in the current study. For isolated, 90° flexed human knee impact experiments at 27J of energy, the regression predicted a high chance of occult microcracking while accepting a 50% chance of gross bone fracture. Occult microcracking was observed in four of six specimens (67%) and gross bone fracture in three of six (50%) specimens.

Past in vivo studies by our group have developed an experimental rabbit model of post-traumatic osteoarthrosis (Atkinson 1996, Newberry 1996, Shelp 1994, Newberry 1995, Haut 1993, Newberry 1995, Newberry:b 1996). Subfracture impacts were delivered at two levels. 'Low' severity impacts did not progress to osteoarthrosis, while 'high' severity resulted in higher tissue stresses and did progress to a chronic joint disease. Theoretical models of these experiments help to define safe and harmful levels of joint tissue stress leading to chronic problems (Table 6). While these data only represent two levels, it may be assumed that the incipient state of stress necessary for pathogenesis of a joint disease may lie somewhere between the low and high severity impact stresses. In the current study, shear and normal stresses in the subchondral plate from rigid interface experiments (Table 7) were approximately 30% and 300%, respectively, greater than the stresses shown to cause disease in the rabbit. While padding significantly limited these stresses, they were still not reduced to safe (i.e. 'low' severity) levels established in our rabbit model. This suggests a more optimized padding system might be utilized to further reduce these stresses to 'safe' levels. This might be accomplished by allowing greater intrusion into the padding system and making contact with the femoral condyles.

The results of the current study suggest the importance of load distribution over the knee during impact which may have implications for future instrument panel designs and the current lower extremity criterion. Two instrument panel design factors appear to be important for occupant injury prevention: 1) the stiffness of the instrument panel should be optimized to distribute the load over the knee (and possibly the femoral condyles) to sufficiently reduce stress levels to prevent acute gross (i.e. bone fracture, ligamentous

injury) and micro- injuries (occult microcracking) and chronic joint pain and morbidity (post-traumatic osteoarthrosis (Newberry 1995)), 2) local incongruities (i.e. plastic heater vents) should be located in areas where knee-instrument panel contact is unlikely (States 1986). In an effort to validate the above suggestions, quantitative field studies of instrument panel designs and associated lower extremity injury frequency are needed to identify design features which aid occupant safety. Experimental methods of evaluating instrument panels may also prove helpful in making additional, more controlled comparisons. In 1969, Wilson developed a self-contained impact apparatus which could be mounted in a vehicle and simulate knee impact into the instrument panel. A hemispherical knee analog mounted on a pendulum impactor head was directed at the instrument panel at variable velocities. A similar method might prove useful in future studies.

The current lower extremity criterion used by the automotive industry is based solely on peak impact load and does not take into account how the load is distributed over the knee. The theoretical and experimental data from the current study suggest that bone and cartilage failures are related to the state of stress in the tissue and not solely the magnitude of the impact load on the knee. While it may be difficult to measure stresses in bone and cartilage in simulated accidents using anthropomorphic dummies, a more indirect approach may prove useful. From the current study it appears that anterior patellar contact area relates to the damaging stresses in the subchondral plate. By instrumenting dummy knees with a transducer to measure contact area (i.e. pressure sensitive film), peak forces on the knee may be indirectly correlated to tissue stresses. This data could be used

to predict the acute (i.e. gross and occult fracture of bone) and chronic (i.e. OA) response of the typical knee joint to impact loading. Future studies will be needed to develop a better understanding of the relationship between contact area, load and tissue stresses.

ACKNOWLEDGMENTS

This study was supported by a grant (R49/CCR503607) from the Centers for Disease Control and Prevention. Its contents are solely the responsibility of the authors and do not necessarily represent the official views of the Centers for Disease Control and Prevention. The authors appreciate the support of Hexcell corporation for their technical and materials support. The authors wish to gratefully acknowledge Ms. Jane Walsh for help in the interpretation of histological slides and Mr. Cliff Beckett for technical support. We are also indebted to Mr. Rick Shumaker and the Michigan Tissue Bank for solicitation of donors and retrieval of joints.

REFERENCES

1. Anderson D, Brown T, Radin E (1991) Stress wave effects in a finite element analysis of an impulsively loaded articular joint. MechE, Part H: J Eng Med 205: 27-34

2. Anderson DD, Brown TD, Yang KH, Radin EL (1990) A dynamic finite element analysis of impulsive loading of the extension-splinted rabbit knee. Journal of Biomechanical Engineering 112: 119-128

3. Arnoldi C (1991) Patellar Pain. Acta Orthop Scand 62: 1-29

4. Ateshian G, Kwak S, Soslowsky L, Mow, V (1994) A stereophotographic method for determining in situ contact areas in diarthrodial joints, and a comparison with other methods. Journal of Biomechanics 27(1): 111-124

5. Ateshian GA, Soslowsky LJ, Mow VC (1991) Quantitation of articular surface topography and cartilage thickness in knee joints using stereophotogrammetry. Journal of Biomechanics 24(8): 761-776

6. Atkinson PJ, Haut RC (1995) Subfracture Insult to the Human Cadaver Patellofemoral Joint Produces Occult Injury. Journal of Orthopaedic Research 13: 936-944

7. Atkinson P, Haut R (1995) Insult to the human cadaver patellofemoral joint: effects of age on fracture tolerance and occult injury. 39th Stapp Car Crash Conference 281-294

8. Atkinson P, Newberry W, Staton T, Garcia J, Altiero N, Haut R (1996) Animal and human studies on injury mechanisms during blunt insult to the knee. 6th CDC Injury Prevention Through Biomechanics 137-160

9. Atkinson P, Haut R (1997) A method for determining regions of diarthrodial joint contact during dynamic loading of the human knee. Trans Orthop Res Soc 656

10. Blankevoort L, Kuiper JH, Huiskes R, Grootenboer HJ (1991) Articular contact in a three dimensional model of the knee. J Biomechanics 24: 1019-1031

11. Bourret P, Corbelli S, Cavallero C (1977) Injury agents and impact mechanisms in frontal crashes about 350 in the field accidents. 21st Stapp Car Crash Conference 215-258

12. Chapchal G (1978) Posttraumatic Osteoarthritis after Injury of the Knee and Hip Joint. Reconstr Surg Traumat 16: 87-94

13. Crandall J, Kuhlmann T, Pilkey W (1995) Air and knee bolster restraint system: laboratory sled tests with human cadavers and the Hybrid III dummy. J Trauma 38: 517-520

14. Davis M, Ettinger W, Neuhaus J, Cho S, Hauck W (1989) The Association of Knee Injury and Obestiy with Unilateral and Bilateral Osteoarthritis of the Knee. American Journal of Epidemiology 130(2): 278-288

15. Donohue MJ, Buss D, Oegema T, Thompson R (1983) The Effects of Indirect Blunt Trauma on Adult Canine Articular Cartilage. The Journal of Bone and Joint Surgery 65-A(7): 948-957

16. Eckstein F, Muller-Gerbl M, Putz R (1992) Distribution of subchondral bone density and cartilage thickness in the human patella. Journal of Anatomy 180: 425-433

17. Gardner DL (1994) Problems and paradigms in joint pathology. J Anat 184: 465-476

18. Grelsamer R, Proctor C, Bazos A (1994) Evaluation of patellar shape in the sagittal plane: A clinical analysis. Amer J Sports Med 22: 61-66

19. Hamerman D (1989) The Biology of Osteoarthritis. New England Journal of Medicine 320(20): 1323-1330

20. Hartemann F, Thomas C, Henry C, Foret-Bruno J, Faverjon G, Tarriere C, Got C, Patel A (1977) Belted or not belted: The only difference between two matched samples of 200 car occupants. 21st Stapp Car Crash Conference 97-150

21. Haut R (1989) Contact Pressures in the Patello-femoral Joint during Impact Loading on the Human Flexed Knee. Journal of Orthopaedic Research 7: 272-280

22. Haut R, Shelp D, LI, X, Altiero N (1993) Studies on the impact response of articular cartilage to blunt impact. Symposium Proceedings: Centers for Disease Control 3: 177-200

23. Hayashi S, Choi H, Levine R, Yang K, King A (1996) Experimental and analytical study of knee fracture mechanisms in a frontal knee impact. 40th Stapp Car Crash Conference 161-171

24. Hayes W (1991) Biomechanics of cortical and trabecular bone: implications for assessment of fracture risk. In: Basic orthopaedic biomechanics, ed Mow and Hayes 93-142

25. Hering W, Patrick L (1977) Response Comparisons of the Human Cadaver Knee and a Part 572 Dummy Knee to Impacts by Crushable Materials. Twenty-First Stapp Car Crash Conference 21: 1015-1053

26. Huberti H, Hayes W, Stone J, Shybut G (1984) Force ratios in the quadriceps tendon and ligamentum patellae. Journal of Orthopaedic Research 2: 49-54

27. Huelke D, O'Day J, States J (1982) Lower Extremity Injuries in Automobile Crashes. Accid Anal & Prev 14: 95-106

28. Johnson-Nurse C, Dandy D (1985) Fracture-Separation of Articular Cartilage in the Adult Knee. The Journal of Bone and Joint Surgery 67-B(10: 42-43

29. Kapelov R, Teresi L, Bradley W, Bucciarelli N, Murakami D, Mullin W, Jordan J (1993) Bone Contusions of the knee;Increased Lesion Detection with fast Spin-Echo MR Imaging with Spectroscope Fat Saturation. Radiology 901-904

30. Kellgren J, Lawrence J (1958) Osteoarthritis and disk degeneration in the urban population. Annals of Rheumatory Diseases 17: 386-396

31. King A, Viano D, Mizeres N, States J (1995) Humanitarian benefits of cadaver research on injury prevention. J Trauma 38: 564-569

32. Li, X, Haut R, Altiero N (1995) An analytic model to study blunt impact response of the rabbit P-F joint. Journal of Biomechanical Engineering

33. Lund A, Ferguson S (1995) Driver Fatalities in 1985-1993 Cars with Airbags. Journal of Trauma 38: 469-475

34. Mackay G, Hill J (1995) The limitations of current seatbelts in Europe - some population considerations. J Trauma 38: 533-537

35. MacKenzie EJ, Siegel JH, Shapiro S, et.al. (1988) Functional Recovery and Medical Costs of Trauma: An analysis by Type and Severity of Injury. Journal of Trauma 28: 281-298

36. Malliaris A, Hitchcock R, Hedlund J (1982) A search for priorities in crash protection. Proceedings of the 1982 SAE International Congress and Exposition 959-991

37. Mcleod W, Moschi A, Andrews J, Hughston J (1977) Tibial plateau topography. The American Journal of Sports Medicine 5(1): 13-18

38. Melvin J, Stalnaker R, Alem N, Benson J, Mohan D (1975) Impact Response and Tolerance of the Lower Extremities. Stapp Car Crash Conf 19: 543-559

39. Minns R, Bremble G, Campbell J (1975) The geometric properties of the human tibia. Journal of Biomechanics 8: 253-255

40. Minns RJ, Birnie AJM, Abernethy PJ (1979) A stress analysis of the patella, and how it relates to patellar articular cartilage lesions. J Biomechanics 12: 699-711

41. Morgan R, Eppinger R, Hennessey B (1991) Ankle joint injury mechanism for adults in frontal automitve impact. 35th Staoo Car Crash Conference 189-198

42. Mow V, Holmes M, Lai W (1984) Fluid transport and mechanical properties of articular cartilage a review. Journal of Biomechanics 17: 377-394

43. Nagel D, States J (1977) Dashboard and bumper knee-will arthritis develop? AAAM proceedings 21: 272-278

44. Newberry W, Atkinson P, Li X, DeCamp C, Altiero N, Haut R (1995) Tissue injuries resulting from blunt impact on the knee. 5th Injury prevention through biomechanics symposium

45. Newberry W, Shelp D, Coles A, Haut R (1995) Chronic alterations in the physiologically relevant properties of cartilage after mechanical insult. Proceedings 41st Meeting of the Orthopaedic Research Society

46. a:Newberry W, Haut R (1996) The effects of subfracture impact loading on the patellofemoral joint in a rabbit model. 40th Stapp Car Crash Conference 149-159

47. b:Newberry WN, Zukosky DK, Walsh JC, Haut RC (1996) Blunt trauma to a joint produces surface damage to cartilage with subsequent changes in subchondral bone. ORS 749

48. Nyquist G, King A (1985) Lower extremities. Rev Biomech Impact Res Inj Auto Env 6: 163-201

49. Otte D (1996) Biomechanics of lower limb injuries of belted car drivers and the influence of intrusion and accident severity. 40th Stapp Car Crash Conference 193-206

50. Patrick L, Kroell C, Mertz H (1965) Forces on tehehuman body in simulated Crashes. Stapp Car Crash Conf 9: 237-259

51. Pattimore D, Ward E, Thomas P, Bradford M (1991) The nature and cause of lower limb injuries in car crashes. 35th Stapp Car Crash Conference 177-188

52. Powell W, Ojala S, Advani S, Martin R (1975) Cadaver Femur Responses to Longitudinal impacts. Stapp Car Crash Conf 19: 561-579

53. Radin E, Ehrlich M, Chernack R, Abernethy P, Paul I, Rose R (1978) Effect of repetitive impulsive loading on the knee joints of rabbits. Clinical Orthopaedics and Related Research 131: 288-293

54. Radin E, Parker H, Pugh J, Steinberg R, Paul I, Rose R (1973) Response of joints to impact loading-III relationship between trabecular microfractures and cartilage degeneration. Journal of Biomechanics 6: 51-57

55. Radin E, Paul I, Rose R (1972) Role of Mechanical Factors in Pathogenesis of Primary Osteoarthritis. The Lancet 3: 519-522

56. Setton L, Zhu W, Mow V (1990) BIphasic poroviscoelastic behavior of articular cartilage. First World Congress of Biomechanics 17

57. Shelp D, Newberry W, LI, X, Dalimonte R, DeCamp C, Altiero N, Haut R (1994) Tissue damage resulting from blunt impact on the knee: animal and cadaver studies. 4th Inj prevention through biomechanics symposium 4: 43-62

58. Shimizu M, Tsuji H, Matsui H, Katoh Y, Sano A (1993) Morphometric Analysis of Subchondral Bone of the Tibial Condyle in Osteoarthrosis. Clin Orthop 229-239

59. Siegal J, Mason-Gonzales S, Dischinger P, Cushing B, Read K, Robinson R, Smialek J, Heatfield B, Hill W, Bents F, Jackson J, Livingston D, Clark C (1993) Safety belt restraintsand compartment intrusions in frontal and lateral motor vehicle crashes: mechan

60. States J (1970) Traumatic Arthritis-- A Medical and Legal Dilemma. Ann Conf of the Amer Assoc for Automotive Med 14: 21-28

61. States J (1986) Adult occupant injuries of the lower limb. In: Biomechanics and medical aspects of lower limb injuries. Warrendale, PA: SAE 97-107

62. Thomas P, Charles J, Fay P (1995) Lower limb injuries-the effect of intrusion, crash severity and the pedals on injury risk and injury type in frontal collisions. 39th Stapp Car Crash Conference 265-280

63. Thompson RC, Oegema TR, Lewis JL, Wallace L (1991) Osteoarthritic changes after acute transarticular load. The Journal of Bone and Joint Surgery 73-A(7): 990-1001

64. Upadhyay S, Moulton A, Srikrishnamurthy K (1983) An analysis of the late effects of traumatic posterior dislocation of the hip without fractures. J Bone Joint Surg 65: 150-152

65. Vellet A, Marks P, Fowler P, Munro T (1991) Occult Posttraumatic Osteochrondral Lesions of the Knee: Prevalence, Classification, and Short Term Sequelae Evaluated with MR Imaging. Radiology 271-276

66. Viano D (1995) Restraint effectiveness, availability and use in fatal crashes: implications to injury control. The Journal of Trauma 38:538-546

67. Viano D (1977) Considerations for a femur injury criterion. 21st Stapp Car Crash Conference 445-473

68. Viano DC, Stalnaker RL (1980) Mechanisms of Femoral Fracture. Journal Biomechanics 13: 701-715

69. Volpin G, Dowd G, Stein H, Bentley G (1990) Degenerative arthritis after intra-articular fractures of the knee. Long-term results. J Bone Joint Surg Br 72: 634-638

70. Wilson W (1969) Evaluating knee-to-instrument panel impacts. Stapp Car Crash Conference 13: 134-148

TABLES

Table 1: *Lower extremity bone fracture injuries by site; data taken from past experimental studies (Patrick 1965, Melvin 1975, Powell 1975, Viano 1980)*

Impact Interface	# of tests	Patella	Femoral Condyles	Femoral Shaft	Femoral Neck	Pelvis	Total Injuries
Rigid Interface	32	27	14	10	4	1	56 injuries
Incidence[&]		84%	44%	25%	13%	3%	
Padded Interface	36	7	11	7	0	5	30 injuries
Incidence[&]		19%	30%	19%	0%	14%	
& Incidence = # of injuries/# of tests							

Table 2: *Material properties for math model*

Tissue	Modulus (MPa)	Poisson Ratio	Reference
Cartilage	20	0.49	Repo/ Atkinson
Cortical/Subchondral Bone	3750	0.3	Mente
Trabecular Bone	300	0.3	Townsend

Table 3: *Paired (right-left) subject impact biomechanical data with rigid and padded impact interfaces*

Interface ⇒	rigid	padded	rigid	padded	rigid	padded	rigid		padded	
	peak contact force		p-f contact pressure		p-f contact area		Knee Joint Injury		Knee Joint Injury	
Spec	(kN)	(kN)	(MPa)	(MPa)	(mm^2)	(mm^2)	Gross*	Micro**	Gross	Micro
H31	6103.4	6861.4	22.6	13.3	381.6	241.3	None	H O Mc	None	None
H32	4654.3	4788.2	11.4	6.4	217.4	99.4	T P Fx	H O Mc	None	None
H33	3324.5	5605.3	11.3	14.9	301.6	161.7	T P Fx	None	None	None
H34	6845.6	6716.8	8.2	11.1	509.3	263.6	None	None	None	None
H35	5839.1	7082.6	12.6	16.9	305.7	251.1	None	H & V O Mc	None	None
H36	3211.8	3860.6	14.8	5.9	260.7	260.9	T P Fx, F C Fx	H & V O Mc	None	None
average	4996.4	5819.1	13.5	11.4	329.4	213.0	3 T P Fx, 1 F C Fx	4 H O Mc, 2 V O Mc	0	0
std dev	1513.4	1298.6	4.9	4.5	103.6	67.3				
* T P Fx = Transverse patellar fracture, F C Fx = Ffemoral condyle fracture, ** H O Mc, V O Mc = Horizontal or Vertical Occult Microcracking (Figure 6)										

Table 4: *Geo*

Specimen	
H31	
H32	
H33	
H34	
H35	
H36	
* See Figure	

Table 5: *Ma*

Interface ⇒	rig
Tissue⇒	Ca
Stresses ⇒	N
average	6.
std dev	5.

Table 6: *Str*

Tissue	
Cartilage	
Cartilage	
SC Bone	
SC Bone	

Table 7: *M*

Tissue	
Cartilage	
SC Bone	

Table 4: *Geometrical variation of test subject patellae*

Specimen	Morphology Ratio (a/b)*	Type Classification *
H31	1.540	Type II
H32	1.315	Type I
H33	1.380	Type I
H34	1.277	Type I
H35	1.252	Type I
H36	1.346	Type I
* See Figure 4 and methods section for explanation		

Table 5: *Maximum normal and shear stresses (MPa) from the math models.....*

Interface ⇒	rigid		padded		rigid		padded		rigid		padded	
Tissue⇒	Cartilage				Subchondral Bone				Trabecular Bone			
Stresses ⇒	Norm	Shear	Norm	Shear	Norm	Shear	Norm	Shear	Norm	Shear	Norm	Shear
average	6.9	6.5	2.0	5.7	94.4	54.8	26.3	25.2	10.1	8.7	2.1	6.6
std dev	5.5	3.2	2.6	2.1	43.5	22.4	21.4	15.5	10.2	4.7	3.3	4.1

Table 6: *Stresses from low and high severity impact*

Tissue	Impact Severity	Max Shear Stress (MPa)	Max Norm Stress (MPa)
Cartilage	Low	6.0	6.3
Cartilage	High	12.9	16.1
SC Bone	Low	16.9	12.6
SC Bone	High	41.8	28.9

Table 7: *Maximum stresses from current study*

	Max Shear Stress (MPa)		Max Norm Stress (MPa)	
Tissue	Rigid	Padded	Rigid	Padded
Cartilage	6.5	5.7	6.9	2.0
SC Bone	54.8	25.2	94.3	25.2

FIGURES

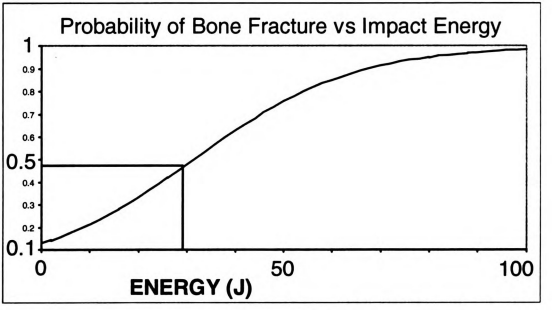

Figure 1

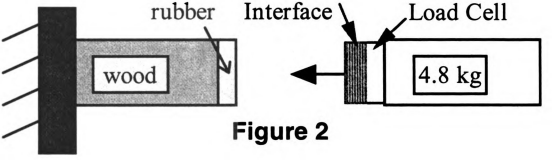

Figure 2

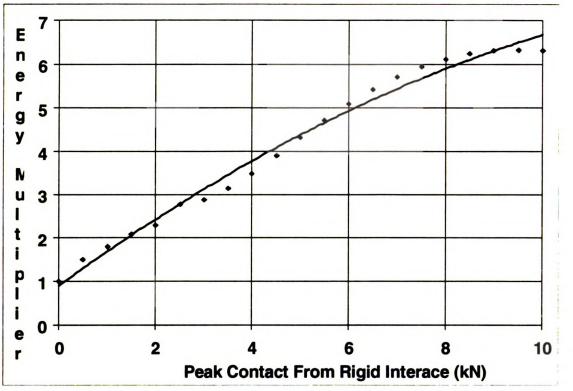

Figure 3

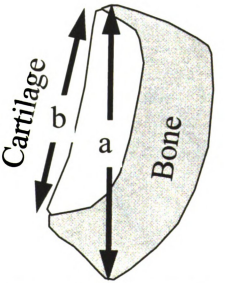

Figure 4: Side view of patella

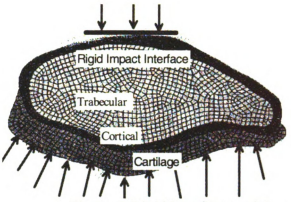

Figure 5: Rigid interface model

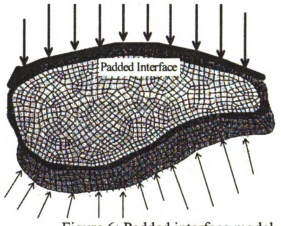

Figure 6: Padded interface model

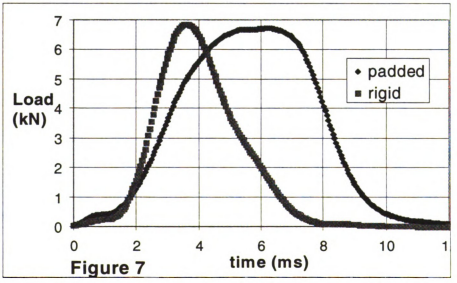

Figure 7

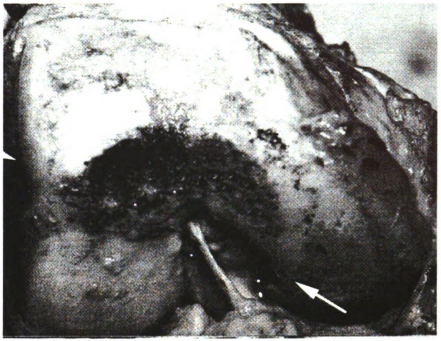

Figure 8: Region of patellofemoral contact on the femoral condyles

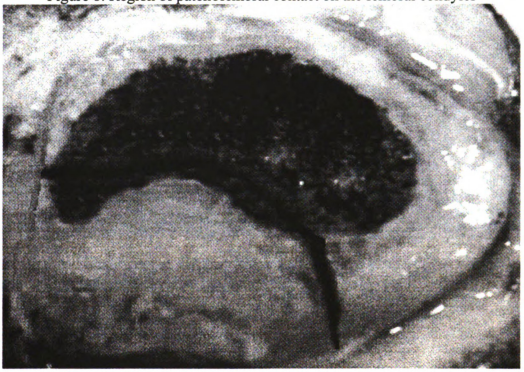

Figure 9: Region of patellofemoral ccntact on the patella. Arrows denote a transverse fracture.

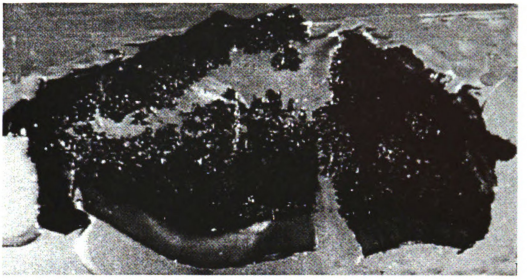

Figure 10: Transverse histological section of a fracture patella.

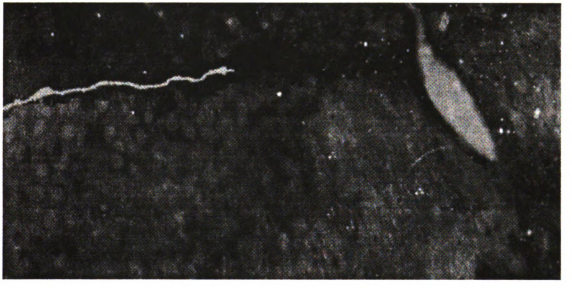

Figure 11: Combination occult trauma: horizontally (left) oriented occult trauma near a vertically oriented occult microcrack (right) (40X).

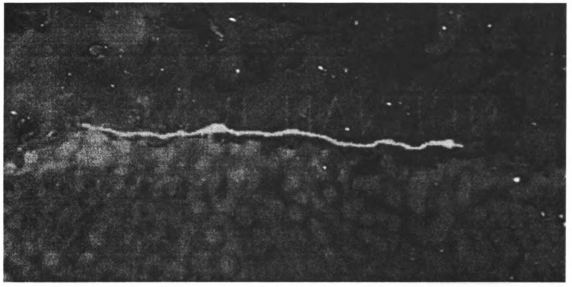

Figure 12: Horizontally oriented occult microtrauma (40X).

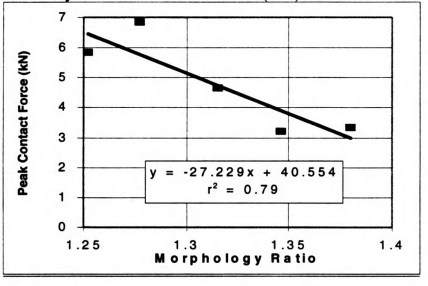

Figure 13

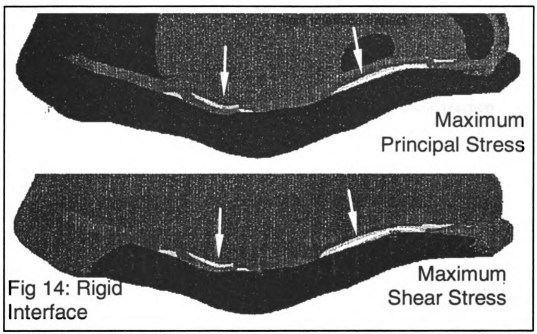

Fig 14: Rigid Interface

Arrows point to regions of maximum stress.

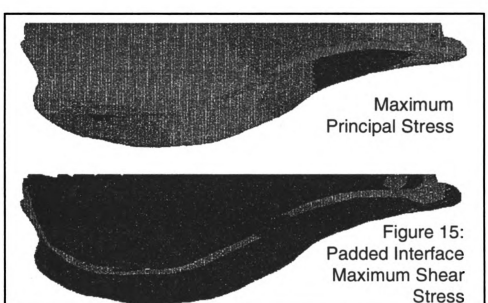

Figure 15: Padded Interface Maximum Shear Stress

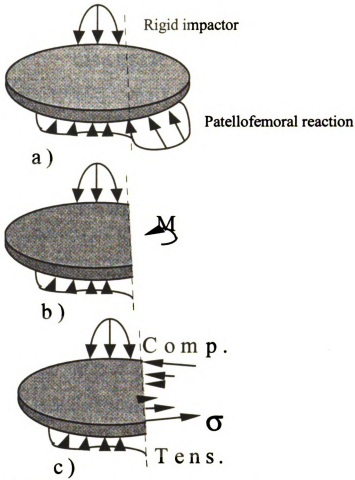

Figure 16: Global bending with a rigid interface

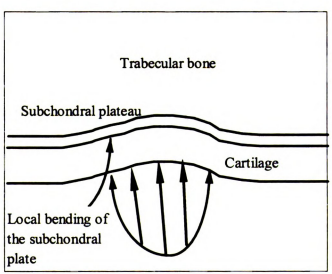

Figure 17: Patellofemoral contact and local bending

CHAPTER 7

HUMAN KNEE IMPACT INJURY THRESHOLDS AND LOCATION VARY WITH FLEXION ANGLE AND IMPACT INTERFACE.

Patrick Atkinson, Jose Garcia, Hasnin Ali*, Nicholas Altiero*, Roger Haut
Orthopaedic Biomechanics Laboratories
*Department of Material Science and Mechanics
Michigan State University

ABSTRACT

Injury to the knee, thigh and hip is currently based on a bone fracture criterion derived from human cadaver impact experiments. Typically a rigid impact interface is used to deliver a blunt insult to the 90° flexed knee. 10 kN is the maximum load allowed during an automotive crash using anthropomorphic dummies. More recent studies, however, suggest that the impact interface and the knee flexion angle influence its response to impact. In the current study, bilateral impacts were delivered to isolated knee preparations of thirty-six cadavers. The cadavers were separated into two test groups. In each test group, subgroups of 6 cadavers were assigned to flexion angles of 60, 90, or 120 degrees. One knee from each subject was impacted at increasing energy levels until gross fracture of bone. In the first group of 18 cadavers, the contralateral knee was impacted once with a rigid interface at a subfracture level. In the second group, the contralateral knee was impacted once with a padded interface (Aluminum Hexcel) at approximately the fracture load in the contralateral knee. The rigid interface experiments

showed that increasing flexion angle was associated with higher fracture loads. The location and mode of injury varied with flexion angle. At 60° of flexion, there was an avulsive failure of the patellar tendon from the distal pole of the patella, at 90° a transverse patellar fracture located centrally on the patella, and at 120° transverse fractures of the proximal pole of the patella, comminuted fractures of the femoral condyles and tibial plateau fractures. Subfracture experiments typically showed occult microcracks at the bone-cartilage interface in regions showing gross fracture in contralateral knees. Padding limited gross and microscopic injury at 90° and 120° flexion, however, injuries still occurred for 60° of flexion. 3-D mathematical models of the patella indicated high shear and tensile stresses in the contact regions corresponding to regions of injury. This study showed that tissue stresses and injury thresholds vary with flexion angle and impact interface.

INTRODUCTION

Lower extremity injury is a significant problem which can lead to considerable hospital stays and extended periods of lost work days (MacKenzie 1988, Huelke 1982). Lower extremity injuries resulting from automotive accidents are second in frequency only to head injuries (States 1986). Within the lower extremity, the knee is the most injured body region due to high speed contact with the instrument panel (Dischinger 1992). Such injurious contact can also occur in sporting activities and falls (States 1970). The resulting injury can be at a fracture or subfracture level, however, subfracture injuries are reported four times as frequently as gross fractures. Unfortunately, the small size and typically occult presence of subfracture injuries can preclude their acute

detection and treatment (Vellet 1991, Kapelov 1993). Clinically, such injuries may be treated as a simple contusion (Tomatsu 1992) or missed entirely. Without proper treatment, such injuries can lead to chronic joint pain and disease, such as post-traumatic osteoarthrosis (Upadhyay 1983, States 1970, Donohue 1983, Thompson 1991).

Several parameters have been hypothesized to be important factors influencing the potential for impact induced injuries in the knee. First, studies have documented a link between the flexion angle of the knee and its tolerance to injury. In automotive accident field studies, Dischinger, et al., (1995) found that shorter automotive occupants of both sexes are more than twice as likely to injure the knee than taller occupants. This may be due to the seat placement for shorter occupants which results in elevated knee flexion angles which might reduce the injury tolerance of the knee. Viano, et al., (1978) used formed interfaces to impact the human cadaver knee and tibia at flexion angles of 45° and 90°. A consistent impact energy was used for all tests and only one impact experiment was conducted for each knee. At 90°, the impact load was 7 kN and gross injuries to the bones and ligaments occurred in all but one specimen. At 45°, the peak load was significantly lower (3.65 kN) and there were no gross injuries. Haut (1989) conducted similar experiments at flexion angles of 60°, 90°, and 110° but restricted the impact to the patellofemoral joint. In addition, progressive experiments were conducted on the same knee at increasing impact energies until gross fracture was noted. Similar to Viano, et al., the fracture load was observed to increase with flexion angle. Unfortunately, in both of these studies there was no investigation of subfracture injuries.

Another parameter which affects knee impact injury is the stiffness of the material which contacts the knee. Extensive experiments have been conducted on seated, fresh

cadavers (Patrick 1965, Melvin 1975, Powell 1975, Viano 1980) in which impact loads were directed at the 90° flexed knee with rigid and padded impactors. Rigid impactors resulted in transverse fractures of the patella, split fractures of the femoral condyles, and mid-femoral shaft fractures in 84%, 44%, and 25% of cases, respectively. Padding reduced fracture to the patella by 65%, to the femoral condyles by 14%, and to the femoral shaft by 6%. Again, however, there was no investigation of subfracture injuries in these studies.

Contact between rigid impact interfaces and the bony anterior surface of the patella likely result in a localized load distribution. The flesh thickness over the anterior patella is approximately 4.8 mm (Hering 1977), offering little protection to a rigid impact. Alternately, padding likely produces increased load distribution over part or all of the patella and possibly the femoral condyles. The localized load distribution associated with rigid interfaces has been implicated in the high incidence of injuries with the rigid interface (Hayashi 1996, Powell 1975). This suggests that the boundary conditions on both the anterior and posterior patella may be important in determining the injury mechanism of patellar fracture. There is some experimental evidence that patellar fractures probably initiate on the retropatellar surface (Viano 1980), however, the exact mechanism of injury is unknown.

While the exact mechanism of fracture injury is unknown, the mechanism of subfracture injuries has been the subject of theoretical and experimental studies. These studies suggest that microfractures of bone and cartilage may be mediated by elevated shear and/or tensile stresses. Theoretical analyses of generalized diarthrodial joint contact (Eberhardt 1990, Ateshian 1994) document elevated shear stresses in the cartilage

at the osteochondral junction as a result of sudden joint loading. These studies hypothesize that this might explain occult osteochondral lesions. Elevated shear stresses at the cartilage surface have also been implicated in the development of cartilage surface fissures. Atkinson, et al., (1998) conducted impact experiments on the tibial plateau using rigid, spherical indentors of various radii. Smaller indentor radii produced a higher frequency of surface lesions which were associated with elevated shear stresses at the cartilage surface. Larger radii created elevated shear stresses at the bone-cartilage interface near the edge of contact suggesting that larger contact areas might be associated with deeper lesions. Because the location and intensity of stresses vary with contact radii, these data suggest that knee joint flexion will likely affect tissue stresses. This results from the changing contact radii between the patella and femur which vary as a function of the flexion angle. Studies of passive joint loading document maximal contact area at 90° of flexion which decreases at 120° and 60° (Huberti 1984). This suggests that extreme flexion angles may produce elevated shear stresses at the cartilage surface due to the disparate contact radii producing the reduced intraarticular contact areas (Atkinson 1998). Alternately, the larger contact areas would indicate contact between larger contact radii which suggest elevated stresses at the bone-cartilage interface.

Subfracture injuries have been documented in knee impact studies in canine and porcine experimental models with the knee flexed 100°-110°. Saggital sectioning reveals occult, horizontal and vertical splitting at the tidemark, and fissures of the articular surface (Tomatsu 1992, Armstrong 1985, Thompson 1991, Donohue 1983). In the canine, these injuries are in the patella and are located within the region of intraarticular contact. For the canine at 100° of flexion, the retropatellar contact area is a narrow band

at the distal pole and extends medial-lateral across the patella. However, differences in the articular geometry of the canine and human knee are such that the contact region in the canine at 100° of flexion is different from the human at the same flexion angle. This makes a direct application of the experimental animal data to the human difficult.

There have been a limited number of subfracture studies on the human. These experiments were conducted at 90° of flexion (Atkinson 1995, Atkinson 1997). Unlike the animal studies, the patellae were transversely sectioned for histological analysis. Occult, horizontal injuries were documented in the region of intraarticular contact which is located in the middle of the patella for the human. The observed absence of fissures or occult, vertical occult microcracks, as seen in the animal studies, may have been due to the plane of sectioning or the shape of the joint. For example, the contact region in the canine which is associated with subfracture injuries (100°) occurs in the human at lower flexion angles (≤60°) (Huberti 1984). It is unknown what effect low and high flexion angles will have on the risk of subfracture injuries in the human knee.

In the current study, subfracture and fracture impact studies were conducted at flexion angles of 60°, 90°, and 120°. Rigid and padded impact interfaces were used to alter the load distribution over the knee. Detailed histological analyses were conducted to identify the type and location of subfracture injuries. A theoretical model of the patella was used to predict the stresses associated with these experiments. Specifically, we hypothesized that: 1) impact loads would increase with flexion angle, and 2) subfracture injuries at lower flexion angles would include cartilage fissures and occult, microfractures, similar to experiments in the canine, and 3) increased load distribution would reduce the incidence of knee injury.

METHODS AND MATERIALS

Experimental protocol

Blunt impact was delivered to isolated, flexed knee joints of 36 human cadavers. The knee joints were randomly assigned to subfracture and fracture level experiments (Table 1). The specific test protocols are provided later. Shortly after death, the patellofemoral joint was examined through a medial incision. Tissues were procured from donors with no prior history of joint trauma and/or evidence of advanced joint pathology (areas of denuded bone, advanced chondromalacia, etc.). Joint preparations were excised approximately 15 cm from the knee proper and stored at -20° C until the day of testing. The tissues were allowed to thaw at room temperature overnight prior to testing. Superficial tissues proximal to the femoral condyle were excised and the femoral shaft was cleaned with alcohol. The femur was potted in a cylindrical steel sleeve with room temperature curing epoxy, and was mounted horizontally to a rigid test frame (Figure 1). Specimens were randomly assigned to be tested at flexion angles of 60°, 90° or 120°. The flexion angle was maintained by constraining the tibia by means of a rigid collar attached to the distal end of the tibia. A loosely knotted tether was attached to the quadriceps tendon to position the patella against the femur. The knot was such that minimal load was required to cause slippage, thus minimizing tensile loads in the tendon during impact. The patella was brushed with India ink and photographed prior to impact to document any baseline surface roughness or fibrillation.

A 4.8 kg free flight impact missile was accelerated to a given pre-impact velocity, while aligned on two steel guide rails and supported on four nylon blocks to minimize friction. A rigid (6061-T6 aluminum) or padded (478 psi crush strength aluminum

Hexcel) impact interface was mounted to the front of a load transducer attached to the front of the missile (Model 3173-2k, Lebow Products, Troy, MI, USA). The impact mass was selected based on previous studies (Atkinson 1995, Haut 1989). Pilot studies indicated that the load transducer and attached mass would not resonate during impact on the human knee. Load data were recorded continuously on a personal computer via a 16 bit A/D board (Model DAS 1600, Computer Boards, Inc., Mansfield, MA, USA). Load data were inertially compensated (Atkinson 1997) and sampled at 20,000 Hz. The impacting mass was accelerated to a predetermined velocity by adjusting the air pressure in a pneumatic impact cannon. Velocity of the mass was measured prior to impact on the knee using two infrared optical sensors (Part No. OR518-ND, Digi-Key Corporation, Thief River Falls, MN). These sensors are designed with a 5 mm separation between the emitter and detector. A metal tab connected to the impact mass crossed the 5 mm gap interrupting the first sensor and then the second. The individual sensors were separated by 76.2 mm to eliminate cross-talk.

All experiments started with a fracture level test on one knee of a cadaver at a given flexion angle using the rigid interface. The protocol consisted of sequentially increasing the velocity of the impact missile in separate experiments, so as to progressively increase the impact energy (2, 10, 22, 38, 60, 86, 112 J). The experiment was terminated when impact loading resulted in a visible fracture of bone. Damage was assessed by visual inspection through lateral and medial incisions in the joint, palpation and documented photographically. For the subfracture experiments, the contralateral limb of each subject was impacted once with the rigid interface at 45% of the impact energy that caused bone fracture in the first limb. The specific level of 45% was taken from experimental studies

(Donohue 1983, Thompson 1991, Atkinson 1995, Atkinson 1997) which document acute subfracture injuries at this energy level. For the impact interface study, each contralateral knee was impacted once with the padded interface at the fracture load for that subject. Typically, an elevated impact energy was needed for the padded interface experiments to produce the same load as the rigid interface experiments. The additional energy was predicted using a previous methodology (Atkinson 1997).

The contact area and contact pressure associated with the impact event was recorded with pressure sensitive film (Prescale, Itochu Int., Quebec, CA). The film was sandwiched between two sheets of polyethylene film (0.05 mm thick/sheet) to prevent exposure to body fluids and help reduce shear loading artifacts (Huberti 1994). The strips of film were sufficiently long to pass through the patellofemoral joint and cover the anterior surface of the patella to measure the distribution of the contact load on the knee. This also minimized frictional forces between the rigid impactor and the knee. To increase the sensitive range of the film, low (2-10 MPa), medium (10-50 MPa), and high (50-139 MPa) range films were stacked to record the contact between the rigid impactor and bony anterior surface of the patella. Low and medium film were stacked for use inside the joint. This specific use of the film was based on pilot experiments conducted to ensure the films would not threshold for typical loads. The calibration of the pressure sensitive film was calibrated in a servohydraulic testing machine (Model 1330, Instron, Canton, MA, USA) using a previous methodology (Atkinson 1995, Hale 1992).

The film was located on the patellar articular surface using a previous methodology (Atkinson 1997). Briefly, a monolayer of gauze placed over the articular cartilage of the patella and Sudan IV biological stain was dusted over the retropatellar surface (Figure 2).

The film packet was inserted into the joint and the impact experiment was conducted. After the impact event, the film packet and gauze were removed and the stain was evenly distributed over the retropatellar surface (Figure 2 A). The articular surface was irrigated with physiological saline to reveal an image of the patellofemoral contact region (Figure 2 B,C) which correlated with the pressure sensitive film. Two reference points were made on the cartilage with a paint pen adjacent to the area of intraarticular contact. The contact region and reference points were transferred to a clear, flexible sheet and the reference points were registered on the film. Following load application, the film was removed from the packet and analyzed using established methods (Atkinson 1998) to determine anterior and posterior contact areas and pressures. The contact area was taken from the low range and the average contact pressure was derived from analysis of all stacked films to derive a composite pressure.

Theoretical modeling-Impact Interface Study

To investigate the state of stress in the patellar bone and cartilage, a reference 3-D finite element model was made of the patella. The model was based on an untraumatized patella with a typical geometry (Grelsamer 1994). To identify a 'typical' patella the 'morphology ratio' was assessed for all patellae. The morphology ratio is defined as the length of the bone divided by the length of the articular surface in a saggital plane. The morphology ratio of the reference patella was 1.30 which represented the average morphology ratio of the subjects in the current study and agrees with average patellae from clinical studies (Grelsamer 1994). The geometry was assessed by taking successive, high resolution transverse MRI slices of the patella. The patella was wrapped in cellophane and fixtured in a plexiglass cage (Figure 3). The cage maintained a fixed

patellar position and located the identification points in the MR images (Figure 3A). The identification points were located by means of a 2.5 cm thick plexiglass track suspended directly over the patellae. Two mm diameter blind holes were drilled in the track directly above the identification points on the patella and a hypodermic needle was used to fill the blind holes with water. Upon imaging the water-filled holes were clearly visible and were used to locate the specific slice and position on that slice of the identification points (Figure 2B). The patellae were imaged transversely in a GE 1.5 T magnet (high resolution extremity coil, no fat suppression, TE=61, TR=11, FA=30°, FOV=8cm x 8cm, 3 mm slices). The cartilage, subchondral bone and trabecular bone geometry and the spatial coordinates of the identification points were digitized into a commercial finite element code (Ansys, version 5.3) and a solid model was constructed (Figure 3C). The material properties were adopted from previous studies (cartilage: E=20 MPa, ν=0.49 (Atkinson 1998), subchondral bone: E=3750 MPa (Mente 1994), ν=0.3, trabecular bone: E=350 MPa, ν=0.3 (Townsend 1975)). The anterior surface was constrained by imposing a zero-displacement boundary condition in the normal elemental direction for all elements making contact with the impactor. It was observed during the experiments that the patella attempted to migrate proximally during the 60° experiments and, to a lesser extent, at 90° (Viano 1978). To account for tensions at the distal pole of the patella due to the patellar tendon, a zero displacement boundary condition which only resisted tension was imposed in the proximal-distal direction for the bone along the insertion of the tendon. The pressure sensitive film data from the patellofemoral joint was discretized to correspond to the cartilage surface layer of elements. The contact pressure was then averaged over each region representing an element face to allow a

direct mapping of the boundary conditions on to the cartilage. All 36 impact interface experiments were mapped onto the reference model and stresses were tabulated at the: cartilage surface, cartilage at the interface with the subchondral bone, subchondral plate, and the trabecular bone in the neighborhood of the subchondral bone.

Histology and Injury Determination: Subfracture Study and Impact Interface Study

Following the impact experiments, patellae were placed in 10% buffered formalin followed by successive decalcification solutions (20% formic acid). Typically each patella was divided into five equal segments by making saggital cuts along the entire length of the patella. Areas of interest included the articular cartilage, the subchondral bone and the trabecular bone (Figure 4). The samples were initially reviewed to document any gross or microscopic injuries. In some cases evidence of fissures or occult cracks were visible at this stage. Two total samples were taken for further histological analysis: one from the medial half and one from the lateral half of the patella. The samples were selected based on evidence of gross or subfracture level injuries. If no injuries were detected in any of the samples, a representative sample was taken from the mid-lateral and mid-medial halves for histological analysis. Samples were processed using established methods (Atkinson 1998) and stained with Safranin O-Fast Green. The sections were read in blinded fashion by two individuals (P.A., J.W.) via light microscopy at 12-400 power. Gross and microscopic injuries were tabulated according to a predefined injury classification scheme (Figure 5).

Statistics

The load-time curve and the pressure sensitive film were analyzed to determine the following parameters: anterior and posterior contact area and mean pressure, peak

contact load, the time to attain peak load and the total contact duration. The time to reach peak load was defined as the time interval from when 50 N of load was first attained after contact until peak load was attained. The contact duration was defined as the time interval from when 50 N was attained after contact until the load pulse returned to 50 N. The contact area, contact pressure, contact load, time to peak load, and contact duration data associated with the subfracture experiments were analyzed with a commercial statistics package (SigmaStat, San Rafael, CA). A one way ANOVA with Student-Neuman-Keuls post-hoc testing was used to detect differences in these data with regard to flexion angle. The frequency of gross fractures, cartilage fissures, and vertical and horizontal occult injuries were documented at each flexion angle and compared with the Chi-Square test.

RESULTS

Subfracture experiments

Impacting the knee with the free-flight missile produced a load-time pulse with an initial short period of low contact load followed by a sharp rise to the peak load. The load then gradually returned to zero (Figure 6). The amplitude and duration of the load-time traces varied with flexion angle. For example, the peak load significantly increased with increasing flexion angle (Table 2). The load at 120° of flexion was approximately double the load at 60° and 30% greater than at 90°. The time to peak load was approximately 5 ms at 90° and 120° of flexion which was approximately half of the time for the 60° experiments. The contact duration was significantly lower for the 90° experiments versus 60° or 120°. The average subfracture impact energy was 18.7 and

16.5 J for the 60° and 90° flexion angles, respectively (Table 3). These energies were approximately half of the average impact energy for the 120° flexion angle. The average anterior contact area was greatest at 90° of flexion and was lower at 60° and 120° flexion angles. The average anterior contact pressure significantly increased with increasing flexion angle. The anterior contact pressure at 60° and 90° was approximately 20% and 40% of the average anterior contact pressure at 120°.

The patellofemoral contact areas were lower than the anterior contact areas at 60° and 90° (Table 4). In addition, for these flexion angles the patellofemoral contact pressures were larger than the anterior contact pressures. The opposite was true at 120° of flexion; on average, the patellofemoral contact area was larger and the contact pressure was lower than on the anterior surface of the knee. In the patellofemoral joint, the maximum contact area occurred at 90° of flexion and was lower at 120° and 60°. Similar to the anterior surface, the patellofemoral contact pressure increased with increasing flexion angle, although the increases were not as significant.

The intra-articular contact area moved proximally with increasing flexion angle (Figures 7, 9-rigid only, 10). At 60° the region of retropatellar contact was a narrow band extending across the distal pole of the patella. This resulted from contact on the femoral groove, approximately a centimeter above the femoral notch. At 90° the retropatellar contact moved centrally on the patella and appeared 'kidney' shaped. This resulted from femoral contact around the upper rim of the femoral notch. At 120° the retropatellar contact was divided into two distinct lobes at the proximal edge of the articular surface and separated at the median ridge. This resulted from contact with both

femoral condyles on either side of the femoral notch and an absence of contact with the femoral groove.

Analysis of the histological samples and sections revealed cartilage surface fissures and occult injuries for all flexion angle groups (Table 5, Figure 8). Even though the impact experiments were conducted at subfracture impact energies, three gross fractures were observed for the 60° flexion angle and two 90° flexion angle experiments. Subfracture injuries were detected in three locations: on the median ridge, on the lateral facet, or the injury extended across the patella and was observed on the median ridge and lateral facet. Cartilage fissures were most frequently detected on the lateral facet and were more common in subjects impacted at 60° versus 120° and 90°, although these differences were not significant. Vertical occult clefts were observed to typically extend across the patella and were observed grossly as a faint shadow when viewing the articular surface. Gross analysis of the samples and microscopic analysis of the histological sections revealed that these microfractures extended from the deep zones of the cartilage, across the subchondral plate and into the trabecular bone. The injuries did not communicate posteriorly to the articular surface and terminated anteriorly in the trabecular core, or, in some cases, in the thick, anterior layer of cortical bone. The vertical clefts were equally represented on the medial and lateral halves of the patella and were observed more frequently as flexion angle increased. Horizontal occult cracks were documented as either a separation at the tidemark or between the calcified cartilage and the subchondral plate. These injuries were most common on the median ridge and were equally represented at all flexion angles. A final classification of avulsive injuries was documented for four of six 60° experiments in which the cortical bone was separated

from the trabecular bone at the distal pole (Figure 8). If this injury was closed (occult or did not communicate to the surface), then the injury was listed as an occult. If the avulsion was opened it was classified as a gross fracture.

Impact interface experiments

The padded interfaces produced a significantly greater amount of contact area over the knee than the rigid interface for all flexion angles (Table 6). The peak loads for the rigid and padded interfaces at 60° and 90° of flexion were not different (Table 7). For the 120° flexion angle, the padded interface peak load was significantly greater than with the rigid interface. For both interfaces, the peak load increased with increasing joint flexion.

The region of extra-articular contact was similar between the interfaces (Figure 9). As flexion angle increased, the region of extraarticular contact moved proximally. The intraarticular regions of contact were similar regardless of interface (Figure 10) with one exception. At 120° of flexion, the medial femoral condyle is in approximately the same plane as the anterior surface of the patella. Thus, impact experiments conducted at this flexion angle typically resulted in contact with both the patella and the femur. An example of a padded impact at 120° is shown (Figure 11).

Gross injuries included transverse or comminuted patellar fractures, split fractures of the femoral condyles (Figures 12, 13), and, in two cases, fracture of the tibial plateau. The majority of the gross injuries were to the patella and the femoral condyles (Table 8). All rigid interface experiments (n=18 for the three flexion angles) resulted in gross fracture of at least one of the bones making up the knee joint. Padded interface experiments resulted in only five gross bone fractures. This represents a 72% reduction

in the incidence of bone fracture at essentially the same load. Subfracture injuries were documented in the patellae impacted with both interfaces and were detected at all flexion angles. Cartilage fissures and vertical occult traumas were common (≈83% frequency) at 60° and 90° of flexion for both interfaces. At 120°, padding reduced the number of subfracture injuries; there were no cartilage fissures and only two subjects suffered occult patellar injuries.

The mathematical model of the impact experiments showed that the maximum shear and tensile stresses at the cartilage surface occurred in different regions (Figure 14). The shear stresses (Table 9) at the cartilage surface were maximal in the region of patellofemoral contact and coincided with regions of greatest contact pressure. The maximum principal stresses at the cartilage surface were typically compressive within the region of contact and tensile outside, and adjacent to, the periphery of patellofemoral contact. The cartilage shear stresses at the interface (Table 9) were slightly larger than at the surface and were typically located adjacent to the maximum surface shear stresses. This coincided with large gradients in the surface stress distribution. The shear stresses at the surface and the interface increased with increasing joint flexion. Similar to the cartilage, the shear and tensile stresses in the trabecular bone were not different for the different impact interfaces and tended to increase with increasing joint flexion.

The shear and tensile stress distributions in the subchondral plate were nearly identical (Figure 15). This was due to a relatively small compressive stress field (< 20% of the tensile stresses) which, based on a simple Mohr's circle analysis, produced tensile stresses which were approximately twice the maximum shear stress for each point in the subchondral bone. Tabulation of the maximum stresses (Table 10) for the 60° subjects

reveals that the average maximum tensile stresses were only reduced 2% with padding versus the rigid interface. The maximum shear stresses were actually 20% greater with padding versus the rigid interface. At the 90° and 120° flexion angles, however, padding reduced both the maximum tensile and shear stresses versus the contralateral experiments conducted with the rigid interface. At 90° of flexion the maximum tensile and shear stresses were reduced 24% and 11%, respectively. Padding produced the greatest reduction in stresses at 120° of flexion; the maximum tensile and shear stresses were reduced 58% and 42%, respectively. For a given interface, the maximum tensile and shear stresses at the 60° and 90° flexion angles were similar (approximately 20 MPa in shear and 40 MPa in tension). The stresses at 120° of flexion, however, were significantly greater, approximately double the stress magnitudes at the lower flexion angles.

Analysis of the principal directions for the subchondral plate revealed tensile stresses acting in the plane of the plate most notably in the proximal-distal direction (Figure 16). This occurred in the region of intra-articular contact and was true for all flexion angles. These tensile stresses may explain the transverse patellar fractures that coincide with the location and direction of the maximum tensile stresses in the subchondral plate (Figure 17). In addition, at 90° and 120° of flexion, there was medial-lateral directed tensile field that also acted within the plane of the subchondral plate. This always occurred in the center of the patella, near the distal pole. The addition of this local tensile stress maxima with the tensile stresses acting in the proximal-distal direction might explain the comminuted patellar fractures (Figure 18).

DISCUSSION

Subfracture experiments

In the current study we investigated the response of the human knee to subfracture transarticular loading at flexion angles of 60, 90 and 120 degrees. We found that the tolerance of the human knee to both gross and microscopic injury increases with flexion angle. Such data may be useful in the clinical setting to aid in the detection and treatment of subfracture injuries. Further, the results of the current study suggest that injury prevention protocols need to account for knee flexion angle to provide optimized protection.

Trends in the experimental data were detected as a function of flexion angle. The contact load, and intra- and extra-articular contact pressures increased with flexion angle while the time to peak load and the contact duration generally decreased with increasing flexion angle. The region of intraarticular contact moved proximally with increasing flexion angle. Subfracture injuries were confined to the posterior side of the patella and were documented within the region of patellofemoral contact. Superficial fissures of cartilage and occult lesions at the bone cartilage-interface were observed for all flexion angles. Superficial fissures were most common in subjects tested at 60° and 120° degrees of flexion, while the number of subjects with occult lesions typically increased with flexion angle. Occult injuries at 60° degrees also included avulsive separations of the cortical bone from the cancellous bone at the respective patellar or quadriceps tendon insertions.

The subfracture injuries documented in the current study are visually similar to those documented in clinical and experimental studies. Cartilage surface fissures have been

documented in human (Zimmerman 1988) and laprine (Atkinson 1998) cartilage following either a single impact or cyclical loading via direct contact of the articular surface with a rigid indentor. Clinically, fissures have been documented via arthroscopy in the ankle and have been associated with chronic pain. Occult vertical clefts have been documented in a chronic OA canine model (Donohue 1983, Thompson 1991) following a single transarticular blow, similar to the current study. In addition, transarticular subfracture impact loads delivered to laprine (Newberry 1996) and porcine (Armstrong 1985, Tomatsu 1992) joints are documented to cause cartilage fissures or occult horizontal cracks, respectively. Regardless of the injury, however, clinical (Johnson-Nurse 1985, Vellet 1991) and experimental (Newberry 1996, Donohue 1983) studies document that superficial and occult injuries are associated with chronic joint pain and degeneration. The occult microfractures documented in the current study might be associated with 'bone bruises' (Vellet 1991). Bone bruises are typically observed adjacent to the osteochondral junction and radiate outward into the trabecular bone (Kapelov 1993). The bruises can be detected via MRI and may represent ruptured arteries (Vellet 1991) in the richly vascularized patella (Arnoldi 1991). Subfracture deformation and compression of the patella have been associated with patellar pain and might be related to a decreased venous drainage and an increase in intraosseous pressure (Arnoldi 1991). While in vivo studies document that these occult lesions can appear resolved after several months, early degenerative changes are documented at 6 months post-insult in 50% of patients suffering bone bruises (Vellet 1991).

The different frequency of subjects suffering cartilage fissures for the various flexion angle groups might be attributed to several factors. First, the reduced frequency of

fissures at 90° might be associated with decreased shear stresses at the surface due to an increase in the contact area (Atkinson 1998). In addition, the cartilage is thickest in the region of contact associated with these experiments. Theoretical studies suggest this would reduce stresses at the articular surface (Eberhardt 1990). Alternately, the region of intraarticular contact coincides with a central medial-lateral band of preexisting surface fibrillation documented previously (Atkinson 1995). An experimental study (Silyn-Roberts 1990) found that it was difficult to mechanically produce a second fissure in the neighborhood of an existing fissure, suggesting that preexisting fibrillation would preclude the development of additional fissures in such a region.

It is reasonable to question whether the subfracture injuries documented in the current study were experimentally produced, an artifact of histological processing, or evidence of a preexisting condition or trauma. This was addressed, in part, in a previous study in which unimpacted, healthy patellae were histologically processed and no subfracture injuries were detected (Atkinson 1995). In addition, the location of the injuries in the current study coincided with the region of intraarticular contact. Because these regions varied greatly with flexion angle, the existence of injuries was easily verified group-by-group. Furthermore, brushing the articular surface with India ink before and after the experiment allowed the visualization of experimentally produced fissures. Finally, the existence of vertical, occult microcracks could be verified via faint shadows in the cartilage which correlated with the histological data.

The experimental data from the current study reflect trends similar to previous studies. Progressive transarticular impact experiments leading to fracture have previously documented a trend of increasing fracture loads with increasing flexion angles

(Haut 1989), although subfracture experiments were not conducted in those studies. Subfracture experiments similar to the current study have been conducted, however, only at a flexion angle of 90° (Atkinson 1995, 1997). The peak load and retropatellar contact pressure from that study deviates by only 10% from the current study. The retropatellar contact area, however, is 30% greater in the current study. This discrepancy is probably related to the film ranges used in the different studies. In the previous study, the lower threshold of the film was 10 MPa versus 2 MPa in the current study. Hence, regions of low contact pressure at the periphery of contact were probably not transduced with the higher threshold film. Experimental (Huberti 1984) and theoretical studies of passive patellofemoral loading document a similar trend with respect to the contact area, region of contact on the retropatellar surface, and the magnitude of the contact pressure. Perhaps not surprisingly the contact pressures documented in the current study are greater (~2-4 times) than intraarticular pressures generated by tensioning the extensor mechanism. This is probably related to the direction and relatively low magnitude of the loads typically attributed to joint flexion during normal activities.

It should be noted, however, that the fracture load data presented in the current study are significantly different than previously documented from experiments conducted on human cadavers. Melvin, et al., (1975) Patrick, et al., (1965) and Powell, et al., (1975)directed impact missiles at the 90 degree flexed knee of whole, seated cadavers using both single and sequential impact protocols. They document fracture loads of approximately 10-17 kN, significantly higher than those of the current study. The increased loads are probably related to the inertial motion of the cadaver and the use of single impact protocols (Powell 1975, Atkinson 1995). The repeated impact protocol

used in the current study likely resulted in accumulated bone microdamage leading to a reduced load at gross fracture. Note, however, that the subfracture experiments in the current study were only impacted once and a range of microscopic injuries and some gross fractures were documented. The subfracture impact energy was based on the energy to cause fracture in the pair-matched contralateral knee. If one assumes the fracture energy may have been attenuated, due to the reasons mentioned above, then the fracture energy was probably conservative. However, subfracture injuries still resulted at 45% of that 'conservative' fracture energy. This suggests that the incipient threshold for the initiation of subfracture injuries is probably less than 45% of the fracture energy. Another reason for the lower than expected fracture loads in the current study was the use of a rigid impact interface. This allowed us to make more unambiguous comparisons to past studies which largely serve as the basis for the current injury criterion used by the automotive industry (Viano 1977).

Finally, the current study suggests that a subfracture knee injury criterion which accounts for the influence of flexion angle would provide the greatest level of protection, both acutely and in the longterm. This would likely produce a more conservative criterion than currently exists. For example, knee injury associated with car accidents is based on gross bone fracture from experiments conducted at a flexion angle of 90°. However, the current study suggests that the knee is less tolerant to gross and subfracture injuries at flexion angles less than 90°. In addition, subfracture injuries are more difficult to detect acutely and are associated with chronic joint morbidity. States (1970) suggested that lower extremity injury criteria should be based on subfracture injury thresholds. This would require the mechanisms for subfracture injury to be established to allow the

design of preventative strategies in car interiors, protective sports equipment, and floor designs for the elderly. Preventing such injuries would reduce the longterm economic and societal costs currently associated with knee trauma.

Impact interface experiments

The current criterion, used by the automotive industry, for knee injury is based on impact loads which produce gross bone fracture at a 90° flexion angle. However, studies have suggested that the contact area over the knee may also be an important parameter in the injury tolerance of the knee, and that at lower flexion angles the knee may be more susceptible to injury. In the current study, paired impact experiments were conducted on isolated human knees flexed 60°, 90°, or 120°.

Fracture producing experiments were conducted on one knee at a given load and the contralateral knee was impacted at the same load with a padded interface. The fractures typically occurred in the patella and were oriented transversely. On average, the padded interface produced a 300% increase in contact area versus the rigid interface. Padding also reduced the incidence of gross injury by 72%.

A theoretical stress analysis of the rigid and padded experiments showed that the shear and tensile stresses in the cartilage and the shear stresses in the trabecular bone were not different for the different interfaces. However, the tensile and shear stresses in the subchondral bone were found to be reduced at the 90° and 120° flexion angles with padding. The tensile and shear stresses were dramatically reduced at 120° of flexion which might explain the absence of patellar fractures and the low frequency of occult patellar injuries. For both impact interfaces, the stresses at 120° were approximately double the stress magnitudes at the lower flexion angles. This might be explained by the

patellar motion at the higher versus lower flexion angles. At 120° of flexion, the patella is driven into the femoral condyles and is essentially undergoes simple compression (Haut 1989; Viano 1978). At the 60° and 90° flexion angles, the patella is both driven into the condyles and undergoes a proximal migration, putting the patellar tendon in tension. Thus, in the region of intraarticular contact, the patella undergoes compression, however, at the distal pole, the cortical and trabecular bone are put in tension. These differences between the lower and higher flexion angles might explain the different loads and stresses documented for the different flexion angles. While both tensile and shear stresses were reduced at 90° of flexion, only the reduction in tensile stresses was significant. At this flexion angle, there was one patellar fracture and numerous vertical occult injuries documented with the padded interface. The benefit of the padding may be the significant reduction in tensile stresses which may have prevented the occult injuries from opening into gross fractures. Padding did not appreciably alter the subchondral bone stresses at the 60° flexion angle. This might explain the incidence of two gross patellar fractures and the high frequency of subfracture injuries at this flexion angle. This also suggests that this flexion angle will be difficult to protect with padding.

For all flexion angles and both interfaces, the tensile stresses were generally maximal within the region of intraarticular contact and the maximum stresses acted within the plate in a proximal-distal direction. These tensile stresses are important as there location and direction are consistent with the observed transverse fractures. The origin of these stresses may be explained by the shape of the intraarticular contact area, which is essentially a wide band of contact across the patella (Figure 19). This is similar to modeling the femoral condyle as a long, cylindrical indentor compressing the

retropatellar surface. This would subject the subchondral plate to local bending which would develop large tensile stresses in the subchondral plate.

In addition to the transverse fractures, comminuted fractures were documented at the 90° and 120° flexion angles. These fractures typically appeared as a transverse fracture with the addition of a proximal-distal oriented fracture emanating from the distal pole. It should be noted that the distal fracture was not in the region of intraarticular contact. The distal fracture may be explained by the contact areas and stress distributions associated with elevated flexion angles. At 90° and 120° of flexion, the intraarticular contact area was essentially two lobes of contact on the medial and lateral patellar facets; this arose from contact with the medial and lateral femoral condyles. This essentially puts the patella in three point bending and generated regions of tensile stress acting in the medial-lateral direction. Alternately, at 60° of flexion, the patella contacted the femoral groove which produced a narrow band of contact across the distal pole of the patella. For this contact, only transverse fractures were documented, again in the region of contact. Analysis of the model revealed that the tensile stresses only acted in the proximal-distal direction; there were no medial-lateral acting tensile stresses. Thus, the contact areas and regions of contact associated with different flexion angles alters the state of stress in the patella and the potential for injury.

The current study shows that the injury tolerance of the knee varies with flexion angle and the degree of load distribution over the knee. These data may be helpful in developing a more comprehensive injury criteria. Such a criterion might account for the flexion angle and the manner in which the load is distributed over the knee. Injury prevention strategies might also benefit from the stress analysis of the patella. For

example, subchondral plate tensile stresses were associated with gross fractures. Thus, injury prevention strategies may be studied theoretically and use the reduction of such stresses as a method to reduce the risk of injury to the knee.

ACKNOWLEDGMENTS

This study was supported by a grant (R49/CCR503607) from the Centers for Disease Control and Prevention. Its contents are solely the responsibility of the authors and do not necessarily represent the official views of the Centers for Disease Control and Prevention. The authors wish to gratefully acknowledge Ms. Jane Walsh for help in the interpretation of histological slides and Mr. Cliff Beckett for technical support. We are also indebted to Hexcel Corporation and Mr. John Porter for technical and materials support. Finally, we wish to thank Mrs. Kathy Pearson and the Michigan Tissue Bank for solicitation of donors and retrieval of joints.

REFERENCES

1. Armstrong C, Mow V, Wirth C (1985) Biomechanics of impact-induced microdamage to articular cartilage: a possible genesis for chondromalacia patella. In: Amer Acad of Orth Surg Symp on Sports Med, ed by G Fenerman. pp70-84

2. Arnoldi C (1991) Patellar Pain. Acta Orthop Scand 62: 1-29

3. Ateshian, G., Kwak, S., Soslowsky, L., and Mow, V (1994) A stereophotographic method for determining in situ contact areas in diarthrodial joints, and a comparison with other methods. Journal of Biomechanics 27(1):111-124

4. Atkinson, T.S., Haut, R.C., and Altiero, N.J. (1998) An Investigation of Biphasic Failure Criteria for Impact Induced Fissuring of Articular Cartilage. J of Biomechanical Engineering (In Press)

5. Atkinson PJ, Haut RC (1995) Insult to the human cadaver patellofemoral joint: effects of age on fracture tolerance and occult injury. 39th Stapp Car Crash Conference: 281-294

6. Atkinson PJ, Haut RC (1995) Subfracture Insult to the Human Cadaver Patellofemoral Joint Produces Occult Injury. Journal of Orthopaedic Research 13: 936-944

7. Atkinson PJ, Garcia JJ, Altiero NJ Haut RC (1997) The influence of impact interface on human knee injury: implications for instrument panel design and the lower extremity injury criterion. 41st Stapp Car Crash Conference, SAE: 167-180. paper 973327

8. Atkinson PJ, MacKenzie C, Haut RC (1998) Joint fracture load prediction using geometrical, physical and pathological measures: the human knee. SAE International Congress: paper 980358

9. Dischinger PC, Kerns TJ, Kufera JA (1995) Lower extremity fracturesin motor vehicle collisions: the role of gender and height. Accident Analysis and Prevention 27(4): 601-606

10. Dischinger P, Cushing B, Kerns T (1992) Lower extremity fractures in motor vehicle collisions: influence of direction of impact and seatbelt use. Proc 36th Conf AAAM Portland, OR pp319-326

11. Donohue MJ, Buss D, Oegema T, Thompson R (1983) The Effects of Indirect Blunt Trauma on Adult Canine Articular Cartilage. The Journal of Bone and Joint Surgery 65-A(7): 948-957

12. Eberhardt, A., Keer, L., Lewis, J., and Vithoontien, V. (1990) An Analytical model of joint contact. Journal of Biomechanical Engineering 112:407-413

13. Eckstein F, Muller-Gerbl M, Putz R (1992) Distribution of subchondral bone density and cartilage thickness in the human patella. Journal of Anatomy 180: 425-433

14. Grelsamer R, Proctor C, Bazos A (1994) Evaluation of patellar shape in the sagittal plane: A clinical analysis. Amer J Sports Med 22: 61-66

15. Hale JE, Brown TD (1992) Contact stress gradient detection limits of pressensor film. J Biomech Eng 114:352-358, 1992

16. Haut R (1989) Contact Pressures in the Patello-femoral Joint during Impact Loading on the Human Flexed Knee. Journal of Orthopaedic Research 7: 272-280

17. Hayashi S, Choi H, Levine R, Yang K, King A (1996) Experimental and analytical study of knee fracture mechanisms in a frontal knee impact. 40th Stapp Car Crash Conference 161-171

18. Hering W, Patrick L (1977) Response Comparisons of the Human Cadaver Knee and a Part 572 Dummy Knee to Impacts by Crushable Materials. Twenty-First Stapp Car Crash Conference 21: 1015-1053

19. Huberti H, Hayes W, Stone J, Shybut G (1984) Force ratios in the quadriceps tendon and ligamentum patellae. Journal of Orthopaedic Research 2: 49-54

20. Huelke D, O'Day J, States J (1982) Lower Extremity Injuries in Automobile Crashes. Accid Anal & Prev 14: 95-106

21. Johnson-Nurse C, Dandy D (1985) Fracture-Separation of Articular Cartilage in the Adult Knee. The Journal of Bone and Joint Surgery 67-B(10: 42-43

22. Kapelov R, Teresi L, Bradley W, Bucciarelli N, Murakami D, Mullin W, Jordan J (1993) Bone Contusions of the knee;Increased Lesion Detection with fast Spin-Echo MR Imaging with Spectroscope Fat Saturation. Radiology 901-904

23. MacKenzie EJ, Siegel JH, Shapiro S, et.al. (1988) Functional Recovery and Medical Costs of Trauma: An analysis by Type and Severity of Injury. Journal of Trauma 28: 281-298

24. Melvin J, Stalnaker R, Alem N, Benson J, Mohan D (1975) Impact Response and Tolerance of the Lower Extremities. Stapp Car Crash Conf 19: 543-559

25. Newberry W, Haut R (1996) The effects of subfracture impact loading on the patellofemoral joint in a rabbit model. 40th Stapp Car Crash Conference 149-159

26. Patrick L, Kroell C, Mertz H (1965) Forces on tehehuman body in simulated Crashes. Stapp Car Crash Conf 9: 237-259

27. Powell W, Ojala S, Advani S, Martin R (1975) Cadaver Femur Responses to Longitudinal impacts. Stapp Car Crash Conf 19: 561-579

28. Silyn-roberts, H. and Broom, N. (1990) Fracture Behavior of Cartilage-On-Bone in response to repeated impact loading. Connective Tissue Research 24:143-156

29. States J (1970) Traumatic Arthritis-- A Medical and Legal Dilemma. Ann Conf of the Amer Assoc for Automotive Med 14: 21-28

30. States J (1986) Adult occupant injuries of the lower limb. In: Biomechanics and medical aspects of lower limb injuries. Warrendale, PA: SAE 97-107

31. States J (1970) Traumatic arthritis--a medical and legal dilemma. Ann Conf of the Amer Assoc for Automotive Med 14:21-28

32. Thompson RC, Oegema TR, Lewis JL, Wallace L (1991) Osteoarthritic changes after acute transarticular load. The Journal of Bone and Joint Surgery 73-A(7): 990-1001

33. Tomatsu T, Imai N, Takeuchi N, Takahashi K, Kimura N (1992) Experimentally produced fractures of articular cartilage and bone. J Bone Joint Surg 3:457-461, 1992

34. Upadhyay S, Moulton A, Srikrishnamurthy K (1983) An analysis of the late effects of traumatic posterior dislocation of the hip without fractures. J Bone Joint Surg 65: 150-152

35. Vellet AD, Marks PH, Fowler PJ, Munro TG (1991) Occult post-traumatic osteochondral lesions of the knee: prevalence, classification, and short-term sequelae evaluated with MR imaging. Radiology 178(1):271-276

36. Vener MJ, Thompson RC, Lewis JL, Oegema TR (1992) Subchondral damage after acute transarticular loading: an in vitro model of joint injury. J Orthop Res 10:759-765, 1992

37. Viano D (1977) Considerations for a femur injury criterion. 21st Stapp Car Crash Conference 445-473

38. Viano DC, Stalnaker RL (1980) Mechanisms of Femoral Fracture. Journal Biomechanics 13: 701-715

39. Viano, D., Culver, C., Haut, R., Melvin, J., Bender, M., Culver, R., and Levine, R. (1978)Bolster impacts to the knee and tibia of human cadavers and an anthropomorphic dummy. Soc.Automotive Engineers :403-428

40. Zimmerman, N.B., Smith, D.G., Pottenger, L.A., and Cooperman, D.R. (1988) Mechanical disruption of human patellar cartilage by repetitive loading In Vitro.. Clinical Orthopaedics and Related Research (229):302-307

TABLES

Table 1: *Experimental design*

Flexion Angle	Subfracture experiments	Impact interface experiments
60°	n=6	n=6
90°	n=6	n=6
120°	n=6	n=6

Table 2: *Load-time data*

Knee Flexion Angle	Peak Load	Time to peak	Contact Duration (Pulse)
	N	ms	ms
60	2394.5±849.5*	9.5±1.1	18.7±1.5
90	3848.0±1511.8	5.4±0.9#	12.6±3.2#*
120	5368.5±1723.3	5.3±1.2#	16.5±3.6
*Significantly different from 120° flexion angle # Significantly different from 60° flexion angle			

Table 3: *Impact energies and anterior contact areas and pressures*

Knee Flexion Angle	Impactor Energy	Anterior Contact Area	Anterior Contact Pressure
Degrees	J	mm^2	MPa
60	18.7±11.5*	603.1±301.2	5.0±1.3*
90	16.5±6.3*	711.1±444.1	10.4±3.1*
120	32.9±4.0	507.9±228.4	23.6±8.8
*Significantly different from 120° flexion angle			

Table 4: *Patellofemoral contact areas and pressures*

Knee Flexion Angle	Patellofemoral Contact Area	Patellofemoral Contact Pressure
	mm^2	MPa
60	431.4±307.9	9.4±4.5
90	651.7±312.6	12.7±5.6
120	609.3±296.9	16.5±4.0

Table 5: *Gross and microscopic injuries from impact with a rigid interface: paired experiments at three flexion angles at fracture and subfracture level impact energies. Injury classifications (A-E) are defined in Figure 5.*

		Fracture level experiments					Contralateral subfracture experiments				
Flexion Angle	Subject	A	B	C	D	E	A	B	C	D	E
60	H72	1	0	1	1	0	0	0	1	1	0
60	H73	1	0	1	0	0	1	0	1	1	0
60	H74	1	0	1	1	0	1	0	0	1	0
60	H75	1	0	1	0	0	1	0	0	1	0
60	H76	1	1	0	1	0	0	1	0	0	0
60	H77	1	1	1	1	0	0	1	0	1	0
	Total Injuries	**6**	**2**	**5**	**4**	**0**	**3**	**2**	**2**	**5**	**0**
90	H57	1	1	1	1	0	0	0	0	0	0
90	H58	1	0	1	0	0	0	0	0	1	0
90	H60	1	1	1	1	0	0	0	1	1	0
90	H63	1	0	1	0	0	1	1	1	0	0
90	H64	1	0	1	0	0	1	0	1	0	0
90	H65	1	1	0	1	0	0	1	1	1	0
	Total Injuries	**6**	**3**	**5**	**3**	**0**	**2**	**2**	**4**	**3**	**0**
120	H66	0	1	1	1	1	0	0	1	1	0
120	H67	1	1	1	0	0	0	0	1	1	0
120	H68	1	0	0	0	0	0	0	0	1	0
120	H69	1	0	1	0	0	0	0	1	1	0
120	H70	0	0	1	0	1	0	1	0	0	0
120	H71	1	0	1	0	0	0	1	0	0	0
	Total Injuries	**4**	**2**	**5**	**1**	**2**	**0**	**2**	**3**	**4**	**0**
Grand Totals for all flexion angles		**16**	**7**	**15**	**8**	**2**	**5**	**6**	**9**	**12**	**0**

Table 6: *Anterior contact area on the cadaver knee*

Flexion Angle	Rigid Impact Interface	Padded Impact Interface
60°	346±127	1494±757*
90°	729±88#	1614±667*
120°	703±114#	2990±626

*Significantly different than 120° padded interface
#Significantly different than 60° rigid interface

Table 7: *Peak loads for paired impact experiments on each cadaver knee (kN)*

Flexion Angle	Rigid Impact Interface	Padded Impact Interface
60°	3.71±1.98	4.31±0.9
90°	5.04±1.4	5.47±1.83
120°	5.76±1.38	8.28±1.2*#
*Significantly different than 120° padded interface #Significantly different than 60° rigid interface		

Table 8: *Gross and microscopic injuries from impact with rigid and padded interfaces: paired experiments at three flexion angles. Injury classifications (A-F) are defined in Figure 5.*

		Rigid Impact Interface Experiments						Contralateral Padded Interface Experiments					
Flexion Angle	Subject	A	B	C	D	E	F	A	B	C	D	E	F
60	H72	1	0	1	1	0	0	0	0	0	0	0	0
60	H73	1	0	0	0	0	0	0	1	1	1	0	0
60	H74	1	1	0	1	0	0	1	1	0	1	0	0
60	H75	1	0	1	1	0	0	0	0	1	1	0	0
60	H76	1	0	1	0	0	0	1	0	0	0	0	0
60	H77	1	0	1	0	0	0	0	0	0	1	0	0
	Total Injuries	**6**	**1**	**4**	**3**	**0**	**0**	**2**	**2**	**2**	**4**	**0**	**0**
90	H57	1	0	1	1	0	0	1	0	1	0	0	0
90	H58	1	0	1	0	0	0	0	0	1	1	0	0
90	H60	1	0	1	0	0	0	0	0	1	0	0	0
90	H63	1	0	1	0	0	0	0	0	1	0	0	0
90	H64	1	1	0	0	0	0	0	1	1	0	0	0
90	H65	1	0	1	0	0	0	0	0	0	1	0	0
	Total Injuries	6	1	5	1	0	0	1	1	5	2	0	0
120	H66	1	0	0	1	0	0	0	1	1	0	0	0
120	H67	0	0	0	1	1	0	0	0	0	0	0	0
120	H68	0	0	0	1	1	0	0	0	0	0	1	0
120	H69	0	0	0	0	0	1	1	1	1	0	0	0
120	H70	1	1	1	0	1	0	0	0	0	0	1	0
120	H71	1	0	0	0	0	1	1	0	0	0	0	0
	Total Injuries	**3**	**1**	**1**	**3**	**3**	**2**	**2**	**2**	**2**	**0**	**2**	**0**
Grand Totals for all flexion angles		**15**	**3**	**10**	**7**	**3**	**2**	**5**	**5**	**9**	**7**	**2**	**0**

Table 9: *Shear stresses in the cartilage at two sites: articular surface and at the tidemark (interface with the bone).*

	Cartilage: surface		Cartilage: tidemark	
Flexion Angle	Rigid	Padded	Rigid	Padded
60°	2.9±1.3	2.2±1.0	3.1±1.1	2.6±1.5
90°	3.0±1.3	2.4±1.4	4.6±3.0	3.5±2.2
120°	8.2±3.0	5.7±2.7	8.1±2.1	6.9±3.4

Table 10*: Shear and tensile stresses in the subchondral bone*

	Shear stress		Tensile stress	
Flexion Angle	Rigid	Padded	Rigid	Padded
60°	18.2±6.3*	21.9±12.2*	36.5±13.3*	35.9±21.0*
90°	22.8±4.8*	20.5± 8.3*	48.1±9.7*	38.9±10.1*&
120°	58.1± 17.2	41.0±23.1&	125.1±37.9	79.4±39.1&
*Significantly different than 120° &Significantly different than the contralateral, rigid interface experiment				

FIGURES

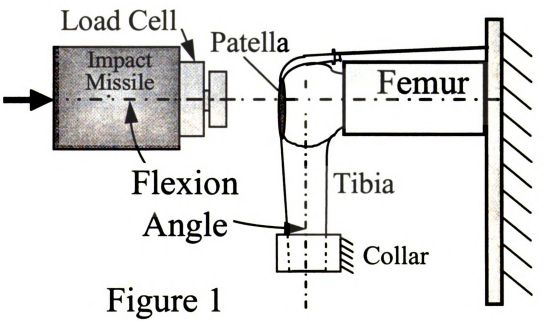

Figure 1

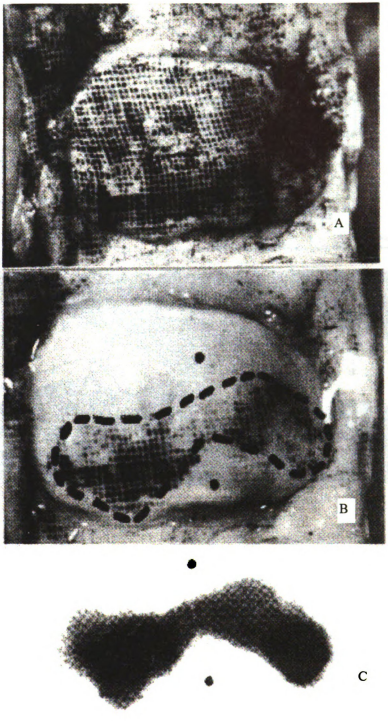

Figure 2

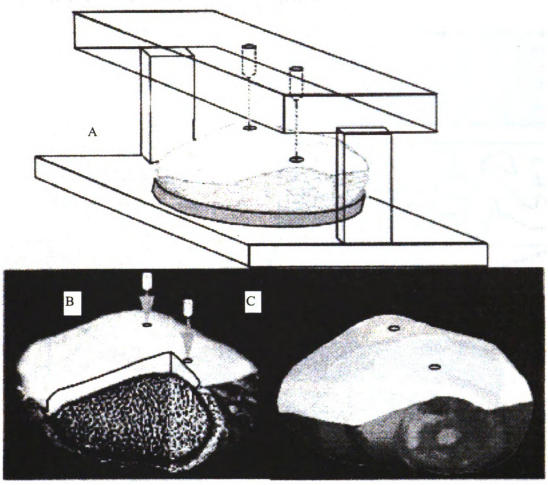

Figure 3

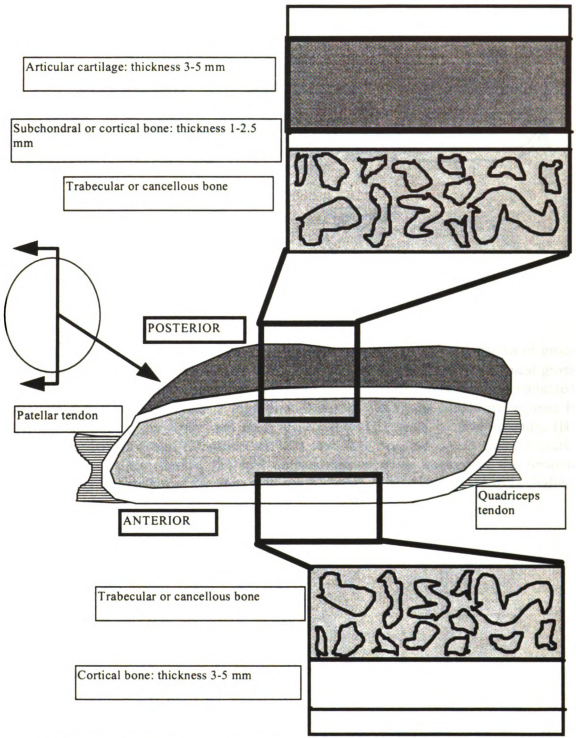

Figure 4: A schematic depicting areas of interest for analysis to identify injuries to the cartilage, subchondral bone, and trabecular bone.

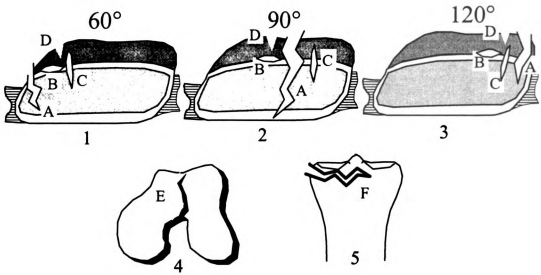

Figure 5: Schematics of a saggital patellar section depicting the typical location of gross and microscopic injuries for the 60°, 90°, and 120° flexion angles (1, 2, 3). Typical gross injuries to the femur (4) and tibia (5) are also shown. The labels correspond to tabulated injury data shown in Tables and . Injuries A-D are specific to the patella and injuries E and F are specific to the femur and tibia, respectively: (A) gross patellar fracture, (B) horizontally oriented occult microfracture, (C) vertically oriented occult microfracture, (D) superficial cartilage fissure, (E) split or comminuted gross fracture of the femoral condyles, (F) gross fracture of the tibial plateau (this injury is also termed a Type I 'Salter' fracture).

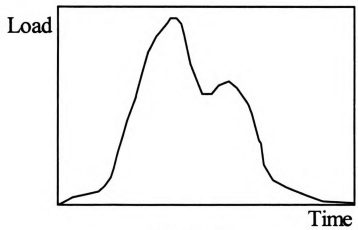

Figure 6

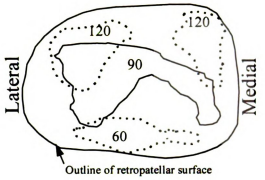

Figure 7

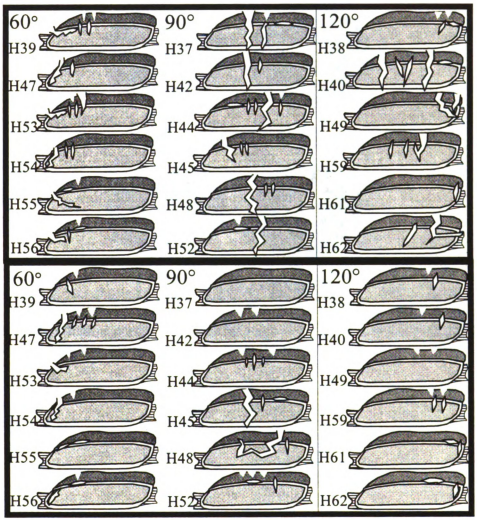

Figure 8: Schematics of patellar injuries documented via analysis of histological samples and sections for subjects in which both knees were impacted with a rigid impact interface in separate experiments. The top box represents fracture level experiments and the bottom box represents the pair-matched contralateral experiments conducted at a subfracture impact energy (45% of the fracture energy). The subject mumber is presented next to each schematic. The schematic and injuries are defined in Figure 4 and 5.

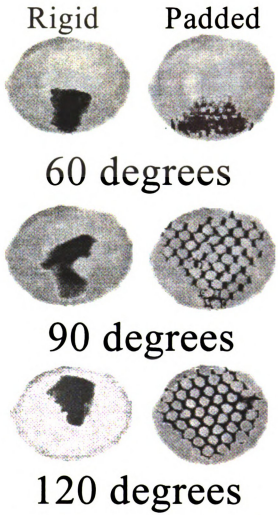

Figure 9: Extra-articular contact regions (between the impactor and the anterior patella) for the rigid and padded interfaces for the three flexion angles.

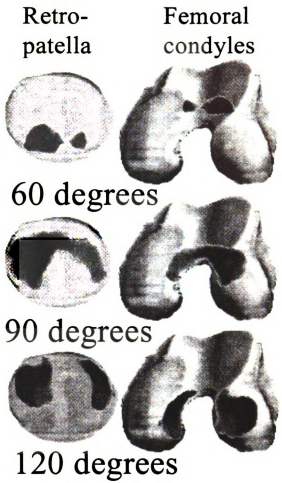

Figure 10: Intra-articular contact regions superposed on the retropatellar and femoral articular surfaces. The regions of intra-articular contact were identical for the impact experiments conducted with rigid or padded impact inetrfaces except as noted in Figure 11.

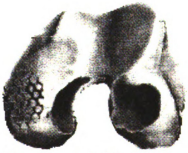

Figure 11: Experiments at the 120° flexion angle with the padding typically resulted in direct contact between the padding and the medial femoral condyle. This occurs because the medial condyle is in a similar plane as the anterior patellar surface for elevated fflexion angles.

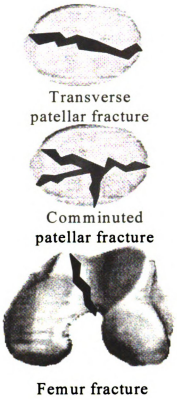

Figure 12: Predominant gross injuries to the patella and femur.

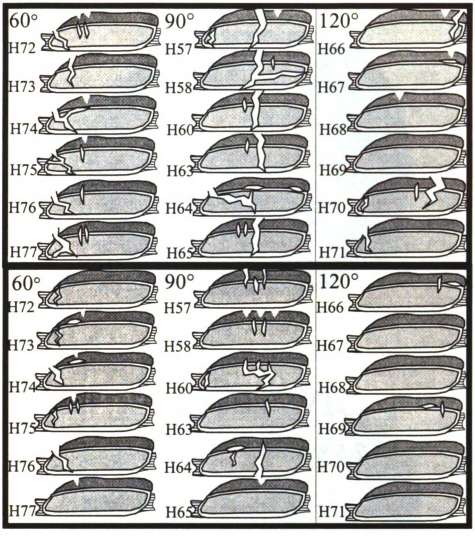

Figure 13: Schematics of patellar injuries documented via analysis of histological samples and sections for subjects in which one knee was impacted with a rigid impact interface in a fracture level experiment. The contralateral knee was then impacted at the rigid interface-fracture load with a padded interface. The top box represents fracture level-rigid interface experiments and the bottom box represents the pair-matched contralateral experiments conducted with the padded interface. The subject mumber is presented next to each schematic. The schematic and injuries are defined in Figure 4 and 5.

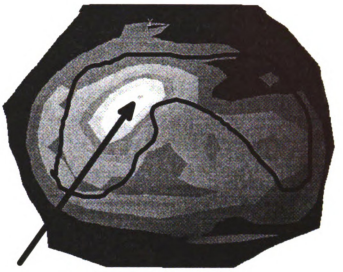

Maximum
shear stress

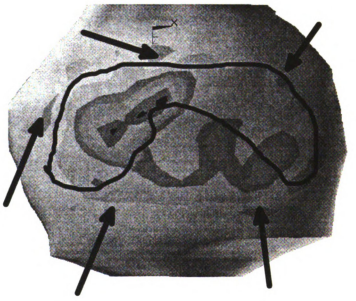

1st principal stress

Figure 14: Arrows point to regions of maximum stress at the cartilage surface for a typical experiment conducted at a 90° flexion angle. The outline depicts the region of intraarticular contact.

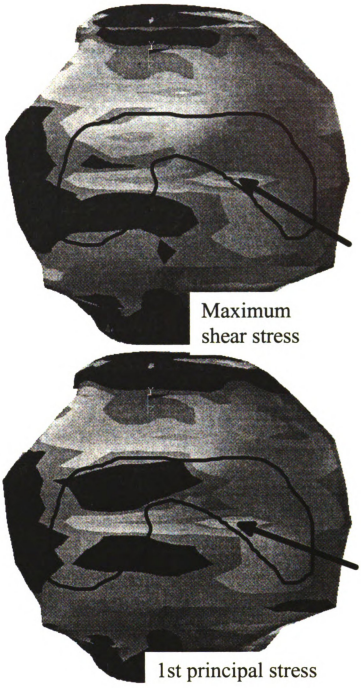

Figure 15: Arrows point to regions of maximum stress in the subchondral plate for a typical experiment at a 90° flexion angle. The outline depicts the region of intraarticular contact.

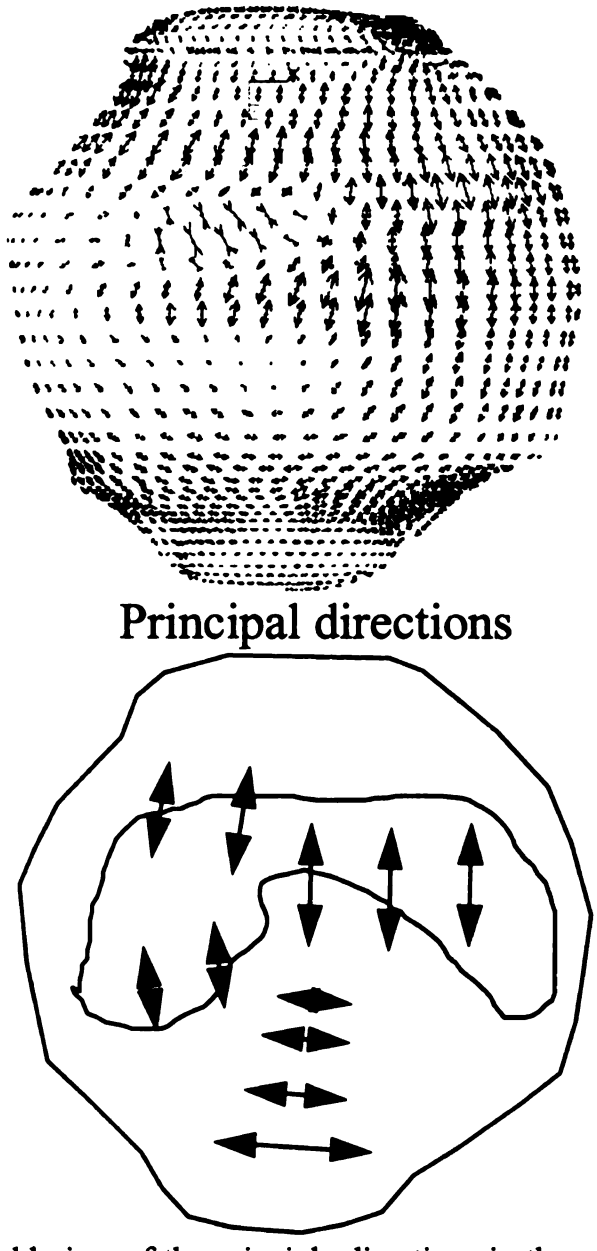

Figure 16: A whole-field view of the principle directions in the subchondral plate and a simplified schematic showing the dominant tensile stresses and their predominant directions for the stress field shown in Figure 14.

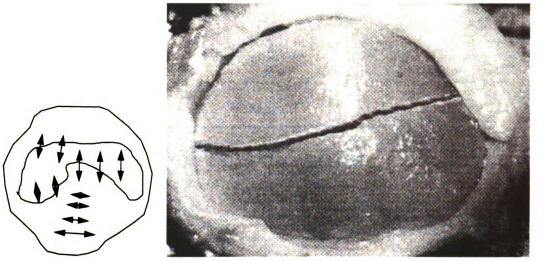

Figure 17: An example of how the tensile stresses acting in the proximal-distal direction (shown at left) are associated with a simple, transverse patellar fracture.

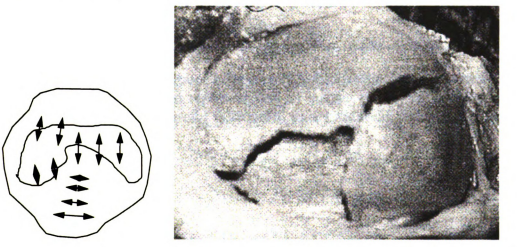

Figure 18: An example of a more complicated, comminuted fracture in which both the proximal-distal and medial-lateral tensile stresses (shown at left) are associated with two planes of fracture.

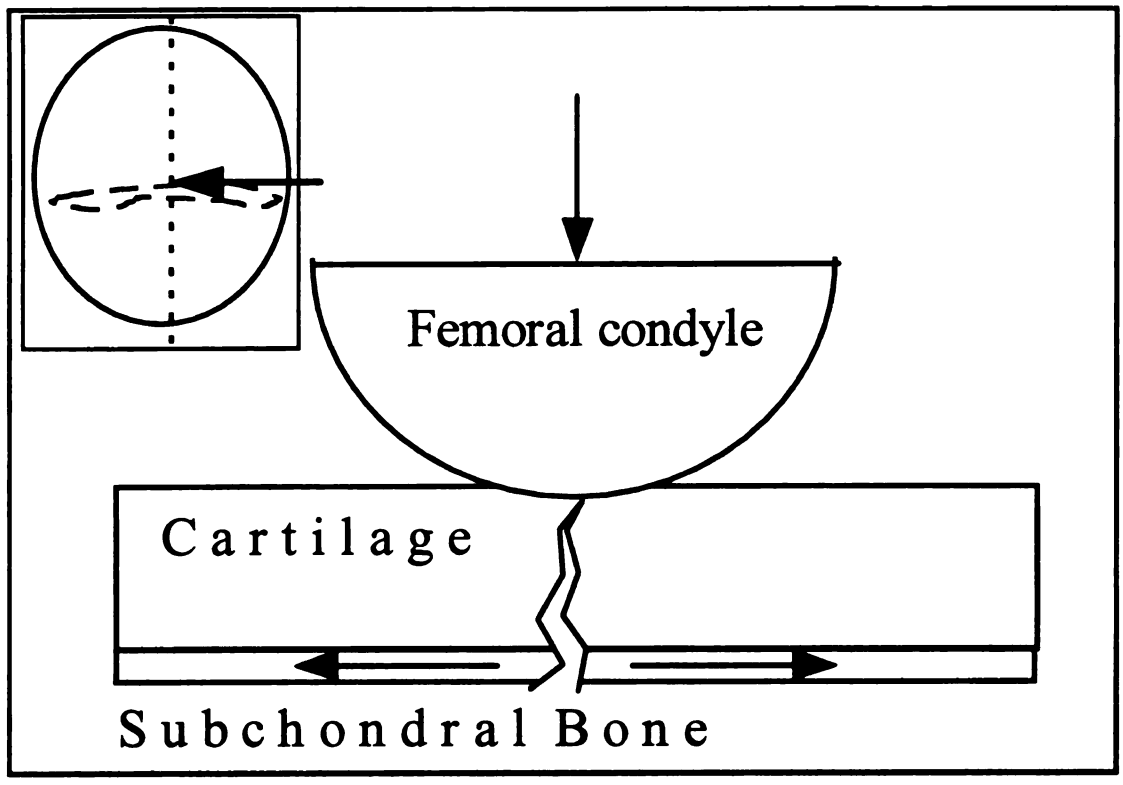

Figure 19: A schematic of the retropatellar contact and a saggital section passed through the patella (inset). An idealized representation of contact (along the saggital section viewed in the direction of the arrow) is modeled as a cylindrical indentor compressing the articular cartilage.

CHAPTER 8

A PROPOSED MODEL TO TRANSFORM CADAVER KNEE INJURY CRITERIA TO THE HYBRID III DUMMY

Patrick Atkinson, Nicholas Altiero*, Roger Haut
Orthopaedic Biomechanics Laboratories
*Department of Material Science and Mechanics
Michigan State University

Chris Eusebi, Vivek Maripudi, Tim Hill, Kiran Sambatur
Breed Technologies, Sterling Heights, Michigan

ABSTRACT

A fracture threshold of 10 kN is currently used in the automotive industry to predict gross fracture of bone to the knee, thigh and hip. However, recent studies show that load alone is not sufficient to predict joint trauma. Experiments on isolated cadaver knees show that increasing the contact area for a given contact force over the knee significantly reduces the occurrence of gross and microscopic injuries at a given contact load over the knee. These data, however, are not directly applicable to the Hybrid III knee because the contact force-area relationships for the cadaver and dummy differ. In the current study transformations were established between the cadaver injury data and the dummy knee. Numerous experiments were conducted on the dummy to establish comparisons with the cadaver data for the isolated knee. Mathematical models were developed to address transformation of these data to the whole dummy. Sled tests were run, using an idealized instrument panel, to show the utility of the new injury curves in the prediction of joint trauma for depowered air bags, restrained versus unrestrained occupants, etc. This study

begins to show a strategy whereby injury data from isolated cadaver knee experiments can be utilized to predict injurious conditions in the automobile crash environment using anthropomorphic dummies.

INTRODUCTION

Traumatic lower limb injuries in frontal car crashes continues to be a significant problem. Numerous field studies conducted in the last 20 years conclude that lower extremity injuries occur in about one of every three car accidents (Bourret 1977, Hartemann 1977, Morgan 1991, Otte 1996, Pattimore 1991, Thomas 1995, Siegal 1993, States 1986). In addition, these studies document that the knee is the most injured body region within the lower extremity. The knee may either suffer fracture or subfracture (contusions, lacerations, abrasions) injuries. The majority of knee injuries result from high speed contact with the instrument panel or steering column. In an effort to prevent the more severe, fracture level injuries, the National Highway Traffic and Safety Administration adopted an injury criterion in 1976 (Viano 1977). The criterion states that axial femoral loads cannot exceed 10 kN when certifying new automobiles with anthropomorphic dummies at a crash velocity of 13.4 m/s (30 mph). The criterion is based on a bone fracture threshold derived from human cadaver impact experiments (Patrick 1965, Melvin 1975, Powell 1975, Viano 1980). These impact experiments, conducted in the 1960's and 70's, delivered impact loads to the 90° flexed knee. Gross fracture at the knee, femoral shaft, or hip occurred at loads ranging from 10-17 kN for these tests conducted on whole cadavers. Analysis of the data from these experiments suggests, however, that peak load may not be the sole parameter of interest. Of the 68

total knee impact experiments, 32 were conducted with a rigid interface and 38 were conducted with padded interfaces of variable thickness and composition. In general, the peak loads were similar, regardless of the impact interface. However, even at similar loads, the padded interface experiments resulted in a 65% and 14% reduction in patellar and femoral condyle fractures, respectively, versus the rigid interface experiments. One explanation may be related to the increased extraarticular contact area over the patella and possibly, the femoral condyles.

Several recent studies specifically address the relationship between peak load, contact area over the knee, and the associated injury potential. In studies on the isolated human cadaver knee, rigid and padded interfaces were used to deliver a single impact load to the isolated knee joint (Atkinson 1997). The protocol consisted of impacting one knee with a rigid interface and then impacting the contralateral knee at the same load with a padded interface. All rigid interface experiments resulted in small contact areas over the anterior surface of the patella. All of these experiments produced gross fractures of the patella or subfracture injuries at the bone-cartilage interface. Alternately, padded impacts resulted in significantly greater contact areas over the patella and no gross or microscopic injuries. Theoretical models of the patella reveal that the shear and tensile stresses in the subchondral plate were reduced 70% with padding. In another study, a stress-based parametric analysis of contact area and impact load shows that greater impact loads can be tolerated with greater contact area over the knee (a:Atkinson 1998). These studies underscore the association between elevated tissue stresses and tissue failure, rather than simply peak load and bone fracture. It should be noted, however, that the magnitude of

the load is still an important variable. Indeed, the stresses in an arbitrary body of material are related to the magnitude of the load as well as its distribution over the body. However, stress is a derived quantity and cannot be experimentally quantified. But, based on the above studies, it appears that contact area over the knee is associated with the magnitude of tissue stresses and the incidence of injury. Thus, knowledge of the impact load and the contact area over the knee might allow a rough estimation of the stress magnitudes. This may provide a more accurate injury criterion than peak load alone.

To establish an injury criterion based on peak load and contact area would require an understanding of the loads and areas associated with impact trauma events. Currently, impact loads are routinely measured in the automotive industry during experimental crash simulations. Instrumented anthropomorphic dummies serve as human surrogates and are designed with a load cell in the femoral shaft. Thus, the load associated with knee-instrument panel contact can easily be recorded. The contact area is not currently measured, however, established methods (i.e. pressure sensitive film, instrumented pressure mats) do exist to measure the contact area. The load-area relationship for the dummy, though, may not be directly applicable to the human. While it is true that the dummy is designed to imitate the human cadaveric response (for which the dummy is based on), limited experimental data (Hering 1977, Nyquist 1974) suggest that the load-area relationship for the dummy can be significantly different from the human. Further, these differences may be accentuated based on the composition of the impact interface (i.e. rigid, padded). The current study was designed to address these issues.

The overall study aim was to develop a transformation between the load-area relationship between the dummy and the human. Impact experiments were conducted on the isolated dummy and cadaver knee using different impact interfaces. The transformation is based on impact energy and empirically derived load-area data. This transformation is based on the fact that impact energy is one of the few parameters which can be independently controlled *a priori*. Thus, while the load-area impact response of the knee is clearly a function of its geometry and material properties, the response of the dummy and cadaver knee was related based on consistent levels of impact energy.

In addition to the isolated knee tests, automotive crash simulations were also conducted using whole anthropomorphic dummies with a variety of restraint scenarios. Load-area data were recorded to provide an example of the data transformation from the isolated cadaver knee to the automotive crash environment with the dummy.

METHODS AND MATERIALS

Experimental protocol

Impact experiments were conducted on the knee of a 50th percentile Hybrid III dummy and a group of 16 pair of isolated cadaver knees with an age of 69±15 years (12 male, 3 female, 1 unknown). The cadavers had an average height of 1.75±0.17m and a mass of 70.4±11.8. The cadaveric data comes from separate, parallel studies of impact trauma. The specific test protocols were similar for the dummy and cadaver knees and are provided later. For the cadaveric experiments, tissues were procured from donors with no prior history of joint trauma and/or evidence of advanced joint pathology (areas of denuded bone, advanced chondromalacia, etc.). Shortly after death, the patellofemoral

joint was examined through a medial incision. Joint preparations were excised approximately 15 cm from the knee proper and stored at -20° C until the day of testing. The tissues were allowed to thaw at room temperature overnight prior to testing. Superficial tissues proximal to the femoral condyle were excised and the femoral shaft was cleaned with alcohol. The femur was potted in a cylindrical steel sleeve with room temperature curing epoxy, and was mounted horizontally to a rigid test frame (Figure 1). Specimens were tested at a 90° flexion angle. The flexion angle was maintained by constraining the tibia by means of a rigid collar attached to the distal end of the tibia. A loosely knotted tether was attached to the quadriceps tendon to position the patella against the femur. The knot was such that minimal load was required to cause slippage, thus minimizing tensile loads in the tendon during impact. The patella was brushed with India ink and photographed prior to impact to document any baseline surface roughness or fibrillation.

The isolated dummy knee was mounted to the testing fixture in a similar fashion as the cadaver knees (Figure 2). The dummy knee component included the distal half of the thigh and the entire lower leg without the foot.

To impart the impact force, a 4.8 kg impact missle was accelerated to a given pre-impact velocity, while aligned on two steel guide rails and supported on four nylon blocks to minimize friction. A rigid (6061-T6 aluminum), 'stiffly' padded (3.3 MPa crush strength aluminum Hexcel), or 'softly' padded (1.65 MPa crush strength aluminum Hexcel impact interface) impact interface (Figure 3) was mounted to the front of a load transducer which was attached to the impact missile (Figure 1,2) (Model 3173-2k, Lebow

Products, Troy, MI, USA). In the dummy tests, the femur load cell (Figure 2) was used as a redundant measure of the impact load. The impact mass was selected based on previous studies (Atkinson 1997, Haut 1989). Pilot studies indicated that the load transducer and attached mass would not resonate during impact on the human knee. Load data were recorded continuously on a personal computer via a 16 bit A/D board (Model DAS 1600, Computer Boards, Inc., Mansfield, MA, USA). Load data were inertially compensated (Atkinson 1997) and sampled at 20,000 Hz.. The impacting mass was accelerated to a predetermined velocity by adjusting the air pressure in a pneumatic impact cannon. Velocity of the mass was measured prior to impact on the knee using two infrared optical sensors (Part No. OR518-ND, Digi-Key Corporation, Thief River Falls, MN). These sensors are designed with a 5 mm separation between the emitter and detector. A metal tab connected to the impact mass crossed the 5 mm gap interrupting the first sensor and then the second. The individual sensors were separated by 76.2 mm to eliminate cross-talk.

The cadaver experiments started with a fracture level test on one knee of a cadaver using the rigid interface. The protocol consisted of sequentially increasing the velocity of the impact missle in separate experiments, so as to progressively increase the impact energy (2, 10, 22, 38, 60, 86, 112 J). The experiment was terminated when impact loading resulted in a visible fracture of bone. In four of the subjects, the contralateral knee was subjected to a single impact with the rigid interface at 45% of the impact energy that caused bone fracture in the first limb (Donohue 1983, Thompson 1991, a:Atkinson 1995). In the remaining 12 subjects, six contralateral knees were impacted once with the stiff

padding and six with the soft padding at the rigid interface fracture load for that subject. Data from experiments with any of the interfaces in which a gross fracture of bone was noted were excluded from further analysis in the current study.

Impact experiments on the dummy knee were conducted in a similar fashion as the cadaver. A similar range of impact energies were used to impact the knee with the rigid and padded interfaces. For the rigid interface, testing was terminated when the maximum load for the dummy femur load cell was approached (13.3 kN). Testing with the padded interface was terminated when successive experiments did not yield additional contact area.

The anterior contact area associated with the impact event was recorded with pressure sensitive film (Prescale, Itochu Int., Quebec, CA). The film was sandwiched between two sheets of polyethylene film (0.05 mm thick/sheet) to prevent exposure to body fluids and help reduce shear loading artifacts (Huberti). This also minimized frictional forces between the impactor and the knee. To optimize the measurement of contact area, low range pressure sensitive film was used (range: 2-10 MPa). The pressure sensitive film was calibrated in a servohydraulic testing machine (Model 1330, Instron, Canton, MA, USA) using a previous methodology (Atkinson 1997). Following the impact experiment, the film was removed from the packet and analyzed using established methods (b:Atkinson 1998) to determine the contact area over the knee. Briefly, the film images were digitally scanned at 150 dpi. A commercial computer code (SigmaScan) was then used to outline the images to determine the contact area.

Transformation protocol

The load-contact area-impact energy data were tabulated for all dummy-cadaver experiments. These data were used to develop a transformation for the load-area relationship between the cadaver and dummy for the impact interfaces used in this study. The protocol essentially consisted of four steps:

1) Tabulate the load-area-energy data for the dummy knee for a given interface:

Example: Rigid interface data presented in Table 1 (note the arbitrary assignments of the data to the given coordinate axes). Ideally, a linear or polynomial fit of the above data in three space would define the dummy impact reponse for the rigid interface over the entire range of the data. This would allow a direct transformation to the cadaver. Unfortunately, regressions are restricted to functions of one variable. This problem was overcome by first performing a linear regression on the load-area data (Figure 4).

2) Next, fit a surface to the area, load, energy data. This was performed by conducting an iterative, nonlinear regression through these data via the Marquardt-Levenburg method (SigmaStat). This requires an assumption of the functional form that will fit the data along with initial value assumptions of the function's constant values. The simplest surface is a plane which can be written as $z=(-ax-by+d)/c$. The program iterates to identify the values of the constants which will minimize the sum squared error (i.e. min Σ [energy data - $(-ax-by+d)/c]^2$) to produce the best fit planar fit of the data (Figure 5).

3) Now, a continuous array of area, load, energy data may be obtained by the following:

A) Write an incremental array of contact areas over a meaninful range determined by the experimental data (Table 2).

B) Using the regression equation determined in 1) above, calculate the corresponding loads for the given contact areas (Table 3).

C) Using the equation determined in 2), calculate the corresponding energy for the given area-load data (Table 4).

4) Match energies between the cadaver and the dummy to transform the area-load data: Example: A cadaver impact experiment with a rigid interface resulted in an area-load data point of 236 mm^2 and 992 N at an impact energy of 2.09 J. Using the table above, this impact energy corresponds to an area-load data point in the dummy of 653 mm^2 and a load of 1742 N. This transformation shows that the dummy load-area data point is greater than the cadaver (Figure 6).

This protocol (step 4) was repeated for the remaining cadaver data points in which the rigid impact interface was used.

The entire procedure (steps 1-4) was repeated for the stiff padding and then the soft padding.

Anthropomorphic dummy tests

In addition to the isolated knee tests, car crash simulations were performed with a whole dummy. These tests were conducted to illustrate the utility of the transformation methodology to a realistic trauma environment. The tests were conducted on a HYGE (HYdraulic Gas Energized) test system using a generic buck and a 50th percentile male dummy. The dummy was placed in the front passenger seat (Figure 7 A,B) placed in the

mid-position. A 76.2 mm thick piece of aluminum Hexcel (1.65 MPa Hexcel) served as the knee bolster (Figure 7 C). The surface of the bolster facing the dummy's knees was covered with a sheet of 'low' range (2-10 MPa) pressure sensitive film (Figure 7 D). Similar to the isolated knee tests, the film was encased in a polyethylene packet secured peripherally to the Hexcel. Two tests were run with the given parameters (Table 5). The femur load cell and inner/outer knee clevis force transducers were sampled per SAE specification J211. The clevis transducers are designed to measure loads transmitted to the knee via foot and/or tibial contact with the toepan and/or instrument panel. The femoral load cell is designed to measure axial loads acting on the thigh. Thus, a portion of the femoral load cell data arises from direct loading of the knee and the remainder represents contact with components distal to the knee. The loads on the knee were therefore taken as the femoral load cell data less the clevis load data. The associated contact area was determined in the same manner as the isolated knee tests. These data were then plotted on a transformed graph to estimate the cadaveric response.

RESULTS

The load-contact area response for the isolated cadaver and dummy knee were fit with linear functions for a given impact interface (Table 6). In general, the linear fits of the data yielded high correlation coefficients. For the cadaver, the rigid interface load-area response was significantly steeper than with padding (Figure 8). There was no difference, however, in slopes between soft or stiff padding. Analysis of the y-intercepts revealed that the rigid interface curve originated near the origin. The padded interface curves, however, intercepted the y-axis well above the origin.

For the dummy, the three impact interfaces resulted in three distinct load-area curves (Figure 9). The slope of the curves increased with increasing impact interface stiffness. In addition, the rigid and 3.3 Hex curves appeared to originate from nearly the same point: 400 sq mm and zero load. The 1.65 Hex curve originated from near the origin.

As in the example given in the Methods section, the load-area data in the dummy was always greater than the cadaver load-area data for a given impact energy. This was true for all impact interfaces. Partly because of this, it was necessary to forward extrapolate some of the padded dummy data to allow transformation of some padded cadaver data points. The transformations are shown for each of the interfaces (Figures 10-12). A consistent x-y scale was used for all of the graphs to allow a direct comparison between the graphs. A summary plot of all the transformed cadaver knee load-area data for the rigid, 3.3 MPa Hexcel, and 1.65 MPa Hexcel interfaces to the dummy knee allows a comparison of the different data associated with the different interfaces (Figure 13).

Anthropomorphic dummy tests

The femur/clevis loads, and associated contact areas for the two sled tests were similar for both tests (Table 7). These load-area data points can be plotted with the data in Figure 13 to provide a comparison with the transformed cadaver data (Figure 14). The dummy load-area data points from the sled tests fall on the 1.65 Hex curve and at a reduced load and area than the majority of the transformed isolated tests.

DISCUSSION

The main objective of the current study was to develop a methodology to convert impact induced load-area data for the cadaver knee to the dummy knee. Currently, the

prediction of knee injury in car crash simulations is assessed with an instrumented dummy. The current injury criterion is based solely on a peak load associated with bone fracture in the human cadaver. However, experimental and theoretical studies show that the injury tolerance of the human knee to impact loading increases with increasing contact area over the knee. Accounting for the load and area over the knee would be yield a more sensitive injury criterion.

To develop a wide range of load-area data points, three impact interfaces were used to impact 16 pair of isolated human cadaver knees and the Hybrid III isolated dummy knee. Separate experiments conducted at increasing levels of energy to gradually increased the load and contact area. The transformation of the cadaver load-area data to the dummy was performed by comparing similar levels of impact energy. For a given impact interface, the load and area in the dummy was always greater than the cadaver. Linear functions provided a good fit of the load-area data for the cadaver and the dummy. The slope of the load-area curves for the dummy were significantly different based on the impact interface. The stiffer interfaces resulted in more elevated slopes. For the cadaver, the slope of the rigid interface curve was greater than with padding, however, no distinction could be made between the padded interface curves.

Analysis of the cadaver and dummy load-area regression lines highlights some differences between the different interfaces and between the dummy and cadaver knees. For example, the wide range of y-intercepts showed that a majority of the load-area curves did not intersect the origin. For the padded cadaver experiments, the load-area curves intersected the positive y-axis, well above the origin. This implies that a finite impact load

is associated with zero contact area. Clearly, this is not a realistic outcome; in general, it would be expected that zero load should be associated with zero contact area. The rigid interface curve did, however, pass very near the origin. One possible explanation for the difference between the rigid and padded cadaver curves is probably related to the impact energies used for the cadaver experiments. The rigid interface experiments started at very low energies which were progressively increased. Thus, data representing low loads and low contact areas were generated with the initial impact energies for a given cadaver. The rigid interface experiments provided a good definition of the cadaver response near the origin and the expected result (i.e. passing through the origin) occurred. Alternately, in the padded cadaver experiments, only one impact was delivered per cadaver at an elevated impact energy. Thus, there was no experimental data at low loads and low contact areas. Additional experiments are needed with the padded interfaces to elucidate the cadaver response for low impact energies.

For the dummy, the load-area curves for all of the impact interfaces passed very near a point approximately represented by a 400 mm^2 contact area and zero load. This suggests that a finite contact area would develop for zero load. Again this appears to be counterintuitive. However, the shape of the anterior dummy knee might account for the large contact areas at low loads. The dummy knee has a rounded profile but is essentially flat in the medial-lateral direction (Figure 15). Thus, even low loads could be associated with large contact areas due to the inherent shape of the dummy knee.

The utility of the transformation presented in the current study could be an assessment of 'safe' pairs of load and area on the knee. Cadaver experiments in which injuries were

documented could be used to establish the load-area injury threshold for a given interface stiffness. If a sufficiently diverse group of interfaces were used, a comprehensive injury threshold could be developed. Based on the experimental cadaver data presented in the current study in addition to injury producing experiments not presented in this study, several fundamental conclusions can be made.

1) **Load and area data points are unique to a given interface.** That is to say, a rigid interface and a styrofoam interface would never yield an identical load and area, regardless of impact energy. Clearly, knee geometry material properties and will vary between cadavers and this will result in some data scatter. However, tests conducted on an 'average' cadaver of a given anthropometry will yield a similar response as the dummy: increasing interface stiffness will yield load-area curves of increasing slope.

2) **For a given impact interface stiffness, there exists a maximum load (and associated area) which can be tolerated without an associated injury.** While this may be intuitively obvious, this idea would allow the data from the current study to be used in conjunction with experiments which resulted in injury to develop a more comprehensive criterion. To illustrate this idea, consider a load area curve for a given interface (Figure 16). After a threshold level of load and area has been attained, injury will occur. A logistic regression superposed on the load area line would identify the statistical probability of injury (Figure 17). Injury probability curves could then be added to identify the injury risk associated with a given load and area (Figure 18).

Similar experiments as those mentioned in the previous example are needed on a wide range of impact interfaces. The relative risk for each interface could again be determined

by conducting logistical regressions along each load-area curve. For example, cadaveric experiments conducted with several impact interfaces might produce injury and non-injury data points (Figure 19). Note that as the impact interface stiffness reduces, the load and area increases before injury occurs. The 50% injury risk has been arbitrarily chosen for this example and is denoted by the arrows for each interface curve. If the 50% injury risk points were connected, the entire field of load-area data points associated with this level of injury risk could be interpolated (Figure 20). Thus, any load-area data point above the 50% curve would be associated with a high probability of injury. Any data points below this line, would be associated with a lower probability of injury. Interestingly, this injury criterion is independent of the impact interface. Thus, tests can be conducted without requiring a material's characterization of the impact interface prior to determining an associated injury risk. Rather, simply the load and area are sufficient to identify the risk of a given impact event.

Currently, the automotive injury criterion is based on gross bone fracture. However, consideration of subfracture or microscopic injuries might be warranted to produce a more conservative criterion. While fracture level injuries of the patella, tibia, and femoral condyles are a well documented impact induced injury, numerous recent studies also document microscopic bone and cartilage injuries (Armstrong 1985, a:Atkinson 1995, b:Atkinson 1995, Atkinson 1997, Donohue 1983, Thompson 1991). These injuries may be even more insidious than gross injuries because they are difficult to detect acutely and are typically not treated. Further, these subfracture traumas have been associated with chronic joint pain and disease (Upadhyay 1983, States 1970). Thus, preventing

subfracture injuries will be an important consideration in new injury criteria. Incidentally, there is theoretical evidence that preventing subfracture injuries would yield a conservative criterion. This is based on the hypothesis that preventing subfracture injuries will also prevent the fracture level injuries. This follows from the idea that fracture level injuries begin as subfracture microfractures which can coalesce and form gross fractures if additional energy is imparted to the joint. Future work is needed to develop a comprehensive injury criterion which accounts for subfracture level injuries, different impact interfaces, and the differences between the dummy and human cadaver knee.

ACKNOWLEDGMENTS

This study was supported by a grant (R49/CCR503607) from the Centers for Disease Control and Prevention. Its contents are solely the responsibility of the authors and do not necessarily represent the official views of the Centers for Disease Control and Prevention. The authors wish to gratefully acknowledge Mr. Cliff Beckett for technical support. We are also indebted to Hexcel Corporation and Mr. John Porter for technical and materials support. Finally, we wish to thank Mrs. Kathy Pearson and the Michigan Tissue Bank for solicitation of donors and retrieval of joints.

REFERENCES

1. Armstrong C, Mow V, Wirth C (1985) Biomechanics of impact-induced microdamage to articular cartilage: a possible genesis for chondromalacia patella. In: Amer Acad of Orth Surg Symp on Sports Med, ed by G Fenerman. pp70-84

2. a:Atkinson PJ, Haut RC (1995) Insult to the human cadaver patellofemoral joint: effects of age on fracture tolerance and occult injury. 39th Stapp Car Crash Conference: 281-294

3. b:Atkinson PJ, Haut RC (1995) Subfracture Insult to the Human Cadaver Patellofemoral Joint Produces Occult Injury. Journal of Orthopaedic Research 13: 936-944

4. Atkinson PJ, Garcia JJ, Altiero NJ Haut RC (1997) The influence of impact interface on human knee injury: implications for instrument panel design and the lower extremity injury criterion. 41st Stapp Car Crash Conference, SAE: 167-180. paper 973327

5. a:Atkinson PJ, MacKenzie C, Haut RC (1998) Joint fracture load prediction using geometrical, physical and pathological measures: the human knee. SAE International Congress: paper 980358

6. b:Atkinson PJ, Newberry WN, Atkinson TS, Haut (1998) A method to increase the sensitive range of pressure sensitive film. Journal of Biomechanics. In review

7. Bourret P, Corbelli S, Cavallero C (1977) Injury agents and impact mechanisms in about 350 frontal crashes in field accidents. 21st Stapp Car Crash Conference 215-258

8. Donohue MJ, Buss D, Oegema T, Thompson R (1983) The Effects of Indirect Blunt Trauma on Adult Canine Articular Cartilage. The Journal of Bone and Joint Surgery 65-A(7): 948-957

9. Hartemann F, Thomas C, Henry C, Foret-Bruno J, Faverjon G, Tarriere C, Got C, Patel A (1977) Belted or not belted: The only difference between two matched samples of 200 car occupants. 21st Stapp Car Crash Conference 97-150

10. Haut R (1989) Contact Pressures in the Patello-femoral Joint during Impact Loading on the Human Flexed Knee. Journal of Orthopaedic Research 7: 272-280

11. Hering W, Patrick L (1977) Response Comparisons of the Human Cadaver Knee and a Part 572 Dummy Knee to Impacts by Crushable Materials. Twenty-First Stapp Car Crash Conference 21: 1015-1053

12. Melvin J, Stalnaker R, Alem N, Benson J, Mohan D (1975) Impact Response and Tolerance of the Lower Extremities. Stapp Car Crash Conf 19: 543-559

13. Morgan R, Eppinger R, Hennessey B (1991) Ankle joint injury mechanism for adults in frontal automitve impact. 35th Stapp Car Crash Conference: 189-198

14. Nyquist GW (1974) Static force-penetration response of the human knee. 18th Stapp Car Crash Proceedings. Paper 741189

15. Otte D (1996) Biomechanics of lower limb injuries of belted car drivers and the influence of intrusion and accident severity. 40th Stapp Car Crash Conference 193-206

16. Patrick L, Kroell C, Mertz H (1965) Forces on tehehuman body in simulated Crashes. 9th Stapp Car Crash Conf: 237-259

17. Pattimore D, Ward E, Thomas P, Bradford M (1991) The nature and cause of lower limb injuries in car crashes. 35th Stapp Car Crash Conference: 177-188

18. Powell W, Ojala S, Advani S, Martin R (1975) Cadaver Femur Responses to Longitudinal impacts. Stapp Car Crash Conf 19: 561-579

19. Siegal J, Mason-Gonzales S, Dischinger P, Cushing B, Read K, Robinson R, Smialek J, Heatfield B, Hill W, Bents F, Jackson J, Livingston D, Clark C (1993) Safety belt restraintsand compartment intrusions in frontal and lateral motor vehicle crashes: mechanisms of injuries, complications and acute care costs. The Journal of Trauma 34:736-759.

20. States J (1970) Traumatic Arthritis-- A Medical and Legal Dilemma. Ann Conf of the Amer Assoc for Automotive Med 14: 21-28

21. States J (1986) Adult occupant injuries of the lower limb. In: Biomechanics and medical aspects of lower limb injuries. Warrendale, PA: SAE 97-107

22. Thomas P, Charles J, Fay P (1995) Lower limb injuries-the effect of intrusion, crash severity and the pedals on injury risk and injury type in frontal collisions. 39th Stapp Car Crash Conference: 265-280

23. Thompson RC, Oegema TR, Lewis JL, Wallace L (1991) Osteoarthritic changes after acute transarticular load. The Journal of Bone and Joint Surgery 73-A(7): 990-1001

24. Upadhyay S, Moulton A, Srikrishnamurthy K (1983) An analysis of the late effects of traumatic posterior dislocation of the hip without fractures. J Bone Joint Surg 65: 150-152

25. Viano D (1977) Considerations for a femur injury criterion. 21st Stapp Car Crash Conference: 445-473

26. Viano DC, Stalnaker RL (1980) Mechanisms of Femoral Fracture. Journal of Biomechanics 13: 701-715

TABLES

Table 1: *Contact area-load-impact energy data from impacting the Hybrid III 50th male knee. See text for specific details regarding the test protocol.*

Contact Area (x)	Impact Load (y)	Impact Energy (z)
550 mm^2	1115 N	2 J
950 mm^2	4180 N	9.1 J
1284 mm^2	7500 N	20.9 J
1420 mm^2	9960 N	35 J
1637 mm^2	11850 N	43.3 J

Table 2: *Array of incremental contact areas*

Contact Area (x)	Impact Load (y)	Impact Energy (z)
651 mm^2		
653 mm^2		
655 mm^2		
657 mm^2 . . .		

Table 3: *Regression-derived load data points associated with the given contact areas.*

Contact Area (x)	Impact Load (y)	Impact Energy (z)
651 mm^2	1722 N	
653 mm^2	1742 N	
655 mm^2	1762 N	
657 mm^2 . . .	1782 N . . .	

Table 4: *Associated impact energies for the given area-load data points. The load and area data were inserted into an equation describing a best-fit plane describing the area-load-energy experimental data.*

Contact Area (x)	Impact Load (y)	Impact Energy (z)
651 mm^2	1722 N	2.00 J
653 mm^2	1742 N	2.09 J
655 mm^2	1762 N	2.32 J
657 mm^2	1782 N	2.53 J
.	.	.
.	.	.
.	.	.

Table 5: *Experimental parameters for crash simulations using a HYGE sled and a Hybrid III 50th male anthropomorphic dummy*

Test	Delta V	Air Bag	Seat Belt
a	14 mph	depowered	none
b	30 mph	none	3-point

Table 6: *Regression parameters describing the load-area relationship for the cadaver and dummy knee using three impact interfaces of variable stiffness.*

cadaver	m	b	r^2
rigid	6.50	130.40	0.63
3.3 Hex	2.15	1758.00	0.94
1.65 Hex	3.17	615.30	0.98
dummy	m	b	r^2
rigid	10.06	-4828.00	0.98
3.3 Hex	3.51	-1374.00	0.99
1.65 Hex	1.42	50.35	0.99

Table 7: *Load-area data from experimental crash simulations with a whole dummy.*

Test	Limb	Contact area (mm^2)	Peak load (N)
a	right	3945.1	5535
a	left	4058.5	5665
b	right	4891.0	5739
b	left	3655.5	6174

FIGURES

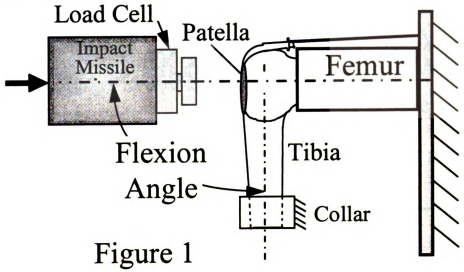

Figure 1

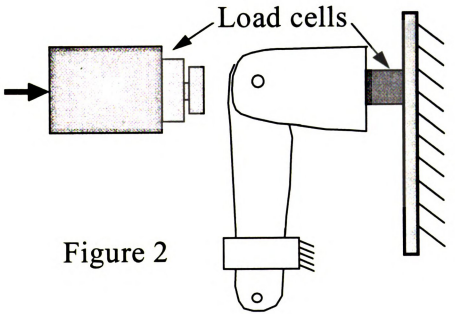

Figure 2

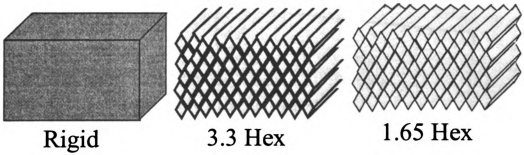

Figure 3

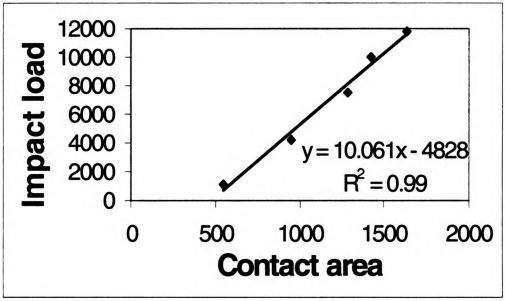

Figure 4: A best-fit linear fit of the load-area data from the rigid interface experiments on the dummy knee.

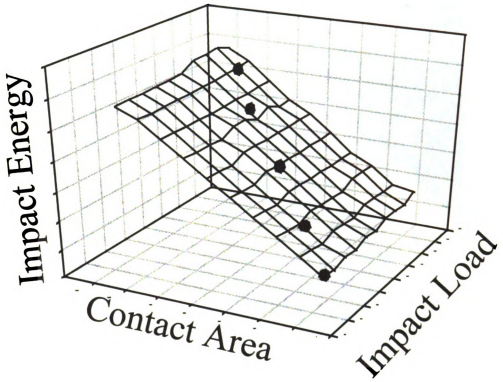

Figure 5: A best-fit plane describing the experimental area-load-energy data points. The plane was determined by iterating to identify the parameters which minmized the sum-squared error. Please see the text for more details on this procedure.

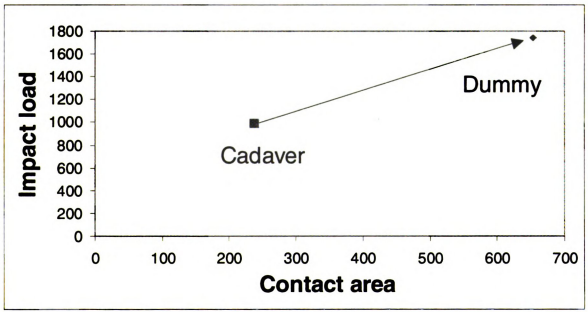

Figure 6: An example of transforming one load-area data point from the cadaver to the dummy

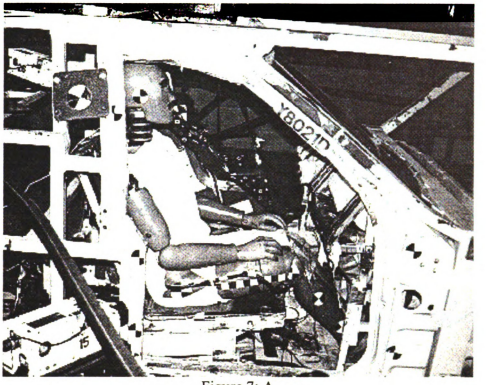

Figure 7: A

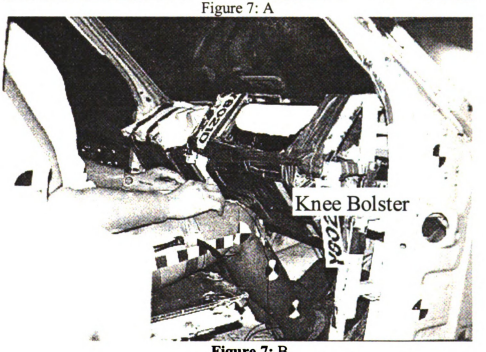

Figure 7: B

Figure 7: The pre-test experimental setup for HYGE sled crash simulations (A,B).

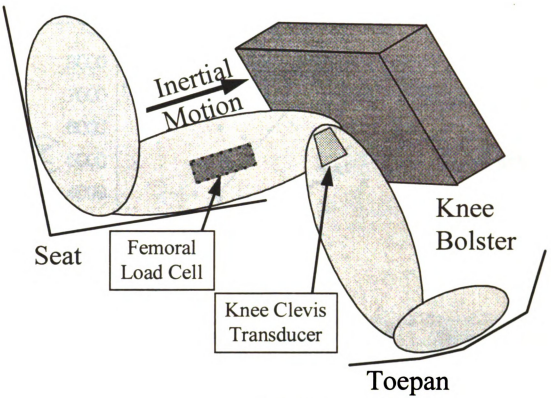

Figure 7: C

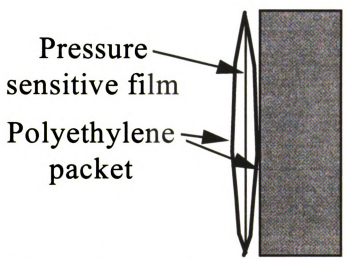

Side view of knee bolster
with attached film packet

Figure 7: D

Figure 7: A schematic of the dummy and the Hexcel knee bolster (C). A schematic sideview of the knee bolster showing the pressure film packet.

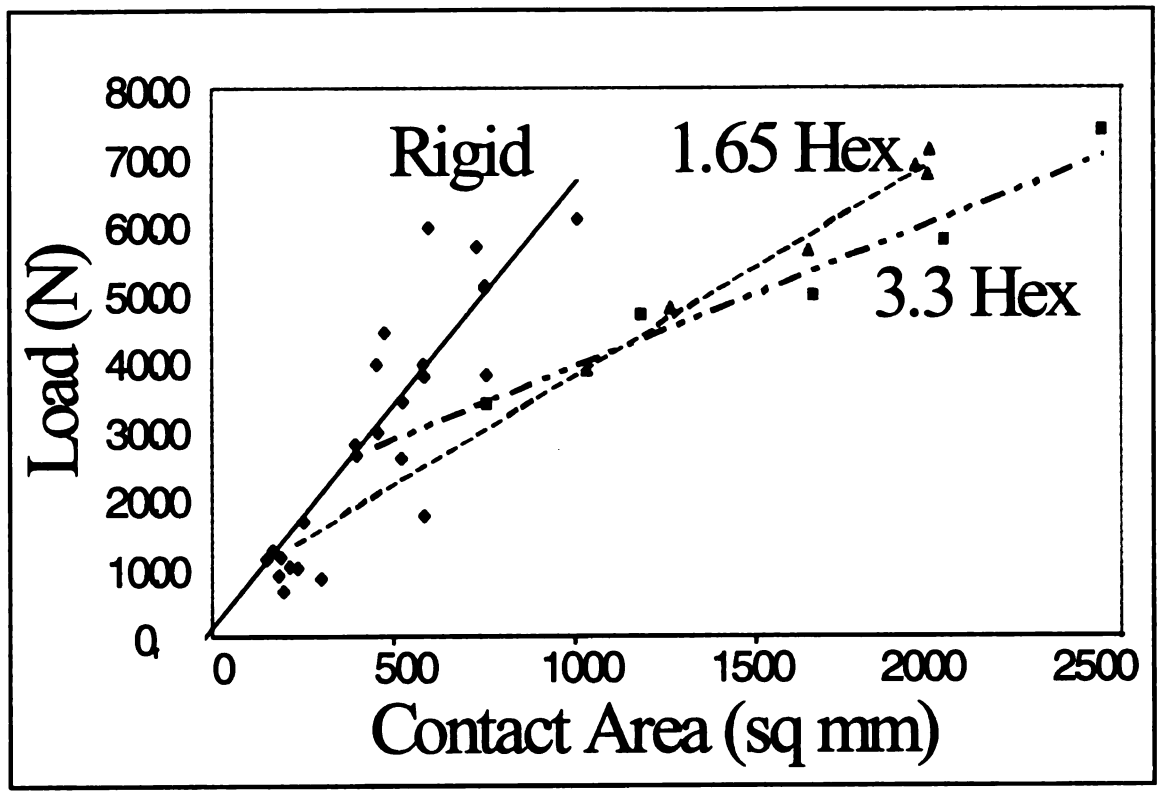

Figure 8

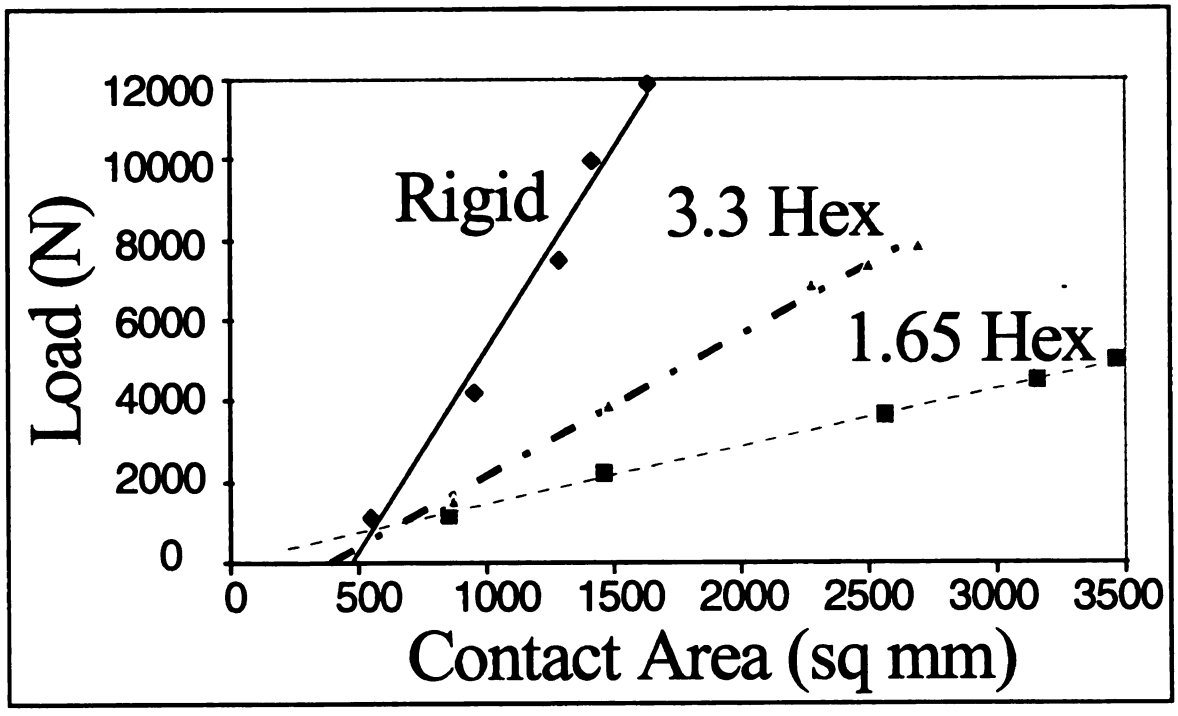

Figure 9

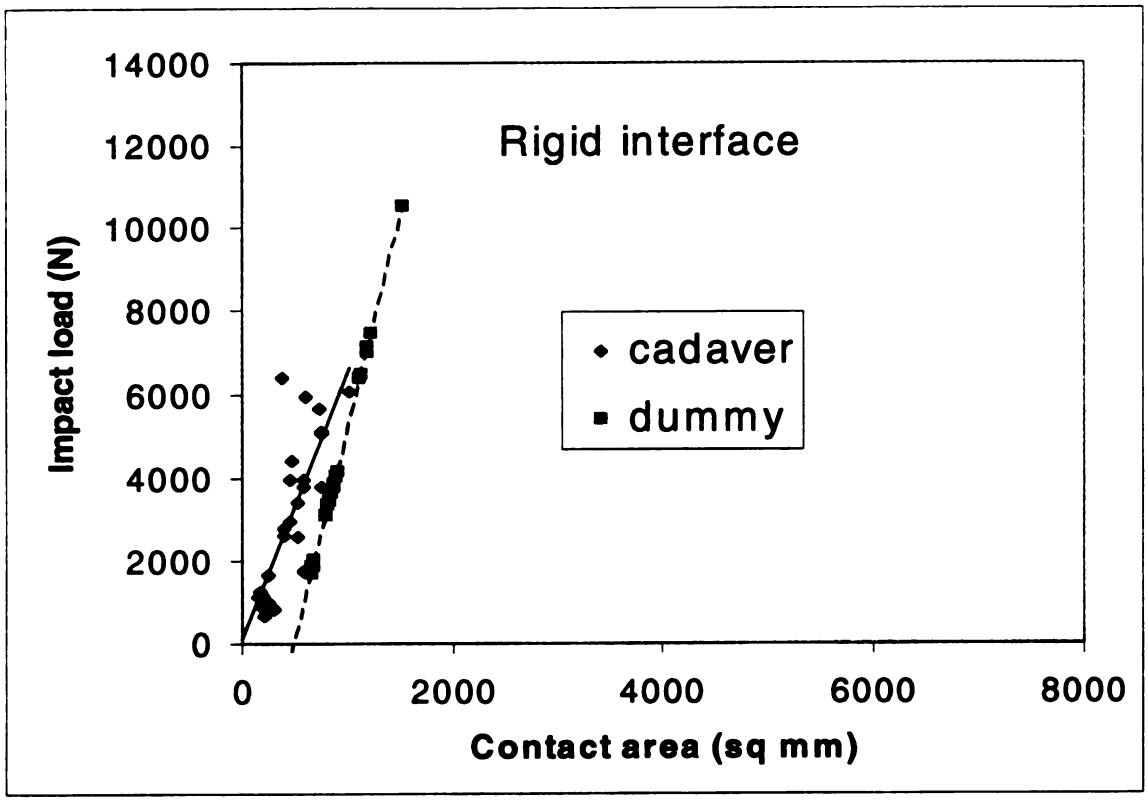

Figure 10

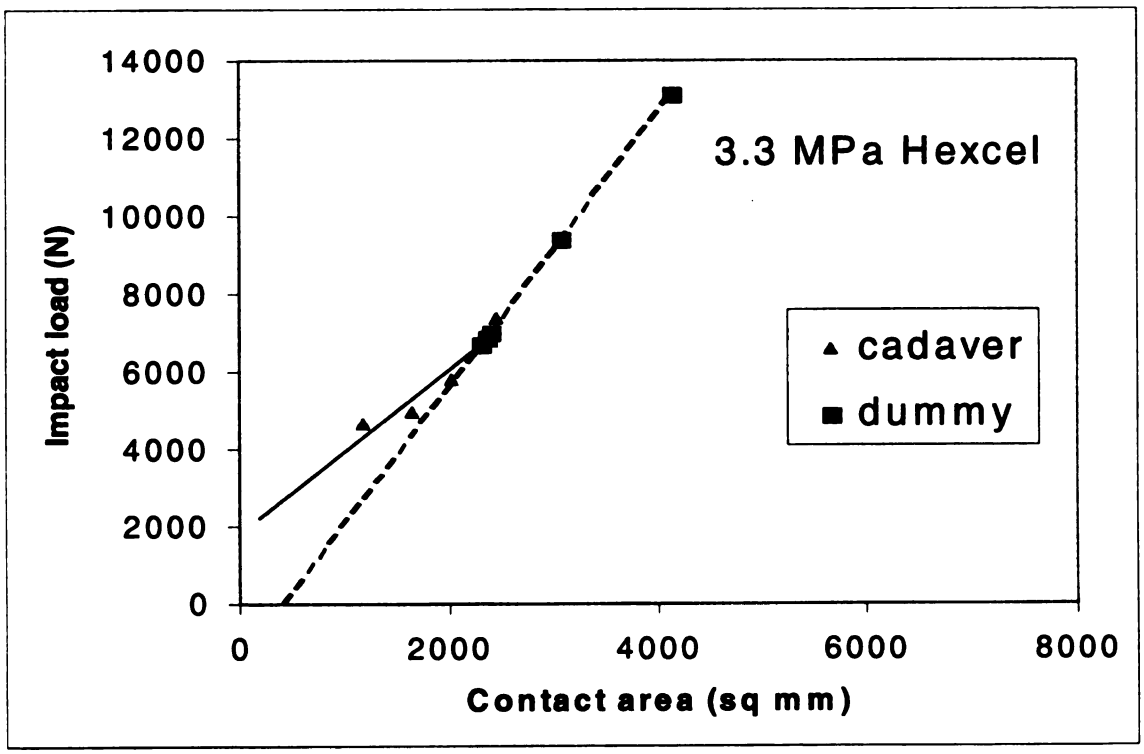

Figure 11

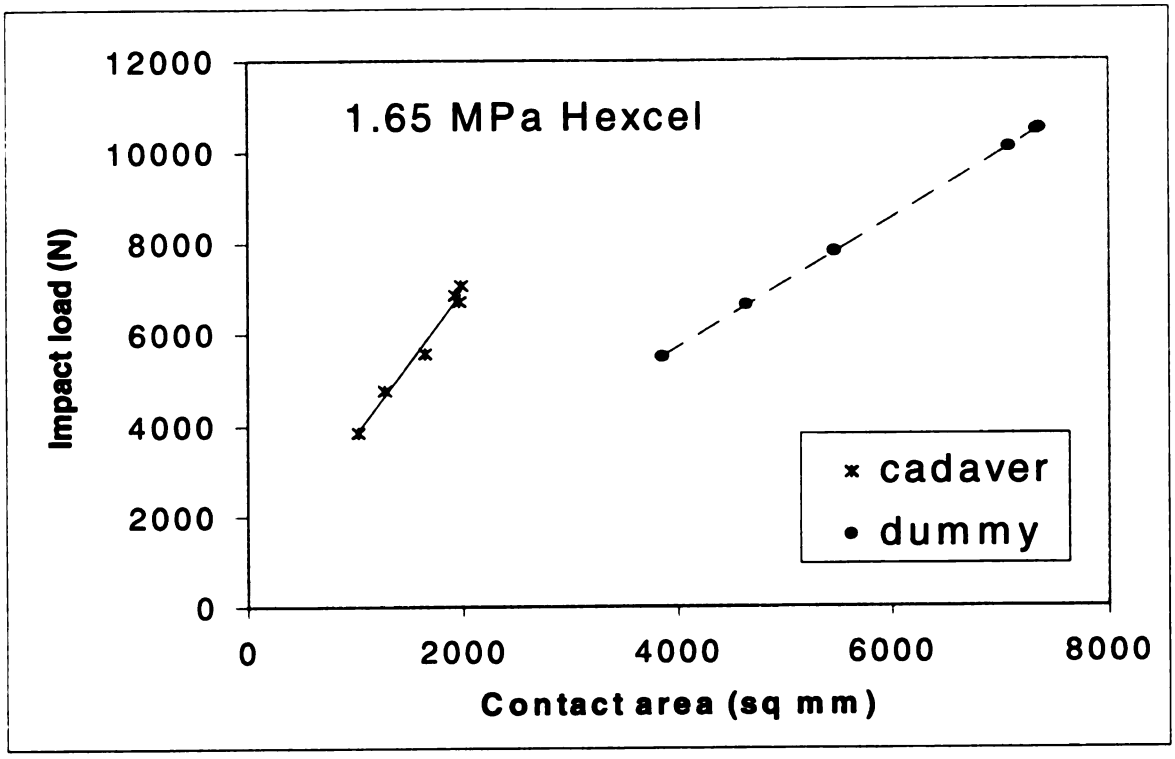

Figure 12

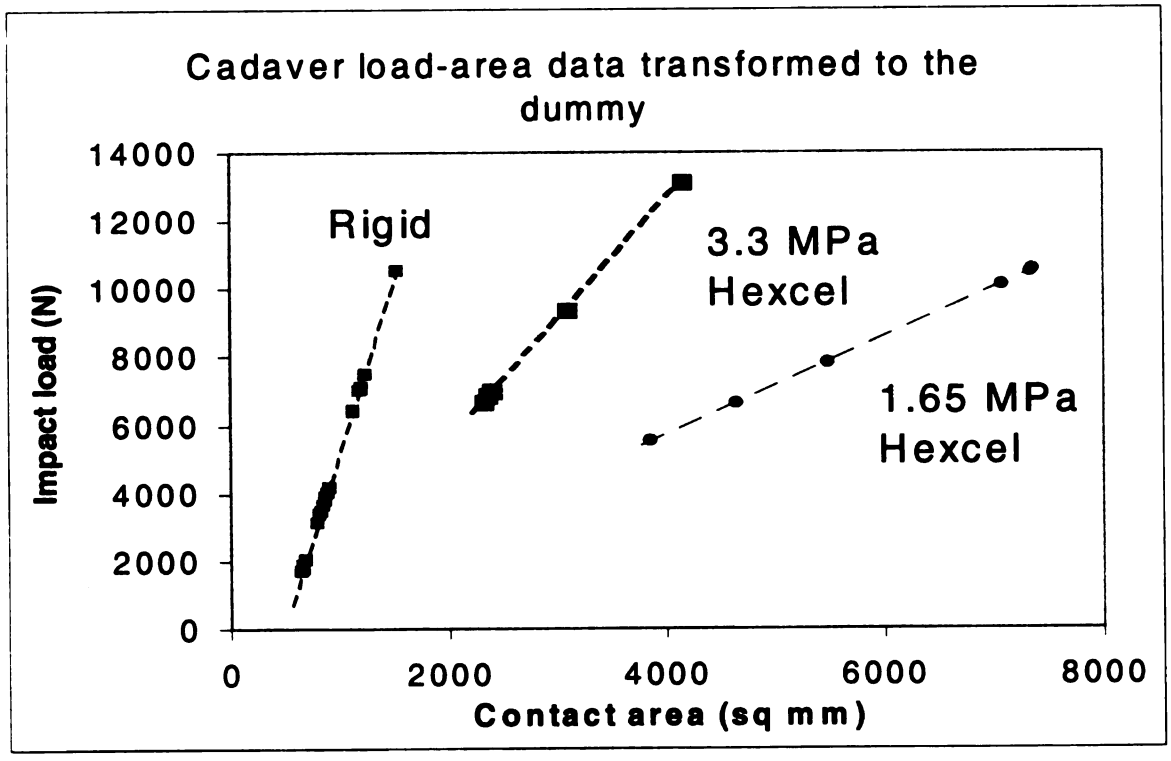

Figure 13

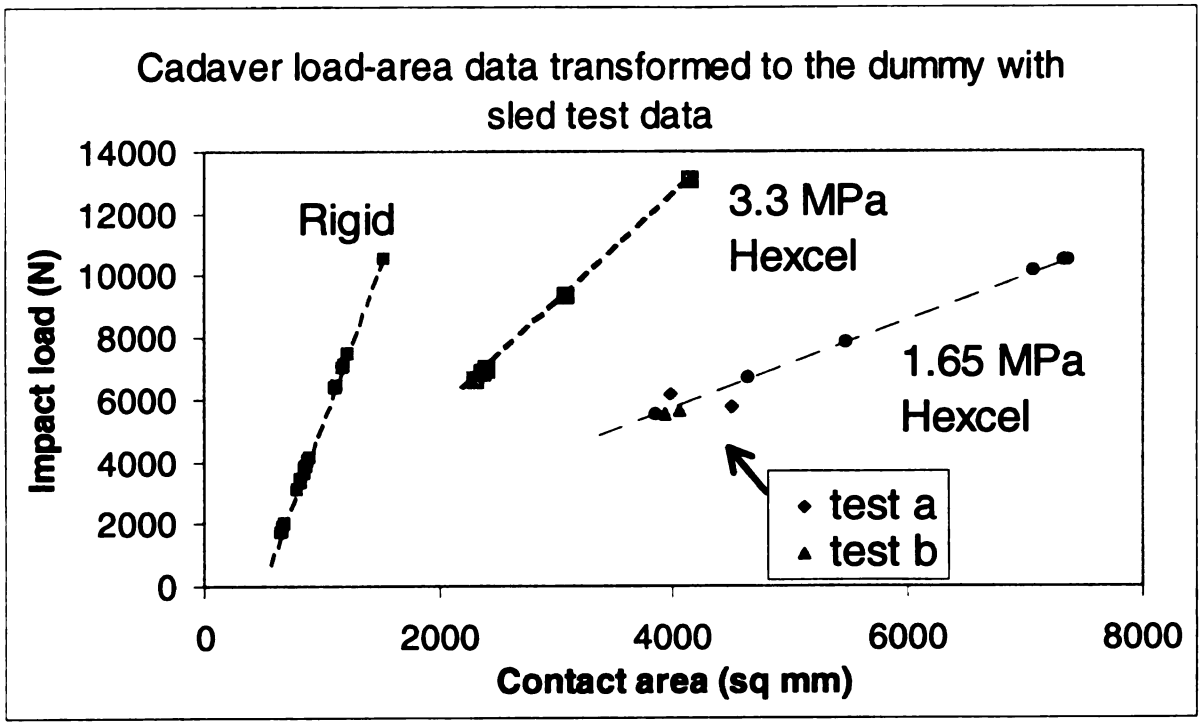

Figure 14

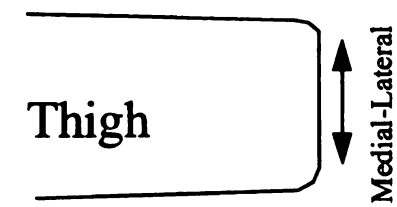

Top View of Flexed Dummy Knee

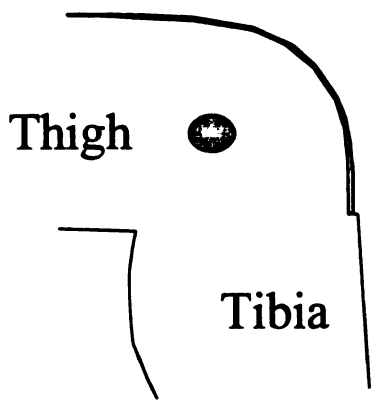

Side View of Flexed Dummy Knee

Figuew 15

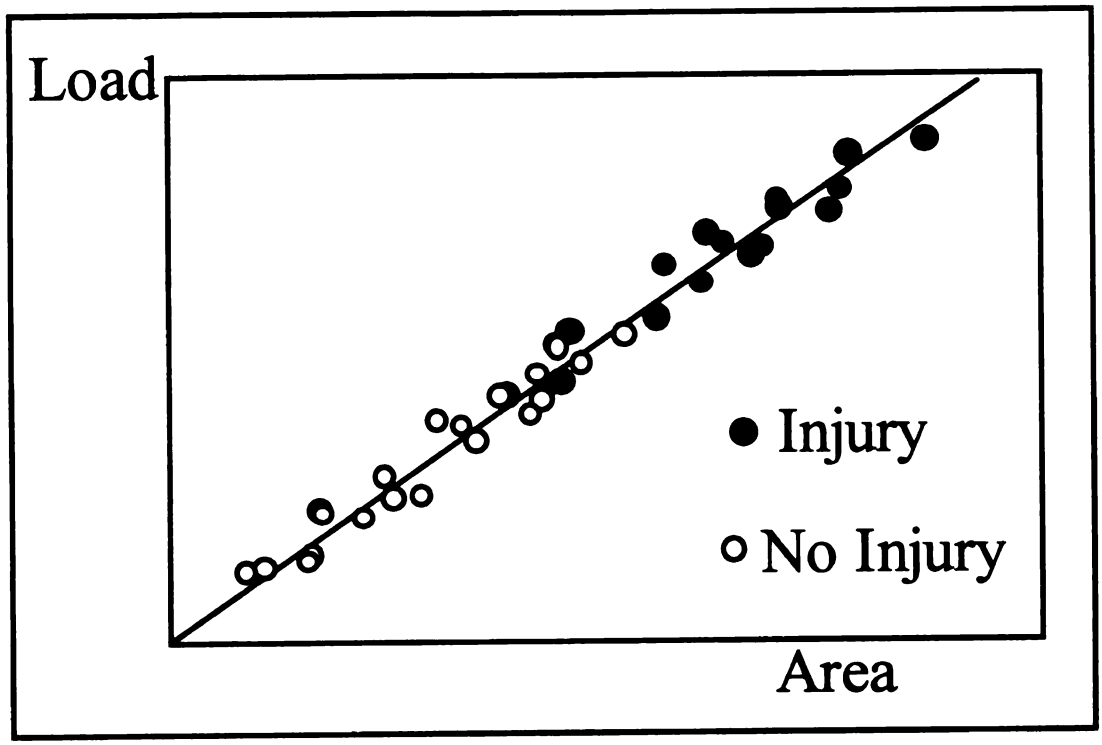

Figure 16

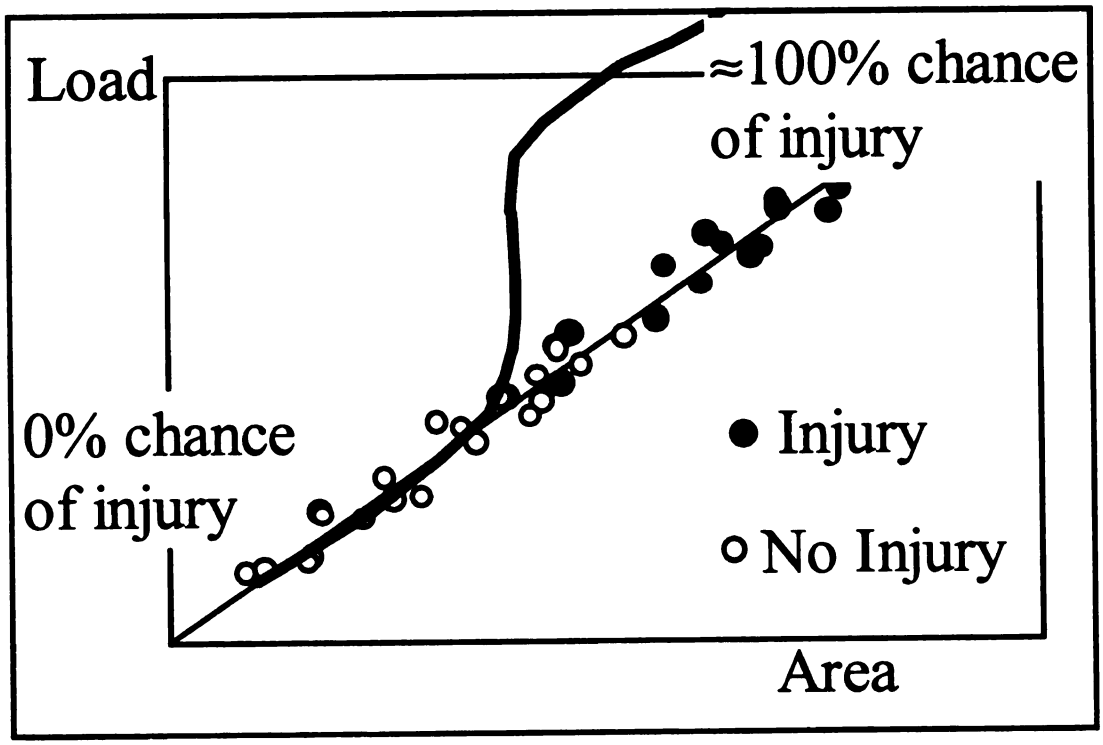

Figure 17

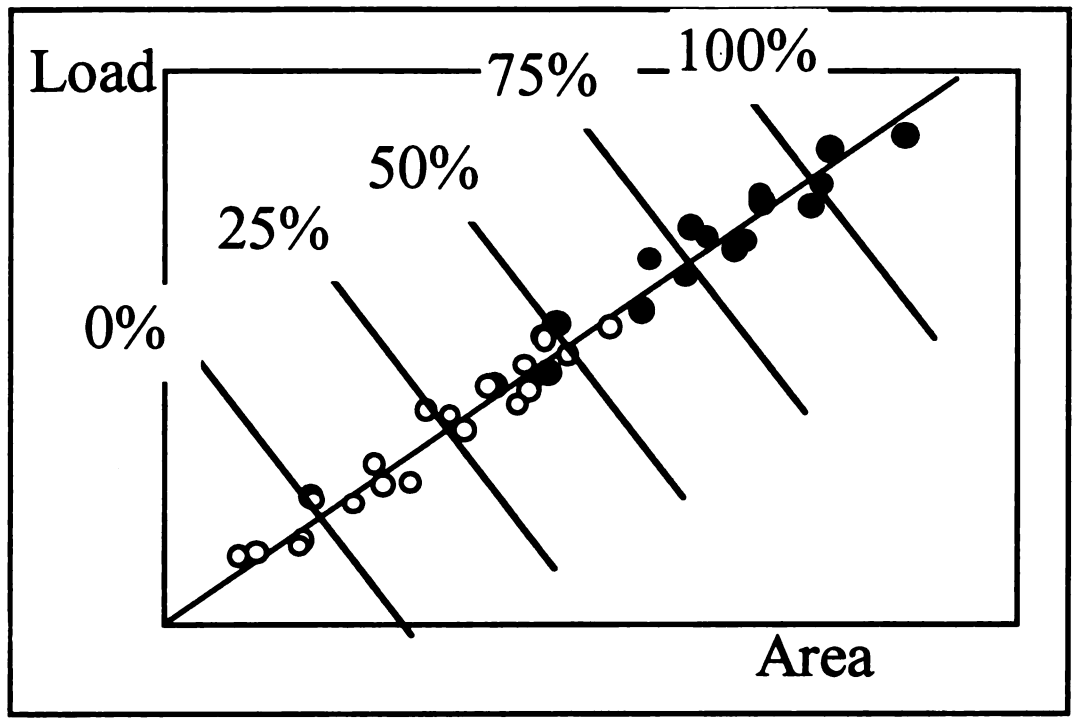

Figure 18

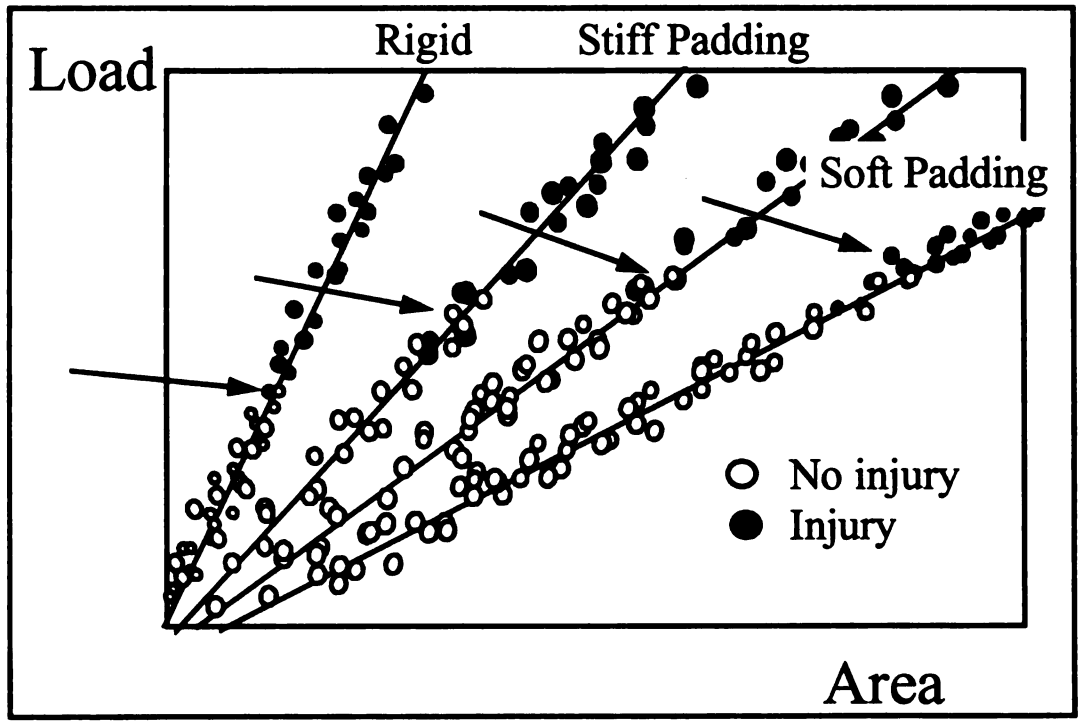

Figure 19

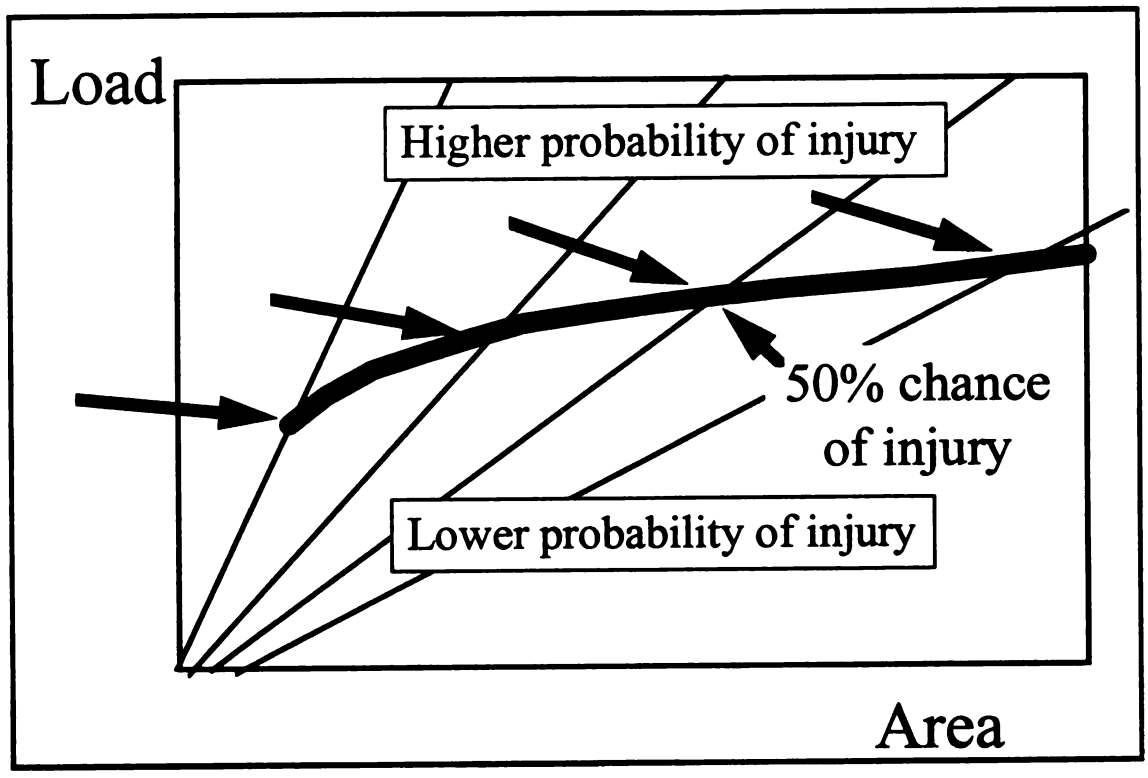
Load
Higher probability of injury
50% chance
of injury
Lower probability of injury
Area

Figure 20

CHAPTER 9

STUDY OVERVIEW AND ADDITIONAL CONSIDERATIONS FOR COMPREHENSIVE JOINT INJURY PREVENTION

Overview

This concluding chapter will provide an overview of the findings presented in chapters 2, 4, 5, 6, 7, and 8. Five main topics will be discussed:

1) The types of subfracture injuries and their probable mechanisms:

Injury data from all chapters will be used in concert with the stress analyses to identify probable injury mechanisms.

2) Injury prevention strategies:

Extraarticular load distribution and joint flexion angles will be discussed.

3) Appropriate injury thresholds I: the influence of inertial loads and stress waves on injury tolerance.

While inertial loads were briefly discussed in chapters 4, 5, 6, and 7, this topic will receive additional attention in this chapter. In addition, the influence of stress waves on joint injury will also be investigated. These topics are important when comparing impact data from various experimental designs.

4) Appropriate injury thresholds II: logistic regressions:

A method will be suggested to incorporate the above mentioned issues into an injury risk curve.

5) The use of theoretical models to design injury prevention strategies:

The implementation of the injury criteria developed in the current study into 'whole-body' theoretical models will be discussed. Such models could be used in car crash simulations

to predict the injury risk to the knee while also providing knowledge of whole body kinematics. Thus, the injury risk to the knee, head, chest, etc. could be predicted from a single model.

1) The types of subfracture injuries and their probable mechanisms:

Three main classifications of subfracture injuries were identified in chapters 2, 4, 5, and 7: vertical occult microfractures, horizontal occult microfractures, and cartilage fissures. All injuries were detected in the region of contact and were associated with elevated shear or tensile stresses. It is noted in passing that gross fractures were also documented and were nearly always observed in the patella, although there were some femoral condyle fractures. The most common patellar fracture was transverse followed by comminuted. The experimental data suggests that the occult traumas may be the precursor to gross fracture. This will be discussed in further detail below.

Vertical occult traumas were detected in regions of high contact pressure gradients at the cartilage surface. This coincided with elevated tensile and shear stresses in the subchondral plate, however, based on the direction of the injury and the principal stress directions, the injury is most likely tensile in nature. Viewed on a saggital plane, the vertical occult traumas traversed the subchondral plate and extended into the deep zones of the cartilage but did not communicate with the articular surface. The trauma also extended in the opposite direction into the trabecular bone. In some of the fracture specimens it appeared that the gross fracture was simply the advanced growth of a vertical occult trauma. This idea was supported by several of the subfracture histological specimens in which vertical occult traumas were documented which had almost communicated with the articular surface. These traumas had also extended in the opposite direction to the anterior surface of the patella. While this injury was technically still occult, an additional amount of energy imparted to the joint would have likely opened the occult fracture into a transverse or comminuted patellar fracture.

Horizontal occult injuries were documented in three categories: separation at the tidemark, separation at the calcified cartilage-subchondral bone interface, or horizontal cracks confined to the subchondral bone. The first two injuries were noted in regions of elevated shear stress in the cartilage at the tidemark. These stress maxima occurred in regions of high contact pressure gradients at the cartilage surface. Microcracks in the subchondral plate were associated with elevated shear stresses in the subchondral plate. In some of the histological data there was occult evidence of a gross fracture connected to a horizontal occult injury. This suggests that horizontal as well as vertical injuries may be precursors to gross fracture.

Cartilage fissures at the articular surface occurred in the center of contact which coincided with regions of elevated shear stress. Tensile stresses were ruled out as a potential mechanism because these maxima were located adjacent to and outside of the region of contact, remote to any evidence of fissures. The fissures appeared in the shape of a 'V': the articular surface was opened and the fissure extended into and terminated in the middle zones of the cartilage. It should be noted that it does not appear likely that cartilage fissures play a role in initiating gross fractures. The histological data shows several specimens in which fissures were the sole injury. In some cases, however, a fissure was located over a vertical occult trauma. An additional amount of energy could open up the fissure to expose the vertical occult trauma and this would be termed a gross fracture. However, it was the vertical occult trauma that actually initiated the injury to the bone.

2) Injury prevention strategies:

Chapters 5, 6, and 7 show that increased extraarticular contact area (via padding) reduces the incidence of fracture and subfracture level injuries. Increased contact area allowed higher loads to be tolerated without gross or microscopic injury. Math modeling of the patella also showed that increased contact area was associated with significant reductions in tensile stress in only the subchondral bone. This finding suggested two

conclusions: 1) vertical occult injuries probably initiated in the subchondral plate, and 2) preventing the occult injuries will prevent the incidence of gross fracture.

While increasing the contact area reduced injury, there were limits on this injury prevention strategy. There is a maximal contact area that can be achieved over the knee. In cases in which the maximal contact area is achieved, there would be a great deal of penetration into the impact interface. This may have negative implications on body kinematics in car accidents. For example, a large penetration into a knee bolster, while protecting the knee, may precipitate unwanted whole body kinematics. Deep penetration into the bolster would move the entire body forward putting the head in potentially life-threatening contact with the header or windshield. Thus, injury prevention in automobiles must be viewed as a system in which body kinematics will change as a function of the car interior.

Another kinematic parameter which affected injury potential in the current study was the knee joint flexion angle. Significantly greater loads and energies were required to produce injury at the higher versus lower flexion angles. This suggests that for scenarios in which knee impact may occur (i.e. car accidents), the car interior should be designed such that impact will occur at higher flexion angles. The experimental data showed that at lower flexion angles ($\leq 90°$) significantly less load was required to produce fracture and subfracture level injuries than at higher flexion angles (120°). This was because the patella attempted to migrate proximally at lower flexion angles. This put the patellar tendon in tension which caused an avulsive injury at the distal pole of the patella. This may explain the lower fracture loads for such experiments as the distal portion of the patellar bone tissue is loaded in tension. This can be contrasted to experiments at higher flexion angles in which the patella was loaded in compression as it was driven into the femoral condyles. In these experiments, the fracture load was nearly twice that for the lower flexion angles. Unfortunately, the influence of flexion angle is not reflected in the current automotive industry safety standards. These standards are based on loads measured with dummies

with an injury tolerance referenced to cadaver experiments conducted solely at 90°. Thus, the dummy cannot accurately predict injury at flexion angles other than 90°. At higher flexion angles, the dummy will understate the tolerance to injury, while the reverse will happen at lower flexion angles. It will be important for these considerations be included in future dummy designs.

3) Appropriate injury thresholds I: the influence of inertial loads and stress waves on injury tolerance.

Inertial Effects

A comparison of the data from the current study with past studies reveals a great difference in fracture load magnitudes. For example, at a 90° flexion angle, experiments on whole, seated, fresh cadavers show fracture at loads of 10-17 kN. In the current study, however, experiments at the same flexion angle were conducted on isolated knees and fracture loads of 5-7 kN were recorded. These data vary by a factor of approximately two. Three potential reasons for these differences are: inertial motion of the cadaver, stress wave effects, and/or strain rate effects. The latter is discounted because the tests on the isolated knees and the whole cadavers all occurred in a similar time frame (about 15 ms). The other two candidates will be discussed below.

'Inertial loads' refers to those loads arising from the rigid body acceleration of a mass where the force is the product of the mass and acceleration. In tests conducted on rigidly constrained, isolated knees, the resulting acceleration is zero. Thus, the load that is measured is simply due to the resistance of the joint tissues to undergo deformation. Alternately, tests conducted on whole cadavers result in an acceleration of the body, in addition to deformation of the tissues. Thus, injury in such experiments will only occur if sufficient deformation of the joint tissue occurs. However, because some of the load is used to inertially move the body, additional load would be needed to achieve an incipient level of deformation at the knee. To study this problem, a lumped mass model was

developed describing the body as two masses: one representing the lower extremity and the other the upper torso. The two body segments were connected by two discrete elements: a spring and dashpot positioned in parallel to incorporate compliance of the system. A pair of non-linear, coupled differential equations of motion were written to describe the impact response of the system. To model the whole cadaver, seated experiments, reasonable masses for a 50th percentile male were prescribed to the two body segments (Figure 1, 2). A frictional force was modeled under the upper body to simulate contact with the seat. An impulsive load was imparted to the 'knee'. The pulse was described as a haversine load-time curve with a 6700 N peak and a 15 ms duration (Atkinson 1995). To model the isolated knee experiments, the same impulsive load was prescribed to the knee, however, the upper body mass was prescribed as infinite to simulate a rigid fixation at the mid-thigh (Figure 1, 2). The equations of motion were solved numerically in MathCad and sample input and output data for the whole body and isolated knee cases are provided (Figures 3, 4).

A sensitivity analysis was conducted to determine the influence of some of the model parameters on the load in the spring and the inertial load associated with the lower extremity (m*a(t)). Specifically, sensitivity analyses were conducted for the impulse time duration (Figure 5), spring constant (Figure 6), and body segment mass (Figure 7) parameters. For infinitesimal impulse time durations (1 μs), the load in the spring for both models was zero and the inertial force of 'm' (the mass of the lower extremity) was identical to the peak applied impulsive force. This occurred because the mass m experienced a very small displacement for short pulse durations. This is the result of its inertial resistance to motion leading to an infinitesimal spring deformation and an associated infinitesimal load in the spring. Equilibrium was maintained by the inertial force in which the product of 'm*a' identically equaled the applied force. For all pulse durations greater than zero, the spring force was always higher in the isolated case than in the whole body case. In addition, the inertial force associated with m was essentially identical for all

impulse durations. More specifically, for time pulses in the range (0ms<t<7ms), the spring force was nonzero. The sum of a spring force and the inertial load approximately equaled the peak applied force. For longer pulse durations (7ms<t<35ms), the peak spring force exceeded the peak applied force, with the greatest spring force occurring in the 15ms to 20ms range. With increasing pulse durations, the inertial force associated with m gradually decreased to approximately 33% of the peak applied force. The elevated spring forces arose from the spring's resistance to the relative displacements of the two body masses and, at the same instant, the load associated with inertially decelerating the mass m. Similarly, the inertial load associated with m decreased at the longer timepoints (>20 ms) as the spring was allowed to deform thus allowing the acceleration of m to diminish at increasing pulse times.

A sensitivity analysis of the spring constant of the knee again revealed that the spring force was greater in the isolated knee model compared to the whole body model. In addition, for the spring constant range (2e+5 N/m < k < 1e+8), the peak spring force in the isolated model was greater than the peak applied force. The whole body model peak spring force followed a similar trend as the isolated model, however, the peak forces were less than the isolated model. For both models, the maximal spring force was documented for spring constants of approximately 1e+6 N/m. This value is identical to experimental measurements of the cadaveric knee spring constant. For larger values of k (k > 1e+6), the inertial force of m was larger for the whole body. This occurred because the elevated spring constant essentially makes the entire whole body system react and move as a rigid body. Such rigid body motion is not possible for the isolated knee model, and thus, the inertial loads are reduced.

A sensitivity of the amount of mass distal to the knee again showed that the forces in the spring were always greater in the isolated knee model. For infinitesimal mass values, the peak spring force is identical to the applied load and the inertial force is zero (because $F_{inertial} = m^*a$ and m→zero). As the mass is increased (1 kg < m < 20 kg), the

spring force and inertial force are increased. This range encompasses 14.2 kg, the realistic mass of the distal lower extremity for the 50th percentile male (Figure 1). For greater mass values (> 20 kg), the spring force decreased and the inertial force steadily increased. This is because there is less spring displacement as the mass value increases because the mass 'm' is undergoing less displacement due to it's increased inertial resistance to motion.

When realistic values of the model parameters are used (pulse time=15ms, k=1e+6 N/m, m=14.2 kg), the whole body model requires 30% more load to achieve the same deformation as the isolated model. The load in the spring and the relative displacement of the lumped masses can be thought of as the stress and strain, respectively, in the thigh. Because tissue failure is considered to be mediated by elevated stresses (and/or strains), the results of the lumped mass model show that the isolated leg is more prone to injury for a given load in comparison to the whole body model. Thus, a comparison of isolated and whole body impact data should take inertial effects into account to make accurate transformations between the two experimental protocols.

Stress Waves

To determine if stress wave transmission could potentially affect the state of stress in the knee joint (for the whole body and isolated lower extremity models shown in Figures 1 and 2), an estimation was made of the speed of a stress wave in the thigh. For such a case it can be shown that the speed is related to the modulus and density by the following equation: wave velocity = $(E/\rho)^{0.5}$. For this simple analysis, the thigh was modeled as a tube of cortical bone. Inserting appropriate values (E=3.75 GPa, $\rho=1.85*10^3$ kg/m^3) into the wave equation yields a velocity of 1424 m/s. Assuming a 20 cm femur length for the isolated case and 40 cm for the whole femur in the whole body case allows the calculation of the time required for the wave to pass down the femur. In the isolated case, the wave reaches the rigid constraint and returns to the knee joint in 0.28ms. This is far less than a realistic pulse duration of 15 ms discussed in the previous

section. Thus, the initial wave initiated by the first part of the applied load will return to the knee as additional load is still being applied from the impact. Thus, wave trains would be constantly passing down the leg, reflecting off the wall, returning to the knee and engaging in a complicated construction/extinction interaction with the applied load and with prior wave trains. This phenomenon is even more complicated because the initial wave trains initiated by the applied load are compressive. At a fixed node such as the rigid constraint, the waves are reflected with the same polarity. That is the stress wave returns to the knee as a compressive wave. However, as the wave reaches the free end at the knee, the stress wave is reflected back up the thigh with a reversed polarity. Thus, the initial trip a wave makes down the thigh is a dilatational wave, compressive in nature. On the second pass, the wave is tensile. One final complication are local reflections at material discontinuities such as the tidemark. At such discontinuities, some portion of the stress will pass through the interface at a diminished magnitude; the remainder of the wave will be reflected. Clearly, the overall effect of stress wave transmission is highly complicated for the above mentioned reasons. In order to capture these effects, a simple finite element model was constructed to model stress wave transmission in the isolated leg and whole body models. Four noded elements were used to develop an axisymmetric model of the knee and thigh (Figure 8). The distal end was comprised of trabecular bone (E=350 MPa, υ=0.3), patellar and femoral subchondral plates (E=3750 MPa, υ=0.3), and a layer of articular cartilage (E=20 MPa, υ=0.49) (Figure 9). The remaining proximal portion of the femur was modeled with trabecular bone. For the whole body model, a layer of very soft elements were placed at the 'hip' to model the nonrigid interaction with the seat back. Similar to the lumped mass model of the previous section, the applied forcing function was a compressive haversine with a peak load of 6700 N and a pulse duration of 15 ms. The quasistatic solution was also computed as a reference for the dynamic stress magnitudes. The maximum and minimum principal stress histories were acquired and the maximum shear stress history was determined from these data (τ_{max} (t) =

($|\sigma_1(t)-\sigma_3(t)|$)/2). These data were tabulated and compared between the whole body model and isolated leg model and the quasistatic solution (Table 1). Peak stresses were determined as well as 'average' stress values in which the stress history was averaged over time.

Reviewing the stresses in the knee as function of time show the stress wave moving through the knee and into the thigh (Figure 10). The shear stress magnitude (which reflects the maximum and minimum principal stress histories) and wave frequency were greatest in the patellar subchondral bone for the isolated knee model (Figure 11). Within a given model (isolated or whole body), the shear stress magnitude and wave frequency were greatest in the patellar subchondral bone versus the femoral subchondral bone (Figure 12). This might explain, in part, why patellar injuries are more common than femoral fractures. With regard to stress magnitudes and temporally averaged stresses, the isolated model suffers approximately 20% greater stresses than the whole body model (Table 1). This suggests that some additional load would be required in the whole body to achieve the same stress state as the isolated knee. Assuming a very simple proportional relationship (although it is probably nonlinear), a 20% increase in load in the whole body case would approach the isolated case. Regardless of the magnitude, as in the case with inertial effects, a comparison of isolated and whole body impact data should take stress waves into account when comparing isolated knee and whole body data.

4) Appropriate injury thresholds II: logistical regressions:

To identify appropriate injury thresholds based on the data presented in the current dissertation, a logistical regression was performed on load-area data from a series of rigid interface cadaver tests (Figure 13) in which fracture and subfracture data are represented. This allowed injury risks to be associated with specific load-area data points. The injury risk for the isolated leg (for which the experiments are based) were used to identify a load-area data point associated with a 50% chance of fracture. This datapoint was then

increased by 50% (30% for inertial effects and 20% for stress wave effects, see above) to estimate the associated risk for the whole cadaver. These data points were then multiplied by 70% to estimate the 50% injury risks for subfracture trauma (Figure 14). The specific level of 70% comes from a study in the human cadaver knee (Atkinson 1995) which showed that subfracture injuries were commonly associated with subfracture impacts at 70% of the contralateral fracture load. Tabulations of the fracture and subfracture 50% injury risk data were tabulated for the isolated leg and whole body cases (Table 2).

5) The use of theoretical models to design injury prevention strategies:

To take the data from the current study and apply it in a pragmatic setting, models useful to injury prevention in car crashes were initiated. The isolated dummy lower extremity's interaction with aluminum hexcel (a simulated instrument panel) was modeled as a first step in designing safer car interiors (Figure 15). This simple model was constructed because corresponding data (presented in Chapter 8) already existed for experimental validation. The thigh, hip, shin, and foot were modeled as rigid, structural bodies. The vinyl skin of the dummy knee and the hexcel were modeled with finite elements. The vinyl was modeled as a viscolelastic solid which obeyed the 'Zener' material model which is essentially a maxwell discrete elemental model in parallel with a spring (Figure 16). The Hexcel was modeled as an elastoplastic solid with different modulae assigned to each orthogonal material direction. For a given material direction there were three values of the modulus: the initial slope (E1), the plateau (E2), and the final steep slope (E3) as the hexcel bottoms out (Figure 17). The different modulae are encountered at specific compaction factors which are defined as the current volume divided by the initial volume. This results in nine modulae and six compaction factors which were determined experimentally by compressing carefully machined samples of hexcel material. The vinyl skin material parameters were taken from previous, unpublished work on the dummy head and then the parameters were 'tuned' based on

baseline experimental validation (bulk modulus=0.82 GPa, long term shear modulus=0.00074 GPa, short term shear modulus=0.00441 GPa, decay constant= 2.48 s^{-1}). By impacting the dummy knee with a free flight inertial mass at the same energy as corresponding impact experiments, the model successfully predicted the peak load and the load-time history within 3% (Figure 18). Future work with this model will include placing the whole dummy in a simulated vehicle to conduct simulated car crashes. By theoretically estimating the load and contact area, the injury risk to the knee can be ascertained. Thus, variables such as instrument panel design and seat positioning can be studied for their effect on lower extremity injury.

REFERENCES

1. Atkinson PJ, Haut RC (1995) Subfracture insult to the human cadaver patellofemoral joint produces occult Injury. Journal of Orthopaedic Research 13:936-944, 1995.

TABLES

Table 1: Stresses values (Pa) for the isolated leg and whole leg solved dynamically and statically.

	Max Princ Stress: Patella	Min Princ Stress: Patella	Max Shear Stress: Patella	Max Princ Stress: Femur	Min Princ Stress: Femur	Max Shear Stress: Femur
Isolated leg peak stress	8.74E+06	-1.06E+07	8.82E+06	8.00E+06	-7.89E+06	7.84E+06
Whole leg peak stress	9.75E+06	-9.67E+06	7.70E+06	7.20E+06	-7.15E+06	7.03E+06
Peak isolated/ peak whole leg	90%	110%	115%	111%	110%	112%
Isolated leg average stress	3.27E+06	-3.27E+06	3.27E+06	2.74E+06	-2.75E+06	2.75E+06
Whole leg average stress	2.68E+06	-2.68E+06	2.68E+06	2.00E+06	-2.02E+06	2.01E+06
Average isolated leg/average whole leg	121.8%	121.8%	121.8%	136.9%	136.1%	136.5%
Peak isolated leg/static solution	108.7%	130.2%	108.9%	127.8%	97.2%	109.2%
Peak whole leg/static solution	121.2%	118.7%	95.1%	115.0%	88.1%	97.8%

Table 2: Loads (N) and contact areas (sq mm) associated with a 50% fracture or subfracture injury risk for different loading scenarios. The increase in contact area and load due to whole body inertial effects and stress waves is given.

	Injury=fracture		Injury=subfracture	
Load case	**Contact Area**	**Impact Load**	**Contact Area**	**Impact Load**
Isolated leg	887.5	5856	566	4099
Whole body: increase= inertial effects	1213	7607	790	5325
Whole body: increase= inertial effects + stress waves	1423	8784	941	6149

FIGURES

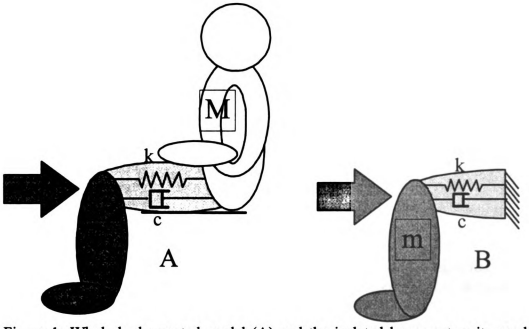

Figure 1: Whole body, seated model (A) and the isolated lower extremity model (B) in which an impact load is delivered at the knee. 'M' (43.4 kg) denotes the mass of the body proximal to the knee and 'm' (14.2 kg) denotes the mass distal to the knee for a 50th percentile individual. 'k' (1e+6 N/m, Atkinson 1995) denotes the spring constant of the knee and 'c' (200 Ns/m) represents the viscous damping coefficient.

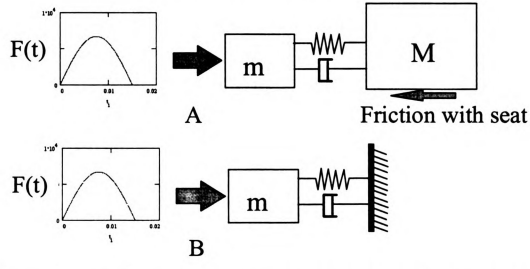

Figure 2: Lumped mass models of Figure 1: the whole body (A) and the isolated knee (B).

$i := 0..2000$

$\Delta t := 0.00001$

$t_i := i \cdot \Delta t$

Whole Body Case

$\alpha := .015$

$P := 6700$

$$F(t) := \Phi(\alpha - t) \cdot P \cdot \sin\left[\left(\frac{1}{\alpha}\right) \cdot \pi \cdot t\right]$$

$m := 14.2 \qquad M := 43.4000 \qquad k := 1000000 \qquad c := 200 \qquad g := 9.81 \qquad \mu := 0.1$

$$a1(v1, x1, v2, x2, t) := \frac{1}{m} \cdot (F(t) - k \cdot (x1 - x2) - c \cdot (v1 - v2))$$

$$a2(v1, x1, v2, x2, t) := \frac{1}{M} \cdot \left[k \cdot (x1 - x2) + c \cdot (v1 - v2) - \mu \cdot M \cdot g \cdot \frac{v2}{|v2|}\right]$$

$$\begin{bmatrix} v1_0 \\ x1_0 \\ v2_0 \\ x2_0 \end{bmatrix} := \begin{bmatrix} 0 \\ 0 \\ 0 \\ 0 \end{bmatrix}$$

$$\begin{bmatrix} v1_{i+1} \\ x1_{i+1} \\ v2_{i+1} \\ x2_{i+1} \end{bmatrix} := \begin{bmatrix} v1_i + a1\left(v1_i, x1_i, v2_i, x2_i, t_i\right) \cdot \Delta t \\ x1_i + v1_i \cdot \Delta t \\ v2_i + a2\left(v1_i, x1_i, v2_i, x2_i, t_i\right) \cdot \Delta t \\ x2_i + v2_i \cdot \Delta t \end{bmatrix}$$

Numerical integration:
Eulerian-tangent method

(A)

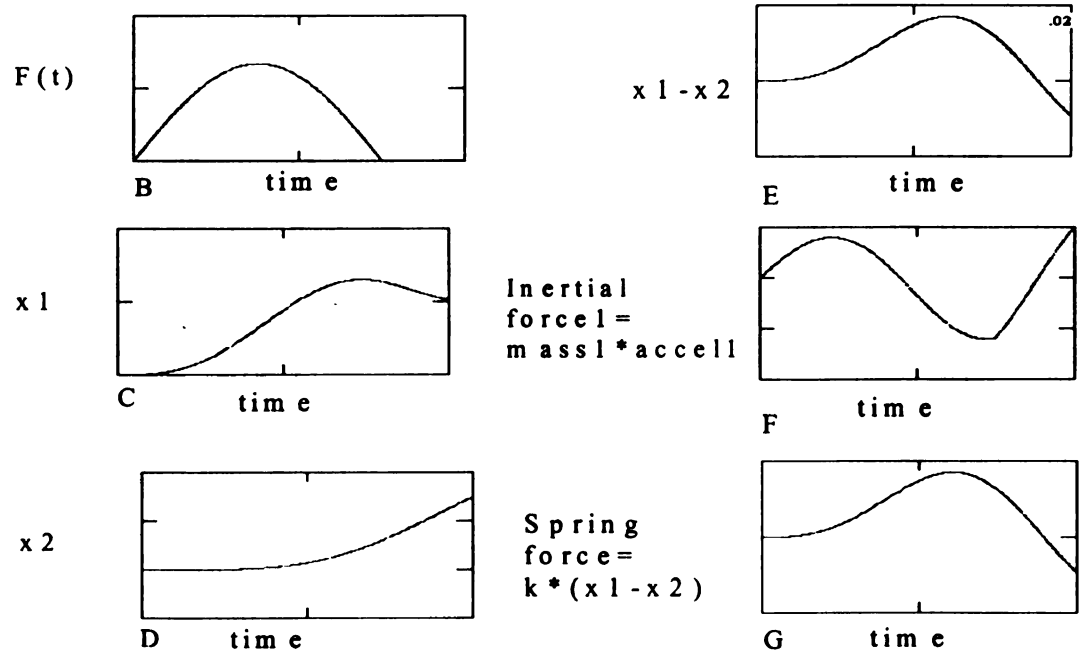

Figure 3: Sample input code (A, for MathCad) to solve the coupled, non-linear differential equations of motion (shown in box) describing the whole body case. Sample output as a function of time is shown in subfigures B-G: the forcing function (B), the displacements of m (C) and M (D), the spring displacement (E), the inertial force of 'm' (F), and the force produced in the spring (G).

$i := 0 .. 2000$

$\Delta t := 0.00001$

$t_i := i \cdot \Delta t$

Isolated Knee Case

$\alpha := .015$

$P := 6700$

$F(t) := \Phi(\alpha - t) \cdot P \cdot \sin\left[\left(\frac{1}{\alpha}\right) \cdot \pi \cdot t\right]$

$m := 14.2 \qquad M := 434000 \qquad k := 1000000 \qquad c := 200 \qquad g := 9.81 \qquad \mu := 0$

$$a1(v1, x1, v2, x2, t) := \frac{1}{m} \cdot (F(t) - k \cdot (x1 - x2) - c \cdot (v1 - v2))$$

$$a2(v1, x1, v2, x2, t) := \frac{1}{M} \cdot \left[k \cdot (x1 - x2) + c \cdot (v1 - v2) - \mu \cdot M \cdot g \cdot \frac{v2}{|v2|}\right]$$

$$\begin{bmatrix} v1_0 \\ x1_0 \\ v2_0 \\ x2_0 \end{bmatrix} := \begin{bmatrix} 0 \\ 0 \\ 0 \\ 0 \end{bmatrix}$$

$$\begin{bmatrix} v1_{i+1} \\ x1_{i+1} \\ v2_{i+1} \\ x2_{i+1} \end{bmatrix} := \begin{bmatrix} v1_i + a1(v1_i, x1_i, v2_i, x2_i, t_i) \cdot \Delta t \\ x1_i + v1_i \cdot \Delta t \\ v2_i + a2(v1_i, x1_i, v2_i, x2_i, t_i) \cdot \Delta t \\ x2_i + v2_i \cdot \Delta t \end{bmatrix}$$

Numerical integration:
Eulerian -tangent method

A

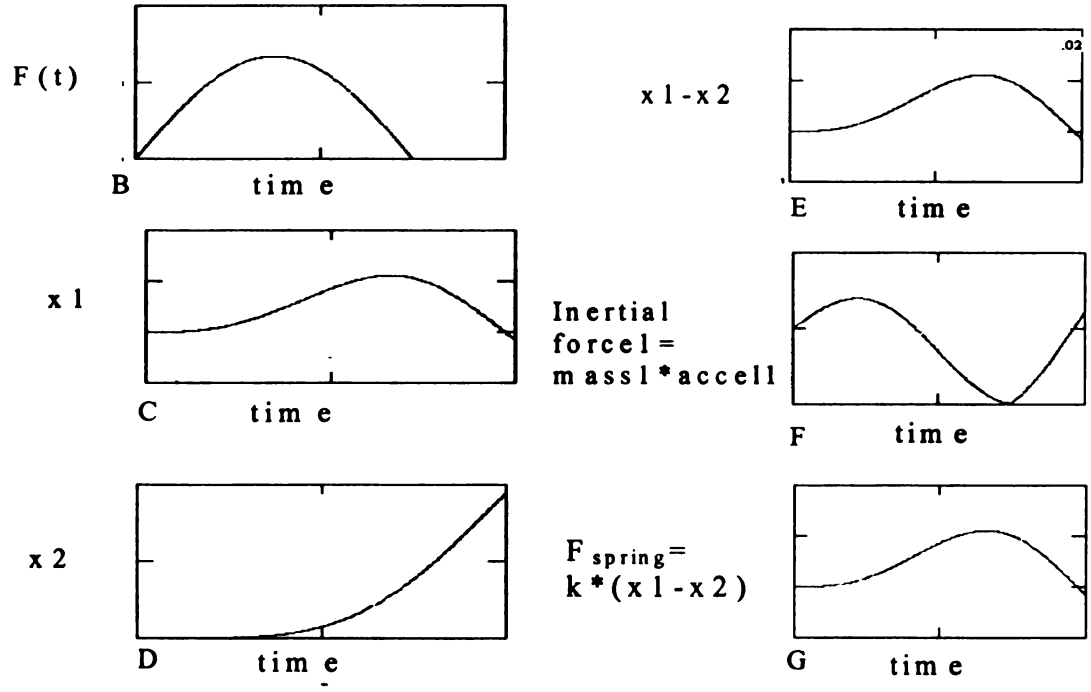

Figure 4: Sample input code (A, for MathCad) to solve the coupled, non-linear differential equations of motion (shown in box) describing the isolated knee case. Sample output as a function of time is shown in subfigures B-G: the forcing function (B), the displacements of (C) and M (D, this displacement is essentially zero), the displacement of the spring (E), the inertial force of 'm' (F), and the force produced in the spring (G).

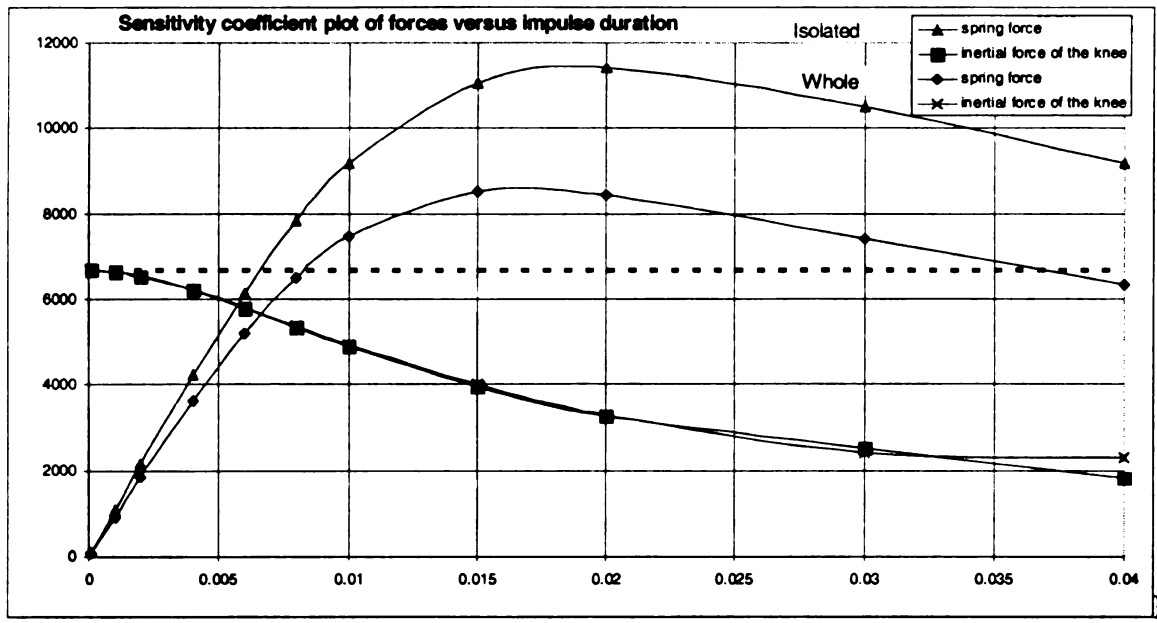

Figure 5: The inertial forces of m and the force developed in the spring for a range of impulse durations for the whole body and isolated leg cases. The dotted line represents the peak applied load at the knee.

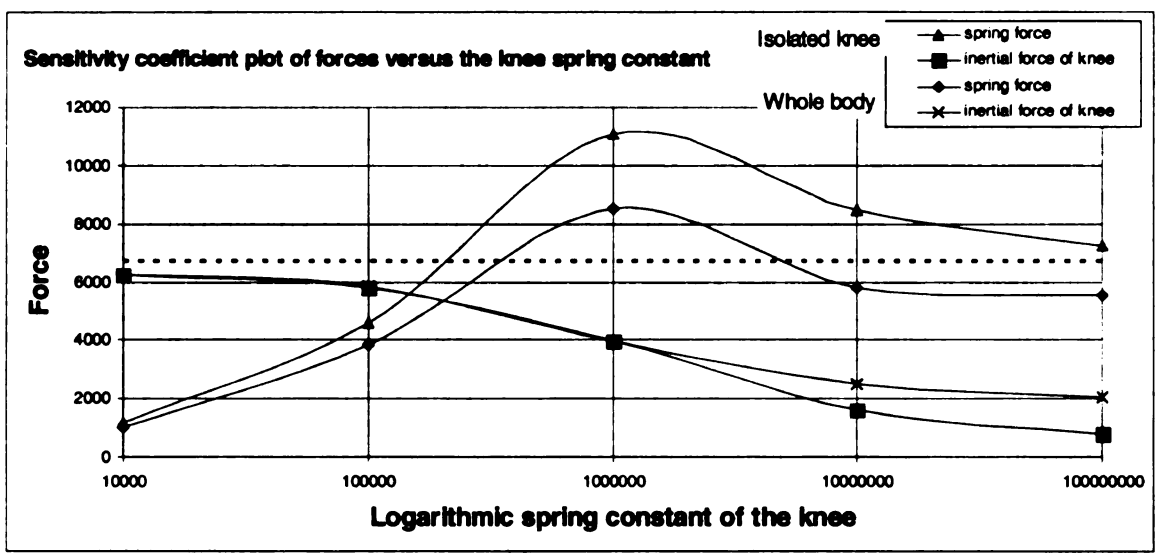

Figure 6: The inertial forces of m and the force developed in the spring for a range of spring constants for the whole body and isolated leg cases. The dotted line represents the peak applied load at the knee.

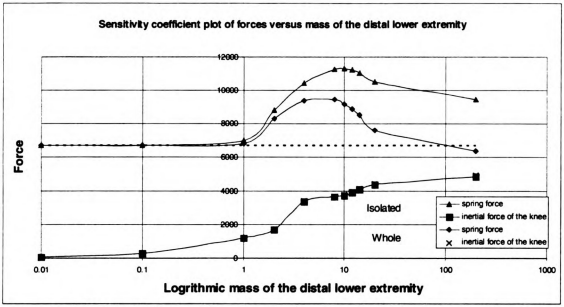

Figure 7: The inertial forces of m and the force developed in the spring for a range of distal lower extremity masses for the whole body and isolated leg cases. The dotted line represents the peak applied load at the knee.

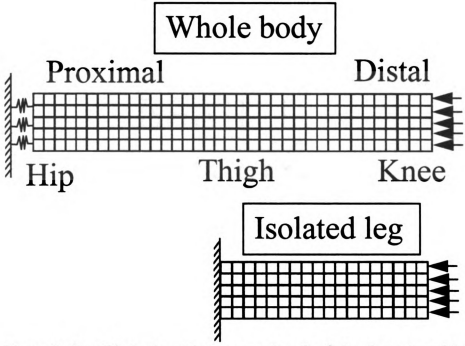

Figure 8: Simplified schematics representing the finite element models used to study the effects of stress waves on the impact response of the whole body and isolated knee experiments.

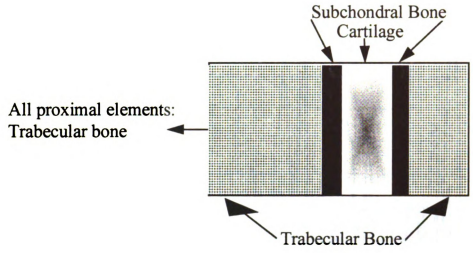

Figure 9: A schematic showing the different material assignements to model the knee.

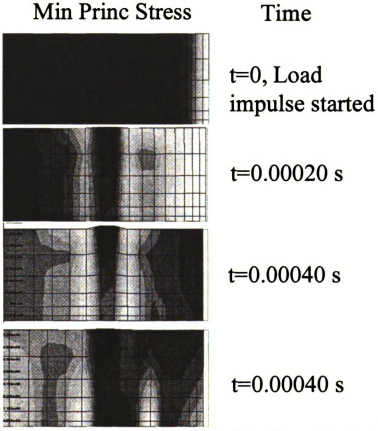

Figure 10: The stresses in the knee and distal thigh (the region depicted in Figure 9) showing the stresses moving up the femur with some reflection at the material discontinuities.

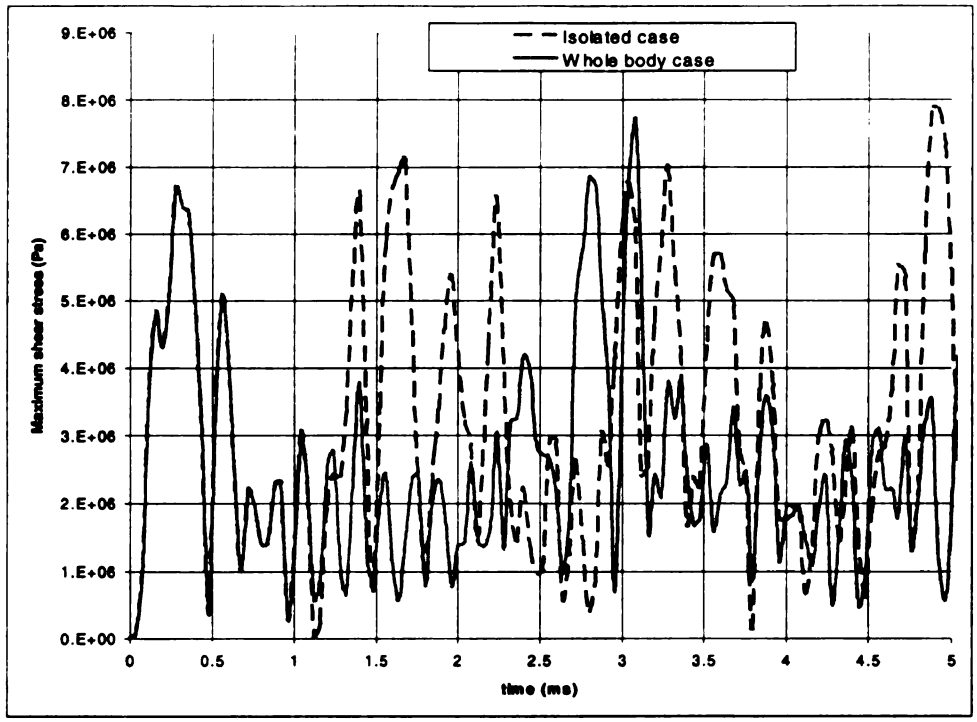

Figure 11: Temporal history of the stress wave magnitude (maximum shear) of a node contained within the patellar subchondral bone for the isolated knee and whole body models for the first 5ms of impact. Note that the stresses are similar for the first 1 ms. For the ensuing time points, the isolated model experiences far more peaks and at higher magnitudes.

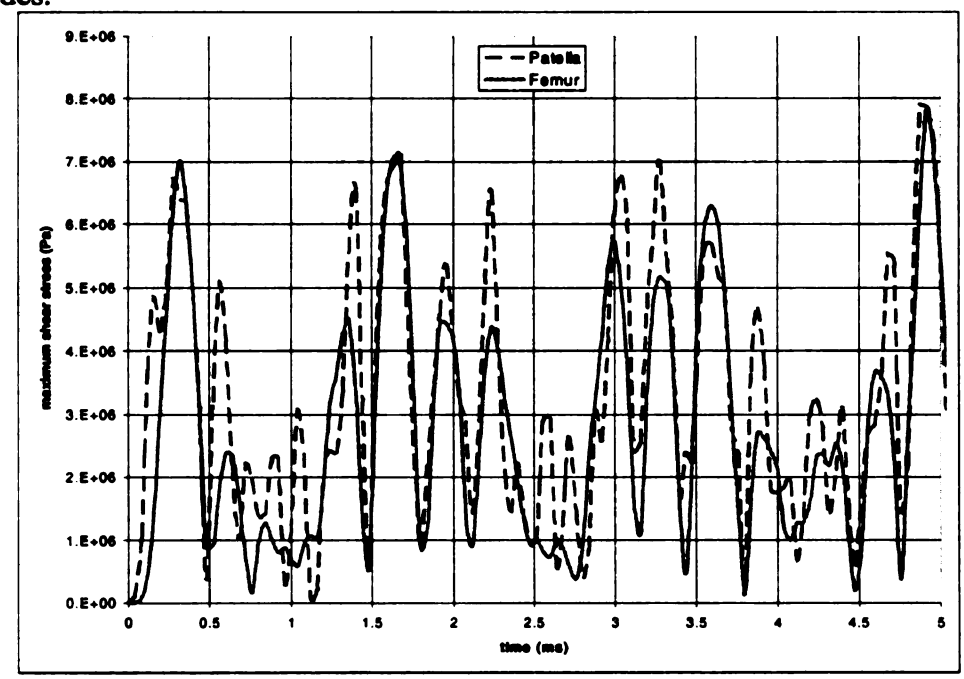

Figure 12: Temporal history of the stress wave magnitude (maximum shear) of two nodes: one contained within the patellar and one contained within the femoral subchondral bone for the isolated knee model only for the first 5ms of impact. Note that the stresses are largely dissimilar similar for all time points. The patellar suffers more oscillations and the stress amplitudes are typically greater than for the femur.

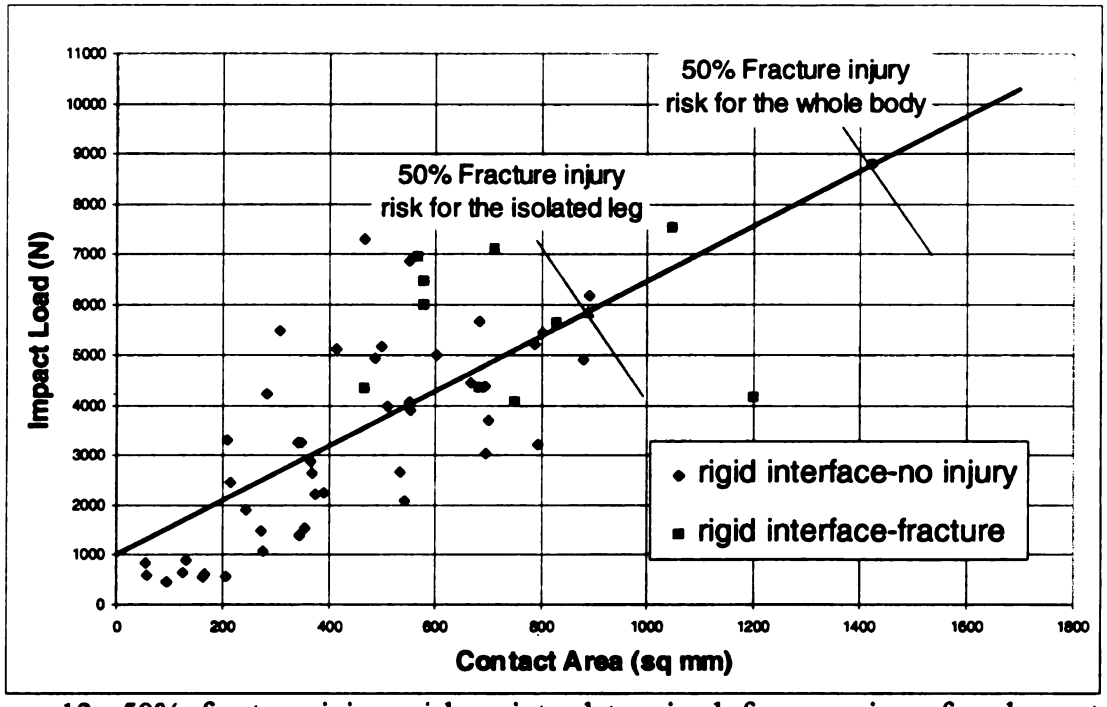

Figure 13: 50% fracture injury risk points determined for a series of cadaver tests performed with a rigid interface. The 50% injury risk for the isolated case was increased 1.5 times for the whole body case to account for inertial effects (30% increase) and stress waves (20% increase). Please see section 3 above regarding these values.

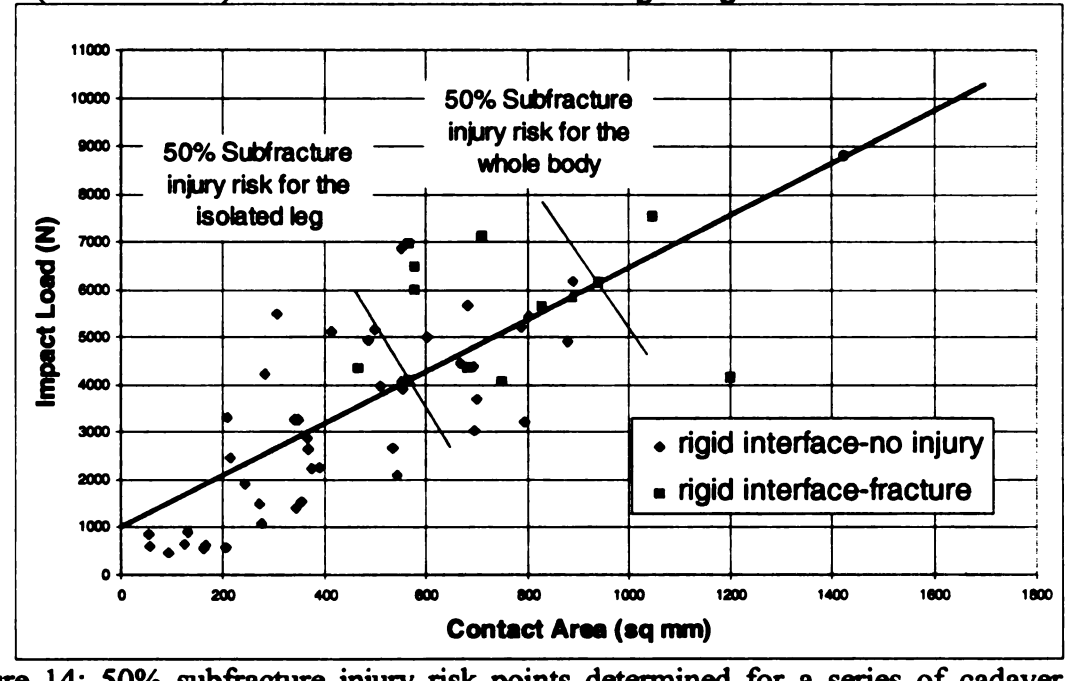

Figure 14: 50% subfracture injury risk points determined for a series of cadaver tests performed with a rigid interface. The 50% risk load-area data points from Figure 13 were multiplied by 70%, the amount of fracture load required to cause subfracture injuries (Atkinson 1995).

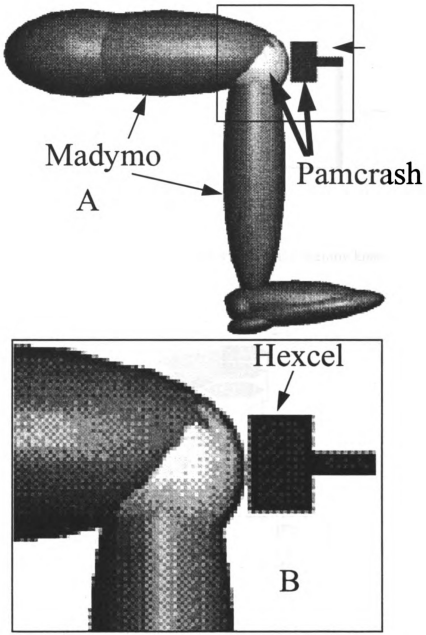

Figure 15: A schematic of a solid model of the dummy lower extremity. The hip is fixed and the hip, thigh, shin, and ankle are modeled as structural elements. The knee dummy skin (9.7 mm thick) and hexcel impact interface are modeled with finite elements. The vinyl material model is shown in Figure 16 and the hexcel material model is shown in Figure 17. The problem with a Madymo-Pamcrash coupled solution in which the Madymo software code accounted for the structural elements and the Pamcrash code accounted for the finite element solution.

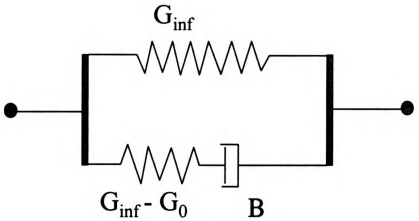

Figure 16: Viscoelastic material model of the vinyl for the dummy knee.

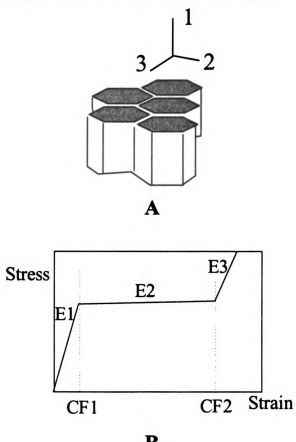

Figure 17: The material directions (A) and the material model for the hexcel. The parameters (three modulae and compaction factors-CF1, CF2) were required for all three material directions and were experimentally determined.

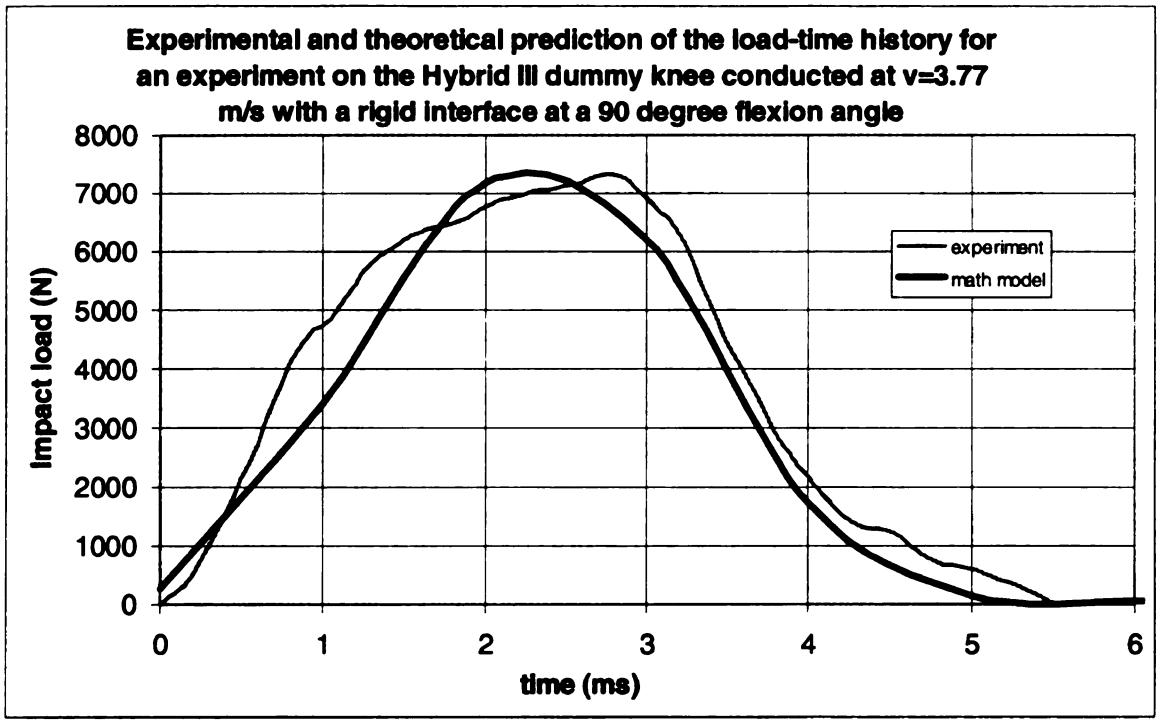

Figure 18: A comparison of the load-time histories from an impact experiment on the dummy and the load-time history predicted by the Madymo-Pamcrash model.